

# Order and transport in interacting disordered low-dimensional systems

Inaugural-Dissertation  
zur  
Erlangung des Doktorgrades  
der Mathematisch-Naturwissenschaftlichen Fakultät  
der Universität zu Köln

vorgelegt von  
**Zoran Ristivojevic**  
aus Kruševac, Serbien

Köln 2009

Berichtersteller: Prof. Dr. Thomas Nattermann  
Prof. Dr. Matthias Vojta

Tag der mündlichen Prüfung: 03. Juli 2009

---

# Contents

<b>Contents</b>	<b>iii</b>
<b>1 Introduction</b>	<b>1</b>
1.1 Physical systems . . . . .	1
1.2 Interacting electrons in one dimension . . . . .	3
1.3 Thin superconducting films . . . . .	7
1.4 Outline of the thesis . . . . .	9
<b>2 Transport in a Luttinger liquid with dissipation</b>	<b>11</b>
2.1 Introduction . . . . .	11
2.2 Model . . . . .	13
2.3 Renormalization group analysis . . . . .	14
2.4 Transport . . . . .	17
2.5 Friedel oscillations . . . . .	20
2.6 Conclusions . . . . .	21
2.A Conductance from the Fermi golden rule . . . . .	21
<b>3 Realization of spin-polarized current in a quantum wire</b>	<b>25</b>
3.1 Introduction . . . . .	25
3.2 Model . . . . .	28
3.3 Resonant tunneling of spinless electrons . . . . .	31
3.4 Weak impurities . . . . .	33
3.5 Strong impurities . . . . .	35
3.6 Transport . . . . .	38
3.7 Conclusions . . . . .	40
3.A Bosonization . . . . .	40
3.B Bosonized model . . . . .	45
<b>4 The effect of randomness in one-dimensional fermionic systems</b>	<b>47</b>
4.1 Introduction . . . . .	47
4.2 Model . . . . .	49
4.3 Rigidities and ac conductivity . . . . .	50

---

---

4.4	Fixed points and phases . . . . .	51
4.5	Mott-glass phase . . . . .	53
4.6	Discussions and conclusions . . . . .	55
<b>5</b>	<b>Vortex configurations in a superconducting film with a mag-</b>	
	<b>netic dot</b>	<b>57</b>
5.1	Introduction . . . . .	57
5.2	Model . . . . .	59
5.3	Ground states with vortices . . . . .	62
5.4	Magnetic field . . . . .	64
5.5	Numerical study of ground states with low number of vortices	67
5.6	Discussions and conclusions . . . . .	72
5.A	Derivation of the model . . . . .	73
5.B	Calculation of $U_{mv}$ . . . . .	77
<b>6</b>	<b>Superconducting film with randomly magnetized dots</b>	<b>79</b>
6.1	Introduction . . . . .	79
6.2	Model and its solution . . . . .	81
6.3	Discussions and conclusions . . . . .	84
6.A	Equivalence between random potentials . . . . .	86
	<b>Bibliography</b>	<b>89</b>
	<b>Acknowledgements</b>	<b>97</b>
	<b>Abstract</b>	<b>99</b>
	<b>Zusammenfassung</b>	<b>101</b>
	<b>Erklärung</b>	<b>103</b>
	<b>Curriculum vitae</b>	<b>105</b>

---

# Introduction

*In this chapter we introduce two different systems that will be considered in this thesis: one-dimensional interacting electronic systems and thin superconducting films.*

## 1.1 Physical systems

Physical systems are very diverse and can be classified in many ways. They can be macroscopically large or microscopically small regarding their size, they can be solid, liquid or gaseous with respect to their state, and there are many other classifications with respect to some property. While some physical systems are well understood, many of them are not. The main obstacle hindering a thorough understanding is the interaction. For systems that we will investigate in this thesis, it is the electromagnetic interaction that is responsible for non-trivial physical effects. The other three fundamental interactions are irrelevant for our considerations.

We begin with a simple example which demonstrates one aspect of the space dimensionality. The electromagnetic potential  $\Phi(\mathbf{r})$  produced by the charge density  $\rho(\mathbf{r})$  is governed by the Poisson equation [1]

$$\nabla^2\Phi(\mathbf{r}) = -4\pi\rho(\mathbf{r}). \quad (1.1)$$

The solution of the previous equation for a single electron placed at the origin depends on the system dimensionality  $d$ . It is given by

$$\Phi(\mathbf{r}) = \begin{cases} -e/|\mathbf{r}|, & d = 3, \\ \text{const} - 2e \log |\mathbf{r}|, & d = 2, \\ 2\pi e|\mathbf{r}| + \text{const}, & d = 1. \end{cases} \quad (1.2)$$

While the electron charge  $-e$  enters the potential in the same way in different dimensions, the spatial coordinate does not. For the interaction between two electrons the previous expression gives the usual Coulomb  $1/r$  interaction in three dimensions, but a logarithmic interaction in two dimensions. We see that even the simplest interacting system shows significant differences in the

---

potential energy behavior. We should be aware that an interacting many body system has quite often an effective interaction that is different from the aforementioned Coulomb interaction. The reason for this are complicated many body interaction processes that occur in reality and which can not be all treated exactly. However, at the end an effective picture emerges as a result of some well suited approximative treatment. For example, it is well known that two electrons of opposite spin and momentum effectively attract each other in superconductors. This occurs due to the presence of phonons that mediate the electron-electron interaction in that particular case.

Apart from interaction, other principles of physics are also involved. Quantum-mechanical indistinguishability of particles classifies them into fermions and bosons, apart from possible exotic particles in some two-dimensional systems. At large temperatures quantum mechanics is not important any more, rather laws of classical mechanics apply. There both kinds of particles behave similarly. At low temperatures fermions and bosons behave quite differently, due to the Pauli exclusion principle. It states that two identical fermions can not occupy the same quantum state simultaneously.

In three dimensions, non-interacting fermions at zero temperature fill the available quantum states up to the Fermi level, while non-interacting bosons condense in a macroscopic quantum state all having zero momentum. This defines the ground state (the state having the lowest possible energy) of non-interacting fermions and bosons. The lowest-lying excitations in the fermionic case occur when a fermion near and below the Fermi level is excited to an empty quantum state above it. In the bosonic case an excitation consists of taking a boson from the rest state, where it has zero momentum, to a moving state.

Effects of interactions in the systems from the previous paragraph are also well understood. Upon switching-on interactions, the Fermi level is still well defined. The low-energy excitations may be described by quasi-particles. They satisfy Fermi-Dirac statistics and carry the same spin, charge and momentum as the original fermions, but have a renormalized mass. These quasi-particles are nearly free and have a finite lifetime, which is inversely proportional to the square of the excitation energy measured relative to the Fermi energy. The theory of interacting fermions in three dimensions is known as Landau's Fermi liquid theory [2].

While interaction between fermions in three dimensions does not qualitatively alter the non-interacting picture, for bosons this is not the case. Weakly interacting bosons become superfluid at low temperatures. Experimentally, a superfluid flows without friction through narrow capillaries at low temperatures. For  $^4\text{He}$  atoms it occurs below the lambda line, at saturated vapor pressure below 2.17 K [3]. Theoretically, due to interactions the

---

lowest part of the spectrum of quasi-particles, which diagonalize the interacting Hamiltonian, becomes linear, which is a necessary condition for the frictionless flow. Excitations of interacting bosons are of collective nature.

The system dimensionality is also very important. Opposite to the three-dimensional case, non-interacting bosons do not condense in one and two space dimensions due to large fluctuations [3, 4]. Quite generally, effects of thermal fluctuations are drastic in two- and less-dimensional systems, preventing long-range order in systems with a continuous symmetry [4, 5].

These are just some very well known facts where the interplay between fluctuations, interaction and dimensionality leads to different physical scenarios. Another very important ingredient is disorder. In solid state physics systems it can be thermal, due to thermal fluctuations, topological, due to topological defects and compositional, due to externally immersed particles into the host system [6]. Effects of disorder are very important, in particular in low-dimensional systems. This will be also shown in this thesis. In the rest of the thesis we will be dealing only with disordered low-dimensional systems, i.e. with one- and two-dimensional interacting systems. More precisely, we focus on systems that are described as if they were effectively low-dimensional. The one-dimensional systems that we consider are interacting electrons, while the two-dimensional systems are thin superconducting films.

## 1.2 Interacting electrons in one dimension

The effects of interactions in one-dimensional fermionic systems are drastic. Fermi liquid theory breaks down and one does not have low-energy excitations that have a single-particle character. Rather, the excitations become collective. Due to their spin and their charge, electrons are described by two kinds of collective excitations, for the charge and for the spin degrees of freedom. These excitations have different velocities, which has also been confirmed experimentally [7]. This phenomenon, that an interacting one-dimensional electron systems has different velocities of collective excitations, is known as spin-charge separation.

In the non-interacting case the Fermi level reduces to two Fermi points,  $\pm k_F$ . Effects of interactions between electrons in one dimension can be treated using the bosonization technique [8]. There, one diagonalizes a fermionic Hamiltonian by going over to a bosonic one. Some details about the procedure are presented in appendix 3.A of chapter 3. Loosely speaking, bosonization translates interacting fermions into free bosons. We should stress here that bosonization properly covers only the low-energy part of the

---

fermionic spectrum, and in the rest of the thesis we should bear this in mind.

In the following we consider only spinless electrons for simplicity. The two parameters that play a role in the bosonic description are the velocity of excitations  $v$  and the Luttinger parameter  $K$ . The velocity of excitations is the Fermi velocity modified by interaction, while the parameter  $K$  controls the interaction. In the non-interacting case we have  $K = 1$ , while for repulsive (attractive) interactions we have  $K < 1$  ( $K > 1$ ). Apart from these two parameters, the bosonic Hamiltonian contains also canonically conjugate position and momentum operators of particles.

Within the classical physics, repulsively interacting electrons in one dimension at zero temperature are equidistantly distributed, where the distance between two electrons is determined by the electron density. However, their quantum-mechanical nature prevents that. The Heisenberg uncertainty relation

$$\Delta x \Delta p \geq \frac{\hbar}{2} \tag{1.3}$$

requires a completely undetermined momentum for an electron that has a specified position. Oppositely, zero momentum of an electron implies that it is positioned everywhere in space with equal probability. A compromise between these two cases is that both the electron's position and momentum are fluctuating quantities. This is a quantum-mechanical consequence. To describe particles, one introduces the operator  $\varphi_i$  which measures the position of the electron, indexed by  $i$  with respect to its classical lattice position. Going over to the continuum limit,  $\varphi_i$  translates into the displacement field  $\varphi(x)$ . The momentum  $\Pi(x)$  is introduced as the canonically conjugated field to  $\varphi(x)$  and they satisfy the bosonic commutation relation

$$[\varphi(x), \Pi(y)] = i\hbar\delta(x - y). \tag{1.4}$$

The two parameters,  $v$  and  $K$ , and the two fields,  $\varphi$  and  $\Pi$ , completely describe the interacting electrons in one-dimension. A new state of matter that arises is called the Luttinger liquid. It is experimentally realized in a number of different systems, which include carbon nanotubes [9, 10], polydiacetylen [11], quantum Hall edges [12], semiconductor cleaved edge quantum wires [13], and in one-dimensional ultra-cold gases [14].

The effects of disorder on Luttinger liquids are also well known. We distinguish between two kinds of disorder, that are an isolated point impurity and densely spaced many weak impurities that act collectively. While some interesting effects may occur when impurities are not static [15], in the following we concentrate only on static impurities.

---

Without impurities a Luttinger liquid is perfectly conducting, so we can say that it has metallic properties [8]. We review the influence of impurities starting from the non-interacting case  $K = 1$ . In the presence of a single impurity the analysis can be done inside the one-body Schrödinger equation, from which we simply conclude that an incident wave (electron) is partially transmitted and partially reflected by a potential barrier created by the impurity. This means the non-interacting system remains metallic due to nonzero transmission. The case with many impurities is more complicated. An electron can coherently backscatter from many impurities and it is not a priori clear whether an electron inserted in the middle of the system can leave it or not. By now it is well established that any disorder in one dimension localizes all electronic states [16, 17], meaning the electron will be localized by disorder. We get an insulating state at zero temperature. Without inelastic scattering processes, the finite temperature conductivity remains zero. When inelastic processes are accounted for, like electron-phonon interaction, the situation changes. With the assistance of phonons, electrons may hop between localized states at any non-zero temperature, leading to a small, but non-vanishing conductivity. This form of electron conduction is known as hopping conductivity [18].

When the interaction is switched on, the situation becomes different. A single point impurity of any strength placed into a Luttinger liquid has a very strong effect. For any repulsive interaction it makes the system insulating at zero temperature [19, 20, 21]. Oppositely, for attractive interaction the presence of an impurity is unimportant and the system remains metallic; this means the phase transition occurs at zero temperature for  $K = 1$ . At finite temperature the conductance vanishes with temperature as a power law controlled by the interaction parameter  $K$ . In this thesis we will consider a system that consists of a single impurity and in the presence of dissipation. Qualitatively, the dissipation may be understood as an inelastic scattering process that diminishes the conductance. We will show that in chapter 2.

Another interesting situation occurs when the two barriers, made by two point impurities, are present in a Luttinger liquid. Somewhat surprisingly and opposite to the single impurity case, the system may be metallic for not too strong repulsive interactions. This rather subtle phenomenon is known in quantum mechanics of non-interacting particles as resonance tunneling [22]. A free particle that impinges on the two-barrier potential always tunnels through the potential. In the special case, when its incident wavevector matches the wavevector it would have if the barriers were impenetrable, there is no reflection and the transmission coefficient is one. This is the resonant tunneling phenomenon.

In the interacting case, when the barriers are large in comparison to the

---

Fermi energy, the island in between them has a well defined charge. For an electron driven by an external voltage, there are two possible ways to overcome the barriers. One option is direct tunneling through both impurities, and the other is the process of sequential tunneling, where an electron first enters the island from one side and then leaves it at the other. The former process is inhibited by the product of strengths of the barriers, while the latter is inhibited by the strength of one barrier and also by the electrostatic repulsion from other electrons that sit on the island. The electrostatic repulsion that prevents an electron to enter the island is known as the Coulomb blockade. When the chemical potential on the island is such that adding another electron to the island has no cost in energy, the Coulomb blockade is lifted. In addition, if the interaction is not too strong, the double-barrier is fully transmitting [20] at zero temperature. When the Coulomb blockade is not lifted, the two impurities effectively act as a single one, and the system is insulating at zero temperature.

An external magnetic field tends to split electrons at the Fermi level. Electrons having different spin projection on the direction of the magnetic field acquire different Fermi momenta. If a double barrier is placed in such a system, an interesting situation may occur. Because electrons of different spin projection have different Fermi momenta, it may happen that just one spin direction resonantly tunnels. This leads to a spin filtering effect. As we know, the effects of interactions are very important in one dimension and they will be examined in chapter 3.

A different kind of disorder is realized when the system contains many impurities that are densely distributed and very weak, so they act collectively. This kind of disorder is called Gaussian disorder. It is characterized by a single parameter, that is the product of the impurity density and the typical squared single impurity strength [8]. The Gaussian disorder couples to the electron density. It tends to deform the electron displacement field according to its minima, while the electrons classically tend to have the displacement field undistorted. The competition between these two effects, the elastic energy and the disorder, crucially depends on the Luttinger parameter  $K$ . For  $K > 3/2$  the elastic term wins and the low-energy properties of the system correspond to the free Luttinger liquid model without disorder. For  $K < 3/2$  the system is disorder dominated and the displacement field is pinned by the disorder. The resulting phase is called the Anderson insulator.

Another kind of ordering in Luttinger liquids occurs when a periodic potential is present in the system. Effectively, the periodic potential may arise due to umklapp processes [8, 23]. It wants to keep the electron displacement field constant in order to minimize the total energy. The displacement field “trapped” by the periodic potential is a ground state of the system as

---

long as the fluctuations of the displacement field, which are measured by  $K$ , are small enough. When  $K$  increases, the displacement field is “less and less arrested” by the periodic potential, becoming free for sufficiently large  $K$ . The low- $K$  phase is known as the Mott insulator for electronic systems. When both the periodic potential and the Gaussian disorder are present, the situation is complicated since the two insulating phases compete. We will consider this issue in chapter 4.

### 1.3 Thin superconducting films

Superconductivity was discovered nearly a century ago. The two hallmarks of superconductivity are perfect conductivity and perfect diamagnetism [24]. Inside the phenomenological Ginzburg–Landau theory, one introduces the local superconducting order parameter  $\psi(\mathbf{r})$  in order to describe the superconducting state. The density of superconducting electrons equals  $n_s(\mathbf{r}) = |\psi(\mathbf{r})|^2$  and is nonzero in the superconducting phase. The correlation function  $\langle \psi^*(\mathbf{r})\psi(0) \rangle$  (where  $\langle \dots \rangle$  denotes an average over the Ginzburg–Landau energy functional) acquires a finite value for  $|\mathbf{r}| \rightarrow \infty$  in three dimensions for temperatures  $T$  smaller than the critical temperature  $T_c$ , which means that there is long-range order for the parameter  $\psi$ . For  $T > T_c$  the correlation function decays exponentially and there is short-range order for the parameter  $\psi$ .

A strong magnetic field always destroys superconductivity. In type-I superconductors this process appears as an abrupt magnetic flux penetration through the whole sample when the external magnetic field exceeds the thermodynamic critical field. In type-II superconductors, for external magnetic fields between the lower and the upper critical field, magnetic flux penetrates the sample only partially in the form of regularly distributed flux lines. The density of superconducting electrons vanishes inside a flux line, and there normal electrons are present. A flux line, also called a vortex, has a typical spatial extension  $\xi$  in the transverse direction. The parameter  $\xi$  is called the coherence length and is a characteristic of the superconductor. The magnetic field around a vortex decays over distances beyond the London penetration depth  $\lambda_L$ . This is the length scale determined by the electromagnetic response of the superconductor. A single vortex line has the energy per unit length [24]

$$\epsilon_1 = \left( \frac{\phi_0}{4\pi\lambda_L} \right)^2 \ln \frac{\lambda_L}{\xi}, \quad (1.5)$$

meaning its energy becomes large for samples long in the direction parallel

---

to the vortex (and the external magnetic field). This explains the fact that vortices do not appear due to thermal fluctuations in three-dimensional superconductors in zero magnetic field. By  $\phi_0 = hc/(2e)$  we have denoted a flux quantum.

Thin superconducting films are effectively two-dimensional systems, where the effect of thermal fluctuations is very pronounced. Divergent fluctuations of the phase of the order parameter at low temperatures prevent a true long-range order of the order parameter. Rather, the low-temperature phase shows quasi-long-range order,  $\langle \psi(\mathbf{r})\psi(0) \rangle \sim |\mathbf{r}|^{-\eta(T)}$ , where  $\eta(T) \sim T$ . The effect of magnitude fluctuations of the order parameter are also very important in two dimensions. We should make a distinction between small fluctuations in the magnitude of  $\psi$ , where  $\psi$  does not vanish, and large fluctuations, where  $\psi$  reaches zero value. The former lead to a slight renormalization of the parameter  $\eta(T)$  for low temperatures [25], and are not important. The latter play a very important role. Points where  $\psi(\mathbf{r}) = 0$  define vortices. As a difference to the three-dimensional case, here vortices appear due to thermal fluctuations, even in the absence of an external magnetic field. We will show this now.

For thin superconducting films it is very important that the magnetic field and the vector potential do not vanish out of the film plane, whereas the order parameter exists only in the film plane. This difference with respect to the three-dimensional case leads to a new effective penetration depth for films,  $\lambda = \lambda_L^2/d_s$ , where  $d_s$  is the film thickness [25, 26]. This affects the single vortex energy, and also the energy of a vortex-antivortex pair separated by a distance  $r$ , which respectively read

$$U_v \approx \varepsilon_0 \ln \frac{\min(\lambda, L)}{\xi}, \quad (1.6)$$

$$U_{vv}(r) = 2\varepsilon_0 \ln \frac{r}{\xi}, \quad r < L < \lambda, \quad (1.7)$$

where

$$\varepsilon_0 = \frac{\phi_0^2}{16\pi^2\lambda} \quad (1.8)$$

and  $L$  is the typical lateral film size. Analyzing the free energy of a single vortex [27]  $F = U_v - TS$ , where  $S = \ln(L/\xi)^2$  we conclude that the two different possibilities arise. For large system sizes,  $L > \lambda$ , the entropy term always prevails, meaning any nonzero temperature leads to the spontaneous appearance of free vortices. This ultimately leads to short-range order of the order parameter and the film loses its superconductivity. The more interesting case is when  $L < \lambda$ . Then, free vortices are created just above the

---

critical temperature  $T_{2D} = \varepsilon_0/2$ . We set Boltzmann's constant to  $k_B = 1$  in the following. Below  $T_{2D}$  the system has only bound vortex-antivortex pairs. They are very important excitations of the amplitude of the order parameter not only in thin films, but in a broad class of two-dimensional systems with continuous symmetry. These systems include superfluid films and planar magnets. Using the renormalization group method one can show that the transition temperature becomes  $T_{2D} = \varepsilon_0(T_{2D})/2$ , where  $\varepsilon_0(T_{2D})$  means that one should use the renormalized value for  $\lambda$  in expression (1.8). This comes from the renormalization of the vortex-antivortex interaction (1.7) due to the presence of other bound vortex-antivortex pairs at low temperatures [25, 28]. Hence, the quasi-long-range order of the order parameter survives at low temperatures  $T < T_{2D}$ , and vortex-antivortex excitations do not destroy this kind of order. The low-temperature phase is superconducting in the sense that it has a nonlinear current-voltage relation of the form  $V \sim I^3$  at  $T \rightarrow T_{2D}^-$ . The high-temperature phase, for  $T > T_{2D}$ , behaves like a normal metal and we have  $V \sim I$  [29].

In this thesis we will consider a thin film in the presence of small magnetic dots placed on top of it. Such magnetic nanostructures can be easily created experimentally and are an interesting tool for probing different physical phenomena [30, 31]. The magnetic substructure creates the inhomogeneous magnetic field in the film and may cause creation and pinning of vortices in the film. It also changes the transport properties and the transition temperature of the superconductor. In particular, in chapter 5 we will consider a single magnetic dot and determine vortex configurations induced by the dot. The vortex configurations depend on the parameters of the dot and also on the superconductor parameters. In chapter 6 we will study a lattice of magnetic dots with random magnetization and determine the phase diagram of the system.

## 1.4 Outline of the thesis

This thesis contains six chapters. After the introductory one, the next three chapters study a Luttinger liquid with impurities, while the last two chapters are dealing with thin superconducting films. In chapter 2 we consider a Luttinger liquid with dissipation and a single impurity. We show that the dissipation changes the conductance behavior at low applied voltages and temperatures, while at higher voltages and temperatures the system behaves as if it was dissipation-free. In chapter 3 we consider a Luttinger liquid in the presence of an external magnetic field and two impurities. We show that such system may have spin-filtering properties for not too strong repulsive

---

interactions. Chapter 4 contains a study of effects of Gaussian disorder on the Mott-insulating state. We show that the intermediate Mott-glass state does not appear, in contrast to some studies. In chapter 5 we calculate the ground state configurations of vortices in the film when a small ferromagnetic dot is placed on the top of the film. In chapter 6 we show that a system that consists of a superconducting film covered by magnetic dots with random magnetization maps to the two-dimensional XY model and infer its phase diagram.

---

# Transport in a Luttinger liquid with dissipation

*In this chapter we study electron transport through a single impurity in a one-channel Luttinger liquid coupled to a dissipative Ohmic bath. For nonzero dissipation, the single impurity is always a relevant perturbation and suppresses transport strongly.*

## 2.1 Introduction

The physics of a particle coupled to a dissipative environment is a fundamental problem [32, 33]. Such theoretical model is realized in many different physical situations, which include damped motion of a particle in an external potential with thermal noise [34], tunnel junctions at low temperatures [35], motion of a heavy particle placed in a Luttinger liquid [36], and a superconducting grain coupled to leads via Josephson junctions [37].

Common for the aforementioned systems is that they are problems of a single degree of freedom. A problem we are interested in is the electron tunneling through a single impurity placed in a Luttinger liquid. Since single particle excitations are absent in interacting one-dimensional systems, one would expect that our case belongs to a different class of problems. However, a closer look reveals that this is also a problem of a single particle; in our case this single particle is played by the fluctuating electron displacement field at the impurity position.

Our main concern in this chapter will be a question of transport in a Luttinger liquid with dissipation and a single impurity. While the Luttinger liquid state can be realized in a broad class of systems, see chapter 1 for some examples, we primarily consider quantum wires. In a one-dimensional quantum wire the transverse motion of electrons is quantized into discrete modes due to finite width of the wire, while the longitudinal motion is free. For simplicity in the following we assume that just one transverse mode is occupied.

---

The wire is connected at its ends to Fermi-liquid leads which are reservoirs of electrons. When one lead has higher electrochemical potential than the other electrons propagate along the wire. If the applied field is an ac field of frequency  $\omega$ , one obtains in the limit  $\omega \rightarrow 0$  the two-terminal conductance  $G(\omega \rightarrow 0) = 2e^2/h$ , provided the length of the wire  $L$  obeys the condition  $L \ll L_\omega = v/\omega$ , where  $v$  denotes the plasmon (excitation) velocity [38, 39, 40]. On the contrary, for  $L \gg L_\omega$ , one observes the low-frequency microwave conductance  $G(\omega) < 2e^2/h$ .

In realistic cases electrons from the wire couple to other degrees of freedom, e.g. to phonons or to electrons in nearby gates. It is usually the effect of screening of long-range Coulomb interaction between electrons due to gates which is considered for one-dimensional conductors [41]. Here we rather consider another effect: the dissipation. The electrons in the nearby gates are degrees of freedom which act as a dissipative bath for the electrons in the wire [32]. In particular, it has been shown recently that the coupling of the electrons from a clean wire to the electrons from surrounding metallic gates results in an Ohmic dissipation of the electrons in the wire [42].

The dissipation introduces a length scale  $L_\eta$ . Above that length scale the electron motion is damped. While the electrons in quantum wires scatter of other electrons and of impurities (if they are present) elastically, the dissipative bath serves a source of inelastic scattering. Losing their momenta in inelastic scattering events, the electrons dissipate energy of the system. On physical grounds it means that the external dissipation increases the resistance of the wire, or equivalently decreases the conductance. What is important here is the ratio between wire's length  $L$  and the dissipative length  $L_\eta$ . Certainly, when  $L_\eta \gg L$ , the effect of the dissipation is very small and hence of no practical importance. In the opposite limit,  $L_\eta \ll L$ , the electron motion in the wire is dominated by the dissipation and one expects that conductance is strongly reduced.

In addition, we are also interested in effects of an isolated impurity placed in the wire. The case without the dissipation is considered in a pioneering work by Kane and Fisher [19]. They found that impurity leaves the zero temperature conductance unchanged, provided the interaction is attractive. This result is independent of the strength of the impurity. For repulsive interaction, on the other hand, the conductance vanishes at zero temperature as  $G \sim V^{2/K-2}$ , where  $V$  is the applied voltage [19, 20, 21, 43]. At nonzero temperatures  $T$  and small voltages the conductance behaves as  $G \sim T^{2/K-2}$ , remaining finite even for  $V \rightarrow 0$ . This is due to thermally excited electrons which tunnel through the impurity.

The question that arises is: what is the influence of dissipation on the transport properties of disordered Luttinger liquids? We address it in the

rest of this chapter. In particular we study the influence of weak dissipation on the tunneling of electrons through a single impurity. This chapter is organized as follows. In section 2.2 we introduce a model for interacting electrons in one dimension in the presence of a single impurity and dissipation. The model is analyzed in using the renormalization group method in section 2.3. In section 2.4 we calculate the conductance of the system at finite voltage and temperature. In section 2.5 we calculate the decay of the mean electron density, which is followed by conclusions. Some technical details are presented in appendix 2.A.

## 2.2 Model

We consider spinless electrons in a one-dimensional wire which are coupled to a dissipative bath. In the center of the wire of length  $L$  is a single  $\delta$ -function like impurity of arbitrary strength. Following Haldane [44], the charge density  $\rho(x)$  can be rewritten as

$$\rho = \frac{k_F}{\pi} - \frac{1}{\pi} \partial_x \varphi + \frac{k_F}{\pi} \cos(2\varphi - 2k_F x) + \dots, \quad (2.1)$$

where  $\varphi(x)$  denotes the bosonic (plasmon) displacement field and  $k_F$  is the Fermi wavevector. The Euclidean action of the system then reads [8]

$$\begin{aligned} \frac{S}{\hbar} = & \frac{1}{2\pi K} \int_{-L/2}^{L/2} dx \int_{-\hbar\beta/2}^{\hbar\beta/2} d\tau \left[ \frac{1}{v} (\partial_\tau \varphi)^2 + v (\partial_x \varphi)^2 - 2\pi K W(\varphi) \delta(x) \right] \\ & + \frac{\eta}{4} \int_{-L/2}^{L/2} dx \int_{-\hbar\beta/2}^{\hbar\beta/2} d\tau \int_{-\hbar\beta/2}^{\hbar\beta/2} d\tau' \frac{[\varphi(x, \tau) - \varphi(x, \tau')]^2}{\{\hbar\beta \sin[\pi(\tau - \tau')/\hbar\beta]\}^2}, \end{aligned} \quad (2.2)$$

where  $\beta = 1/T$ . For  $K \ll 1$  Eq. (2.2) describes also a charge or spin density wave, while  $K \rightarrow 0$  corresponds to the classical limit.  $W(\varphi)$  is the impurity potential which is a periodic function of periodicity  $\pi$ . The last part in the action (2.2) describes Ohmic dissipation [32]. It was derived from a pure Luttinger liquid coupled electrostatically to a metallic gate in Ref. [42], where it was found that such a coupling is only relevant for  $K < K_\eta = 1/2$ . This fact can be taken into account by writing  $\eta = \eta_0 \xi_\eta^{-1}$  where  $\xi_\eta$  denotes the Kosterlitz-Thouless correlation length diverging at the transition  $K \rightarrow K_\eta - 0$  and  $\eta_0$  is a dimensionless coupling constant. Since there may be other sources of dissipation which survive also for  $K > 1/2$ , in the following we assume that  $\eta > 0$ .

---

In treating the influence of the impurity we first consider the zero temperature case. After Fourier transforming

$$\varphi(x, \tau) = \int \frac{d\omega}{2\pi} \int \frac{dk}{2\pi} \varphi_{k,\omega} e^{ikx+i\omega\tau}, \quad (2.3)$$

the harmonic action reads

$$\frac{S_0}{\hbar} = \frac{1}{2\pi K} \int \frac{d\omega}{2\pi} \int \frac{dk}{2\pi} \left[ \frac{1}{v} \omega^2 + vk^2 + K\eta|\omega| \right] |\varphi_{k,\omega}|^2. \quad (2.4)$$

The last term of Eq. (2.4) describes the (weak) damping of the plasmons of complex frequency  $\omega_P \approx v(k + i/(2L_\eta))$ , where  $L_\eta = 1/(K\eta)$  is the dissipative length. The upper cutoff for momentum and frequency are  $\Lambda$  and  $\omega_c$ , respectively.  $\omega_c = \min\{v\Lambda, E_{\text{diss}}/\hbar\}$  where  $E_{\text{diss}}$  corresponds to the maximal energy which can be dissipated by the dissipative bath. For simplicity we will assume that  $E_{\text{diss}} > \hbar v\Lambda$ , so that  $\omega_c = v\Lambda$ . Since the impurity acts at one point in space, the action is harmonic outside the impurity position. One can then get an effective action by integrating out all degrees of freedom outside the impurity. Then, the resulting effective impurity action reads

$$\frac{S}{\hbar} \approx \frac{1}{\pi K} \int \frac{d\omega}{2\pi} \sqrt{\omega^2 + Kv\eta|\omega|} |\phi_\omega|^2 - \sum_{n=1}^{\infty} w_n \int d\tau \cos(2n\phi), \quad (2.5)$$

where  $\phi_\omega = \int d\tau \phi(\tau) e^{-i\tau\omega}$  and  $\phi(\tau) \equiv \varphi(x=0, \tau)$ . Since  $W(\phi)$  is a periodic function it is decomposed into a Fourier series in Eq. (2.5). As can be seen from Eq. (2.5), for low frequencies,  $\omega < v/L_\eta$ , the behavior of the system is controlled by the dissipation. For very large values of  $\omega$  and sufficiently small dissipation,  $\eta \ll \Lambda/K$ , the effective action (2.5) includes also a contribution  $\sim \int \frac{d\omega}{2\pi} \omega^2 |\phi_\omega|^2$  [8], while in the opposite case of large dissipation,  $\eta \gg \Lambda/K$ , it contains a term  $\sim \int \frac{d\omega}{2\pi} |\omega| |\phi_\omega|^2$ . This high frequency limit will be important for the analysis of the model in the strong impurity limit that we perform in the next section.

## 2.3 Renormalization group analysis

In the following we will perform a renormalization group analysis of the effective model given by Eq. (2.5). For weak impurity strength we can calculate the renormalization of  $w_n$  perturbatively. This gives for the flow equations of  $w_n$

$$\frac{dw_n}{dl} = \left( 1 - \frac{n^2 K}{\sqrt{1 + \eta K e^l / \Lambda}} \right) w_n. \quad (2.6)$$

There is no renormalization of  $K$  and  $\eta$ . This can already be argued from the fact that  $K$  and  $\eta$  are bulk quantities which cannot be renormalized by the local perturbation from the impurity. On a more formal level, one finds from integrating out the high frequency modes in Eq. (2.5) that one does not obtain terms depending in a nonanalytic way on frequency, see Refs. [19, 34].

For  $\eta = 0$  we recover from Eq. (2.6) the result of Kane and Fisher [20], namely that the impurity is a relevant perturbation for repulsive interaction  $K < 1$  and irrelevant for attractive interaction  $K > 1$ . As soon as the dissipation is switched on, the downward renormalization saturates at a length scale  $l^*$  given by  $e^{l^*} \approx \Lambda L_\eta$ . Thus the impurity is a relevant perturbation even for attractive interaction, provided the dissipation remains finite in this region. If the dissipation results from the coupling to gate electrons, as considered in Ref. [42],  $\eta$  renormalizes to zero for  $K > 1/2$  and hence the impurity potential renormalizes to zero for  $K > 1$ .

Motivated by the fact that a weak impurity flows toward strong impurity limit, we will consider now the system starting initially from very large impurity strength. Then the cosine terms of impurity potential are important and the displacement field gets locked in their minima. The main contribution to the partition function comes from configurations  $\phi(\tau) = n\pi$  with  $n$  integer, interrupted by kinks which connect these pieces. These multi-kinks configurations are saddle points of the effective action (2.5). For very large impurity strength kinks are narrow, and hence are characterized by the high frequency limit of the action (2.5).

For sufficiently weak dissipation,  $\eta \ll \Lambda/K$ , the resulting saddle point equation is the sine-Gordon equation in one dimension. It has a kink solution that interpolates between  $\phi = n\pi$  and  $\phi = (n+1)\pi$  in a narrow region of width  $\delta \sim 1/\sqrt{w_1}$ . Outside that narrow region the solution very rapidly reaches the values  $\phi = n\pi$  and  $\phi = (n+1)\pi$ .

In the opposite case of strong dissipation,  $\eta \gg \Lambda/K$ , the resulting saddle point equation is the sine-Hilbert (or Peierls-Nabarro called by some authors) equation [45, 46, 47]. As a difference from the sine-Gordon equation, it has a ‘nonlocal’ derivative of the displacement field  $\int d\tau' [\phi(\tau) - \phi(\tau')] / (\tau - \tau')^2$  instead of  $d^2\phi/d\tau^2$ . A kink solution for the sine-Hilbert equation is also localized within a scale  $\delta \sim 1/\sqrt{w_1}$ , but as a difference from the sine-Gordon case this solution has a long power law tail away from its center toward values  $\phi = n\pi$  and  $\phi = (n+1)\pi$ . The important consequences of that fact is a significant interaction energy between two kinks separated by a distance  $d$  proportional to  $\ln(L/d)$ . For the sine-Gordon case this interaction is exponentially small with the distance between kink centers and is negligible for separations larger than the kink width. In the following we will consider only the weak dissipation case.

---

A saddle point solution  $\phi_s(\tau)$  of the effective action (2.5) with  $n$  kinks and  $n$  antikinks can be written as

$$\phi_s(\tau) \approx \pi \sum_{i=1}^{2n} \epsilon_i \Theta(\tau - \tau_i), \quad (2.7)$$

where  $\epsilon_i = \pm 1$  and kinks satisfy the electroneutrality condition  $\sum_{i=1}^{2n} \epsilon_i = 0$ .  $\Theta(\tau)$  is the Heaviside step function and  $\tau_i$  are the kink positions. In frequency space the saddle point configuration can be written as

$$\phi_{s,\omega} \approx \frac{i\pi}{\omega} \sum_{i=1}^{2n} \epsilon_i \exp(i\omega\tau_i). \quad (2.8)$$

We should emphasize that in addition to the interaction between kinks due the high frequency limit, exponentially small in the present case, an extra interaction is present due to the low frequency part of the quadratic part of the action (2.5). The low frequency part does not influence the shape of kinks, but contributes to the partition function. The partition function of the system is a sum over all possible saddle point solutions, and reads

$$Z = \sum_{n=0}^{\infty} \sum_{\epsilon_j = \pm 1} \frac{t^{2n}}{\delta^{2n} (n!)^2} \int d\tau_1 \dots d\tau_{2n} \exp \left[ \frac{2}{K} \sum_{i < j} \epsilon_i \epsilon_j f(\tau_i - \tau_j) \right]. \quad (2.9)$$

Here  $t \sim \exp(-S_{\text{kink}}/\hbar)$  is the tunneling transparency of the impurity and  $S_{\text{kink}} \sim \sqrt{w_1}$  denotes the action of an isolated kink.  $\delta$  is a short time cutoff of the order of the kink width. The partition function (2.9) is valid in the dilute kink gas approximation [48] when the overlap of kinks is neglected. The stronger the impurity is, the narrower the kink is and the smaller the tunneling transparency is. Then the dilute kink gas approximation is very well justified. The kink interaction is encoded into  $f(\tau)$  and is given by the expression

$$f(\tau) = \int_0^{\omega_c} d\omega \frac{\sqrt{\omega^2 + vK\eta|\omega|}}{\omega^2} [1 - \cos(\omega\tau)]. \quad (2.10)$$

In the limit of  $\omega_c\tau \gg 1$  we obtain, up to an additive constant, an interpolating expression

$$f(\tau) \approx \ln \omega_c\tau + \sqrt{2\pi v\eta K\tau}. \quad (2.11)$$

The logarithmic interaction prevails for small kink-antikink distances  $\tau$ , while for larger  $\tau$  the interaction exhibits a power law behavior. The different

behavior of  $f(\tau)$  is very important and will determine different transport characteristics when one changes the external parameters (voltage or temperature).

A strong impurity can alternatively be considered as a weak link between the two half-wires  $x < 0$  and  $x > 0$ , respectively. It is therefore convenient to rewrite the partition function (2.9) in a form in which  $t$  denotes the strength of the nonlinear terms. This can be done in the standard way, Refs. [21, 48], with the result  $Z = \int \mathcal{D}\theta e^{-S_{\text{eff}}[\theta]/\hbar}$  with

$$\frac{S_{\text{eff}}}{\hbar} = \frac{K}{\pi} \int \frac{d\omega}{2\pi} \frac{\omega^2}{\sqrt{\omega^2 + v\eta K|\omega|}} |\theta_\omega|^2 - 2t \int d\tau \cos 2\theta(\tau). \quad (2.12)$$

We can now consider the renormalization of  $t$  which is given by

$$\frac{dt}{dl} = \left( 1 - \frac{\sqrt{1 + \eta K e^l / \Lambda}}{K} \right) t. \quad (2.13)$$

Again  $\eta \equiv 0$  reproduces the known result of Ref. [20] that the weak link is renormalized to zero for  $K < 1$ . In the dissipative case the weak link is renormalized to zero for all  $K$  provided  $\eta$  remains finite. Thus from Eq. (2.6) and Eq. (2.13) we conclude that the impurity is always a relevant perturbation.

## 2.4 Transport

So far we were concentrated on equilibrium properties. However, one is often interested in transport characteristics of the system. In this section we calculate the current  $I$  through the impurity when the voltage  $V$  is applied to the ends of the wire. Their ratio determines the conductance  $G = I/V$ .

In the case without impurity one may use the linear response theory [8]. In the limit of large system sizes  $L \rightarrow \infty$  and for low frequencies  $L_\omega \gg L_\eta$  one gets finite conductivity  $\sigma(\omega \rightarrow 0) = \frac{e^2}{h} 2KL_\eta$ . On the other hand for very weak dissipation, when  $L_\eta \gg L_\omega \gg L$ , we know the result for the static conductance  $G = e^2/h$ . While in the former result the conductance of the wire is purely determined by the dissipation, in the latter case the dissipation is very weak and does not change the result for a clean quantum wire. Knowing the connection between the conductance  $G$  and the conductivity, which is in one dimension  $G = \sigma/L$ , one may write an interpolating expression for the static conductance

$$G = \frac{e^2}{h} \begin{cases} 1, & L \ll L_\eta, \\ \frac{2KL_\eta}{L}, & L \gg L_\eta. \end{cases} \quad (2.14)$$

In the case with impurity we have shown that impurity strength flows to large values. Under an applied external voltage electrons tunnel through the impurity. The tunneling rate  $\Gamma$  and hence the current follows from the expression [49]

$$\hbar\Gamma = 2T\text{Im} \ln Z(V), \quad Z = Z_0 + iZ_1, \quad (2.15)$$

where  $Z(V)$  denotes the partition function in the presence of an external voltage.  $Z_0$  includes the (stable) fluctuations of the  $\phi$  field close to a local minimum  $\phi = n\pi$ , whereas  $Z_1$  includes the voltage driven (unstable) fluctuations which connect neighboring minima  $\phi = n\pi \rightarrow (n+1)\pi$ . Since the strength of the impurity is renormalized to large values, we can use the saddle point approximation employed in the previous section for the calculation of  $Z$ . To obtain the saddle point action it is sufficient to consider a configuration consisting of a pair of kinks separated by a distance  $\tau$ . Then we have

$$\frac{S(\tau)}{\hbar} = \frac{2}{K}f(\tau) + \frac{2S_{\text{kink}}}{\hbar} - \frac{eV}{\hbar}\tau. \quad (2.16)$$

Here we have taken into account that the voltage creates into the action (2.5) a term  $-eV \int d\tau \phi / (\hbar\pi)$ . Note that two-terminal voltage applied to the leads is, in general, different from the four-terminal voltage  $V$  which is relevant for tunneling. However, if the wire is not too long and the impurity is strong both voltages are approximately the same. The saddle point follows then from

$$\frac{2}{K}f'(\tau) - \frac{eV}{\hbar} = 0. \quad (2.17)$$

This gives for larger voltages for the saddle point  $\tau_c \approx 2\hbar/(eVK)$  and hence for the current

$$I \sim \exp \left[ -\frac{S(\tau_c)}{\hbar} \right] \sim t^2 \left( \frac{eV}{\hbar\omega_c} \right)^{2/K}, \quad eV \ll \hbar\omega_c. \quad (2.18)$$

Taking into account quadratic fluctuations around the saddle point, we get an additional factor  $-1$  in the exponent in the previous formula, i.e. we reproduce the result of Kane and Fisher [20] for the conductance  $G \sim (eV/\hbar\omega_c)^{2/K-2}$ . On the contrary, for smaller voltages we get for the saddle point  $\tau_c \approx 2\pi\eta v\hbar^2/(e^2V^2K)$  and hence

$$I \approx A(V) \exp \left[ -\frac{S(\tau_c)}{\hbar} \right] = A(V)t^2 \exp \left( -\frac{\mathcal{C}_1\eta}{\kappa eV} \right), \quad eV \ll \frac{\eta}{\kappa}. \quad (2.19)$$

From fluctuations around the saddle point one gets for the prefactor  $A(V) \sim (\eta/\kappa(eV)^3)^{1/2}$ , while the numerical constant is  $\mathcal{C}_1 = 2$ . Here we have introduced the compressibility  $\kappa = K/(\pi v\hbar)$ . The cross-over between regimes (2.18) and (2.19) happens at  $eV/\hbar \approx \eta v$ . An independent calculation using the Fermi golden rule approach gives similar results, see appendix 2.A for more details.

In the case of non-interacting electrons  $\kappa$  coincides with the density of states. Then Eq. (2.19) can be obtained from the following argument: the probability that an electron tunnels over a distance  $r$  is proportional to  $Pr(r) \sim \exp(-2r/L_\eta)$ . To find the minimal  $r$  the number of states which can be reached has to be at least of the order one, i.e.  $\kappa eVr \approx 1$ . Inserting this into  $Pr(r)$  gives Eq. (2.19) apart from a numerical factor.

As expected, the dissipation reduces the current with respect to the Kane-Fisher result strongly. This means that the tunneling density of states into the end of a semi-infinite Luttinger liquid with dissipation  $\rho_{\text{end}}(E)$  is suppressed at low energies more than a power law found in the dissipation free case [20]. The current through the impurity may be written as

$$I \sim t^2 \int_0^{eV} dE \rho_{\text{end}}(E) \rho_{\text{end}}(eV - E). \quad (2.20)$$

Then using Eq. (2.19) we get

$$\rho(E) \sim \exp\left[-\frac{\mathcal{C}_1 \eta}{4\kappa E}\right]. \quad (2.21)$$

Next we consider finite temperatures. In this case the extension of the  $\tau$  axis is finite. Hence there will be a cross-over from Eq. (2.19) to a new behavior when the instanton hits the boundary, i.e. if  $\tau_c \approx \hbar/T$ . This  $eV$  to  $T$  dependence cross-over happens for  $eV \approx T$ . For larger  $T$  the current is given by

$$I \approx t^2 B(T) \exp\left[-\sqrt{\frac{\mathcal{C}_2 \eta}{\kappa T}}\right] V, \quad T \ll \frac{\eta}{\kappa}. \quad (2.22)$$

The instanton calculation gives for the numerical constant  $\mathcal{C}_2 = 8$ . The prefactor  $B(T)$  may be obtained from the Fermi golden rule approach, and is equal  $B(T) \sim T^{-2} (\kappa T/\eta)^{1/4}$ . More details can be found in appendix 2.A. In the dissipation free limit the conductance becomes  $G \sim (T/\hbar\omega_c)^{2/K-2}$ .

A simple way to reproduce formula (2.22) follows from integration of the flow equation for the transparency (2.13) and truncating the renormalization

group flow at the thermal de Broglie wavelength  $\hbar v/T$  of the plasmons [8]. This gives an effective tunneling transparency

$$t_{\text{eff}} \sim t \frac{\hbar v \Lambda}{T} \exp \left[ - \sqrt{\frac{4\eta}{\pi \kappa T}} \right]. \quad (2.23)$$

The total current is then proportional to  $t_{\text{eff}}^2$  which agrees with result (2.22) apart from the value of  $\mathcal{C}_2$  and the prefactor. Result (2.22) resembles variable range hopping in disordered quantum wires. Indeed, it can be written in the form  $I \sim \exp \left[ -\sqrt{\mathcal{C}_2/(K\kappa L_\eta T)} \right] V$ , which agrees with the variable hopping result if we replace  $L_\eta$  by the correlation length  $\xi_d$  of the disordered system [50]. This type of behavior has been indeed observed in quasi-one-dimensional  $\text{La}_3\text{Sr}_3\text{Ca}_8\text{Cu}_{24}\text{O}_{41}$ , but attributed to variable range hopping [51].

## 2.5 Friedel oscillations

The presence of an impurity in a metal produces Friedel oscillations in the electron density [52]. The asymptotic form of the density in  $d \geq 2$  dimensions behaves as

$$\rho(x) \sim \frac{\cos(2k_F x + \zeta)}{r^d}, \quad (2.24)$$

where  $r$  is the distance from the impurity,  $k_F$  the the Fermi vector and  $\zeta$  is a phase shift. Effects of interactions in  $d \geq 2$  can be incorporated by Fermi liquid theory and does not change  $x^{-d}$  decay. On the other hand in an interacting system in  $d = 1$  dimension Fermi liquid theory breaks down. There the decay is slower for repulsive interactions, and behaves as  $x^{-K}$ , and faster for attraction  $K > 1$ , where behaves as  $x^{1-2K}$ . It is obviously controlled by the interactions [53, 54].

In the present situation the dissipation is present and is expected to change the density profile at distances larger than  $L_\eta$ , provided the system size is large enough. In this section we calculate the charge density oscillations. To determine the averaged charge density we write

$$\langle \rho(x) \rangle = \frac{k_F}{\pi} - \frac{1}{\pi} \langle \partial_x \varphi \rangle + \frac{k_F}{\pi} \cos(2k_F x) e^{-2\langle \varphi^2(x) \rangle}, \quad (2.25)$$

where the average  $\langle \dots \rangle$  is taken with respect to the full action (2.2). The disorder average in the first term vanishes. To calculate the second term we remark that in the presence of dissipation the impurity is always a relevant perturbation and its strength grows under renormalization, see Eqs. (2.6)

and (2.13). To determine the large scale behavior of  $\langle \rho(x) \rangle$  it is therefore justified to assume that  $\varphi$  is fixed at the defect. The fluctuation  $\langle \varphi^2(x) \rangle$  is therefore identical to  $\frac{1}{2} \langle (\varphi(x) - \varphi(-x))^2 \rangle_0$ , where  $\langle \dots \rangle_0$  is the average with respect to the quadratic action (2.4), see Ref. [47]. From this one finds

$$\langle \rho(x) \rangle \sim \frac{k_F}{\pi} \cos(2k_F x) \begin{cases} |x|^{-K\left(1+\frac{1}{2\pi\Lambda L_\eta}\right)}, & x \ll L_\eta, \\ 1 + \frac{KL_\eta}{|x|}, & x \gg L_\eta. \end{cases} \quad (2.26)$$

For smaller distances  $x \ll L_\eta$  we get the well known power from Luttinger liquids, while for  $|x| \gg L_\eta$  the decay saturates.

## 2.6 Conclusions

In this chapter we have considered a Luttinger liquid model with Ohmic dissipation. In such a system on length scales larger than the dissipative length  $L_\eta$  the elementary excitations (plasmons) become diffusive and the displacement fluctuations become strongly suppressed restoring translational long range order (some kind Wigner crystal, but not due to the unscreened Coulomb interaction [55]). For large system sizes the system gets finite conductivity, which is paralleled by diverging superfluid fluctuations. We have shown that weak dissipation has a dramatic effect on transport properties of a Luttinger liquid with a single impurity. The voltage and temperature dependence of the conductance is reduced from power laws in the dissipation free case to an exponential dependence, Eqs. (2.19) and (2.22), respectively.

## 2.A Conductance from the Fermi golden rule

In this appendix we will calculate the conductance for the system we have introduced in this chapter using the Fermi golden rule approach. We closely follow the paper by Furusaki and Nagaosa [21] where the conductance of a Luttinger liquid with a single impurity is calculated. In our case the presence of dissipation changes the quadratic part of the action, producing a change in the conductance. For strong cosine potential the displacement field tend to stay in one of the minima of the cosine from Eq. (2.5) at zero temperature. At finite temperature and finite small applied voltage the displacement field tunnels to a neighboring minimum, because the applied voltage tilts the potential landscape. The increase of the displacement field physically corresponds to the motion of electrons through the system due to the applied voltage; this is expressed in terms of the conductance.

---

Rather than working directly with the model (2.5) for strong impurity, we consider the problem in terms of an equivalent model which gives the same partition function, see Refs. [21, 56]. The equivalent model is given as a system of linear harmonic oscillators to which is coupled the single degree of freedom—in our case the displacement field  $\phi(\tau)$ . Then calculating the voltage driven tunneling probability for the displacement field  $P_{\phi_0 \rightarrow \phi_1}$  from where  $\phi$  changes from  $\phi_0$  to  $\phi_1$  one gets the current  $I = e(P_{0 \rightarrow \pi} - P_{\pi \rightarrow 0})$  in the lowest order of the tunneling probability matrix element  $t$ . The final expression for the current reads [21]

$$I = et^2 \left[ 1 - \exp\left(-\frac{eV}{T}\right) \right] \int_{-\infty}^{+\infty} dz \cos\left(\frac{eV}{\hbar}z\right) \times \quad (2.27)$$

$$\exp\left\{-\pi \int_0^{\infty} d\omega \frac{J(\omega)}{\omega^2} \left\{ [1 - \cos(\omega z)] \coth\left(\frac{\hbar\omega}{T}\right) + i \sin(\omega z) \right\}\right\},$$

where

$$J(\omega) = \frac{2}{\pi K} \sqrt{\omega^2 + Kv\eta|\omega|}. \quad (2.28)$$

Physically, the current is produced by the electron tunneling from one to another minimum of the cosine term which forms the potential landscape. In the previous expression only the processes for tunneling into a neighboring minimum have been taken into account. In principle one should also take tunneling processes into the second (and higher order) nearest neighboring minimum, but these processes are expressed as higher powers of  $t$  and are neglected in Eq. (2.27).

The evaluation of Eq. (2.27) can be done in limiting cases when  $J(\omega) \sim |\omega|$  and  $J(\omega) \sim |\omega|^{1/2}$ . In the latter case by taking the exponential cutoff  $\exp(-\omega/(Kv\eta))$  which mimics the frequency range where the dispersion comes purely from dissipation, one gets for  $T = 0$  the result

$$I = 2\pi e \hbar t^2 \exp\left[\frac{4}{K} - \frac{eV}{\hbar Kv\eta}\right] \sqrt{\frac{\eta}{\kappa(eV)^3}} \exp\left[-\frac{4\eta}{\kappa eV}\right]. \quad (2.29)$$

In the former case again by taking the exponential cutoff  $\exp(-\omega/\omega_c)$  one gets

$$I = \frac{\pi e t^2}{\omega_c \Gamma(2/K)} \exp\left[-\frac{eV}{\hbar\omega_c}\right] \left(\frac{eV}{\hbar\omega_c}\right)^{\frac{2}{K}-1}. \quad (2.30)$$

For nonzero temperatures one can also get the result for the conductance by evaluating expression (2.27). In the dissipative regime it reads

$$I \sim \frac{\hbar e^2 t^2 V}{T^2} \left(\frac{\kappa T}{\eta}\right)^{1/4} \exp\left[-\sqrt{\frac{C_2 \eta}{\kappa T}}\right], \quad (2.31)$$

under the assumption  $eV \ll T \ll \eta/\kappa$ . For the numerical factor we get  $\mathcal{C}_2 = \frac{9}{4} \left( \frac{16\sqrt{2}}{\zeta(3/2)} \right)^{2/3} \approx 9.49$ . For larger temperatures one gets the power law result

$$I \sim \frac{e^2 t^2 V}{\hbar \omega_c^2} \left( \frac{T}{\hbar \omega_c} \right)^{2/K-2}, \quad (2.32)$$

which is the well known result for the conductance of a Luttinger liquid with a single impurity at nonzero temperatures [19, 20].

---

This page intentionally left blank

# Realization of spin-polarized current in a quantum wire

*In this chapter we consider an interacting quantum wire, modeled as a spinfull one-channel Luttinger liquid, placed in an external magnetic field. For the case of two point-like impurities embedded in the wire, under a small voltage bias, the spin-polarized current occurs at special points in the parameter space, tunable by a single parameter. Complete spin-polarization may be achieved at sufficiently low temperatures, provided repulsive interactions are not too strong.*

## 3.1 Introduction

In quantum mechanics it is well known that a one-dimensional plane wave incident on a high potential barrier is always partially transmitted. This effect is called quantum tunneling and does not exist in classical physics. When the same plane wave impinges on a symmetric double barrier, it can be completely transmitted. This surprising effect occurs only for certain wavevectors, otherwise the plane wave is partially reflected and partially transmitted. This phenomenon, when the double barrier is transparent, but the individual one is opaque, is called resonant tunneling [57]. In optics, this phenomenon is in essence of a Fabry-Pérot interferometer, made of two parallel highly reflecting mirrors. Its transmission spectrum as a function of wavelength of incident light exhibits peaks of high transmission corresponding to resonances. The resonance tunneling effect can be explained as destructive interference of all reflected partial waves from the two barriers, leading to perfect transmission.

In addition to its wave nature, an electron has a charge. Therefore, the electron transport in interacting one-dimensional systems is affected by the Coulomb interaction. This is strikingly seen when a potential barrier, created by a point impurity, is present in the system. When a voltage is applied at the ends of the system, the impurity reflects (backscatters) electrons pushed by the voltage, and tends to suppresses the transport. The conductance, which

---

is proportional to the transmission of electrons, vanishes with the voltage for any strength of repulsive interaction [19, 20].

When two point impurities are present in the system, they make an island. Knowing the physical picture of the single barrier, one would naively expect that the conductance of electrons is again strongly suppressed. However, this is not generally the case since the resonant tunneling effect also exists in the present situation. It explains perfect transmission through the island under some conditions. We can obtain them using a simple reasoning [8, 20], as will be explained now.

For weak impurities, the electron displacement field is just slightly perturbed by them and tends to be constant in order to minimize the energy. The condition for resonant tunneling follows from the requirement that the lowest harmonic of the electron density, that couples to the impurity potential, vanishes. For not too strong repulsion this leads to perfect transmission. In the opposite case, higher order harmonics of the electron density become important and destroy the resonance.

Direct tunneling through both impurities has very low probability, when the impurities are strong. Rather, the process of sequential tunneling is important. Strong impurities do not allow the leakage of charge under a small applied voltage, and the island has a well defined charge on it. In the ground state, this charge is fixed to an integer, which is determined by the position of the Fermi level. An empty state on the island is important for sequential tunneling. The process of electron transfer to the island is penalized by the electrostatic energy, that occurs due to the existence of electrons at the island which fill the energy states below the Fermi level. This process, when the host electrons prevent the other to enter the island, is known as the Coulomb blockade. However, when the distance between the impurities, or the gate voltage at the island, is such that the states on the island that differ by one electron become degenerate in energy, the Coulomb blockade is lifted. Under such circumstances, an electron can enter the island from one side and then leave at the other. While the Coulomb blockade does not hinder such process, the barrier strength does. Knowing that the barrier strength is irrelevant quantity for sufficiently strong quantum fluctuations in the system with a single barrier, we expect the same in the present case. Quantum fluctuations in these systems are measured by the Luttinger parameter  $K$ , which also measures the interaction strength. It turns out that the critical value of  $K$ , when the two barriers become irrelevant, is inside the region of repulsive interaction. This makes the effect of resonant tunneling of interacting one-dimensional electrons more realistic and interesting. The resonant condition in both limits of strong and weak impurities is the same,  $\cos(k_F a) = 0$ . Here,  $k_F$  is the Fermi wavevector and  $a$  is the distance between impurities.

---

Until now we considered spinless electrons. Including the electron spin degree of freedom, there will be no differences for weak impurity strengths. Again, there is perfect transmission for not too strong repulsion, when a single parameter, such as the distance between impurities or the voltage on the island, is tuned [20]. However, important differences appear in the large-barrier limit. Resonant tunneling is also possible in that case, but the interpretation of this effect is different than in the spinless case and is based on the Kondo effect. When the number of electrons on the island is an odd integer, the spin on the island is degenerate. Then, the electron from the island may tunnel out of it, being replaced by an electron which enters from outside and which has opposite spin. In such way the electrons may be transferred through the island at no energy cost. The resulting current is non-spin-polarized due to  $SU(2)$  spin symmetry. In contrast to resonances in the spinless case when the charge state on the island is required to be degenerate, in the case with spin is needed a degenerate spin state. For electrons with spin, the aforementioned “charge” resonance mechanism is also possible, but requires more than one parameter to be tuned. Hence, it is difficult to achieve such resonances in practice.

Switching on a magnetic field, the electron spin symmetry is broken. Electrons having different spin projections on the direction of the magnetic field become different particles, having different Fermi momenta and different spin. Assuming the field is not too strong to completely polarize the system, there are four Fermi points instead of two. The resonant tunneling phenomenon occurs for certain momenta of incident particles for a fixed distance between the impurities. In the case with magnetic field, electrons of one spin direction can fulfill the resonance condition, while electrons having the other spin direction need not. This simple observation leads to the appearance of a spin-polarized current in the case of non-interacting electrons at low temperatures under a small voltage bias at the ends of the system.

In literature little attention has been devoted to the question of transport in Luttinger liquids in an external magnetic field. Theoretical studies have shown that spin-polarized current may occur due to a strong degree of electron polarization [58], spin-dependent interactions [59], a large Fermi velocity difference of electrons having different spin [60, 61] or due to a magnetic impurity [62]. Spin-orbit interaction in combination with a magnetic field may also enhance the degree of current polarization [63, 64, 65].

In contrast to the previous studies, we take into account neither Fermi velocity asymmetry nor strong electron polarization. Rather, our study is based on the phenomenon of resonant tunneling. By tuning a single parameter, that changes the Fermi wavevector, we can reach a point where the resonance condition is achieved for only one spin direction in the interacting case.

---

Electrons having other spin direction are strongly reflected by the barriers, like in the single impurity case, giving a spin-polarized current. Pictorially, two strong impurities may serve as a spin filter for electrons traversing the wire.

This chapter is organized as follows. In section 3.2 we introduce a model of interacting electrons in one dimension in an external magnetic field with two impurities. In section 3.3 we present the theory for resonant tunneling of spinless electrons [20, 66], that is needed later for the analysis of the case with magnetic field. We analyze our model (for weak magnetic fields) in the limit of weak impurities in section 3.4 and in the limit of strong impurities in section 3.5. From these two limiting cases we infer the renormalization flow and possible new fixed points. In section 3.6 we consider transport properties of the system. Section 3.7 contains conclusions. Some technical details are postponed to the appendices.

## 3.2 Model

We consider electrons in a one-dimensional quantum wire along the  $x$  axis at zero temperature. The effect of temperature is briefly discussed in section 3.6. An external magnetic field is applied to the wire. Since electrons are confined in transverse directions to the wire, the orbital effect is suppressed and the magnetic field only polarizes electrons. Hence, the direction of the magnetic field relative to the wire is unimportant for our study. In the non-interacting case the magnetic field splits electrons in momentum space. At the Fermi energy  $E_F$  the momentum splitting is  $|k_{F\uparrow} - k_{F\downarrow}| \approx \Delta/(\hbar v_F)$  for  $\Delta \ll E_F$ , where  $k_{Fs}$ ,  $v_F$  and  $\Delta$  are the Fermi momenta of spin- $s$  electrons ( $s = \uparrow, \downarrow$ ), the Fermi velocity and the Zeeman energy, respectively. The Hamiltonian of an electronic system that have split momenta by a magnetic field, in the external potential impurity potential  $V(x)$  can be described by the Tomonaga–Luttinger model

$$H = \sum_s \int dx \left\{ -i\hbar v_F \left[ \psi_{Rs}^\dagger(x) \partial_x \psi_{Rs}(x) - \psi_{Ls}^\dagger(x) \partial_x \psi_{Ls}(x) \right] + V(x) \rho_s(x) \right\} + \frac{1}{2} \sum_{s,s'} \int dx dx' W(x-x') \psi_s^\dagger(x) \psi_{s'}^\dagger(x') \psi_{s'}(x') \psi_s(x), \quad (3.1)$$

where  $\psi_{Rs}(x)$ ,  $\psi_{Ls}(x)$  are the annihilation operators for right- and left-moving spin- $s$  electrons,  $\psi_s = \psi_{Rs} + \psi_{Ls}$  is the annihilation operator for spin- $s$  electrons,  $\rho_s = \psi_s^\dagger \psi_s$  is the electron density of spin- $s$  electrons, and  $W(x-x')$  is the screened Coulomb interaction between electrons.

---

We first consider the system without impurities,  $V(x) = 0$ . Then, the model (3.1) describes an interacting quantum wire with four Fermi points. In that case the interaction terms split into inter-subband and intra-subband interaction terms [67]. While intra-subband terms describe interaction in subsystems consisting of interacting electrons of spin up and spin down, inter-subband terms couple these two subsystems. For spin independent interaction, the electrons stay in their bands during scattering processes (interaction), and the only allowed low-energy processes are forward and backward inter-subband scattering, see appendix 3.A.

In the following we consider only weak magnetic fields,  $\Delta \ll E_F$  when the momentum splitting of the electrons is small. In other cases things are more complicated and one should use more elaborate approaches, like one used in Ref. [58]. While mutually non-interacting subsystems consisting of spin up and spin down electrons in the bosonized representation are described by the standard Luttinger liquid Hamiltonian (see Eq. 3.38) in terms of bosonic fields  $\varphi_\uparrow, \varphi_\downarrow$  with the Luttinger parameter

$$K = \left( 1 + \frac{\widetilde{W}(0) - \widetilde{W}(2k_F)}{\pi \hbar v_F} \right)^{-1/2}, \quad (3.2)$$

the inter-subband interaction is diagonalized in symmetric  $\varphi_\rho = (\varphi_\uparrow + \varphi_\downarrow)/\sqrt{2}$  and antisymmetric  $\varphi_\sigma = (\varphi_\uparrow - \varphi_\downarrow)/\sqrt{2}$  combinations of these fields. The action of the system without impurities then reads

$$\frac{S_0}{\hbar} = \sum_{\ell=\rho,\sigma} \frac{1}{2\pi K_\ell} \int dx d\tau \left[ \frac{1}{v_\ell} (\partial_\tau \varphi_\ell)^2 + v_\ell (\partial_x \varphi_\ell)^2 \right], \quad (3.3)$$

where

$$K_\ell = K \left( 1 \pm \frac{K^2 \widetilde{W}(0)}{\pi \hbar v_F} \right)^{-1/2}, \quad (3.4)$$

with the convention that the upper(lower) sign corresponds to  $\ell = \rho(\sigma)$ . The velocities of excitations are  $v_\ell = v_F/K_\ell$ . A detailed derivation is given in appendix 3.A. We have obtained that interacting electrons in a weak magnetic field are described by the Luttinger liquid action (3.3) with spin and charge degrees of freedom separated.

Non-trivial effects come from impurities. We consider two point-like impurities, modeled as  $\delta$ -functions of equal strength  $V$ , placed at  $\pm a/2$ . Introducing the displacement fields at the impurity positions  $\phi_{1s}(\tau) = \varphi_s(-a/2, \tau)$

and  $\phi_{2s}(\tau) = \varphi_s(a/2, \tau)$ , the bosonized form of the electron–impurity interaction reads

$$\frac{S_1}{\hbar} = \sum_s \frac{V}{\hbar\pi\alpha_s} \int d\tau [\cos(2\phi_{1s} + k_{F_s}a) + \cos(2\phi_{2s} - k_{F_s}a)], \quad (3.5)$$

where  $\alpha_s$  is the short distance cutoff. Some details about the previous formula are given in appendix 3.B.

To proceed further in analyzing the full action  $S_0 + S_1$  it is useful to integrate out all degrees of freedom outside the impurities. In that way one gets an action in terms of four fields fluctuating in imaginary time. For low frequencies,  $|\omega| \ll v_\ell/a$ , the effective action can be written in the form

$$\frac{S_{\text{eff}}}{\hbar} = \sum_\ell \int \frac{d\omega}{2\pi} \frac{|\omega|}{\pi K_\ell} \left( |\phi_{\ell+}(\omega)|^2 + \frac{1}{4} |\phi_{\ell-}(\omega)|^2 \right) + \frac{1}{\hbar} \int d\tau V_{\text{eff}}, \quad (3.6)$$

where the effective potential energy  $V_{\text{eff}}$  reads

$$V_{\text{eff}}(\phi_{1\uparrow}, \phi_{2\uparrow}, \phi_{1\downarrow}, \phi_{2\downarrow}) = \sum_\ell U_\ell \phi_{\ell-}^2(\tau) + \sum_s V_s [\cos(2\phi_{1s} + k_{F_s}a) + \cos(2\phi_{2s} - k_{F_s}a)]. \quad (3.7)$$

We have introduced  $U_\ell = \frac{\hbar v_\ell}{2\pi a K_\ell}$ ,  $V_s = \frac{V}{\pi\alpha_s}$  and the fields

$$\phi_{\ell+} = \frac{1}{2\sqrt{2}}(\phi_{1\uparrow} + \phi_{2\uparrow} \pm (\phi_{1\downarrow} + \phi_{2\downarrow})), \quad (3.8)$$

$$\phi_{\ell-} = \frac{1}{\sqrt{2}}(\phi_{2\uparrow} - \phi_{1\uparrow} \pm (\phi_{2\downarrow} - \phi_{1\downarrow})). \quad (3.9)$$

The effective potential energy (3.7) consists of two types of terms: the charging energy

$$E_C = \sum_\ell U_\ell \phi_{\ell-}^2 \quad (3.10)$$

suppresses fluctuations of the charge on the island between the impurities, while the cosine terms tend to fix the displacement fields at the impurity positions. The part of the action (3.6) with  $|\omega||\phi_{\ell-}|^2$  should be understood as a fluctuating correction to  $E_C$  and is important at resonance points for strong impurities, when  $\phi_{\ell-}$  are undetermined.

Without inter-subband interaction the two subsystems of electrons, each having one spin direction and Fermi momentum, do not mutually interact

and each of them is analogous to the spinless case [20]. For the spinless case we know that resonant tunneling, and hence perfect transmission, occurs only at special values of the product  $k_{Fs}a$ , which means this condition may be satisfied just for one subsystem, meaning the spin-polarized current occurs. The inter-subband interaction is a new interaction in our system that distinguishes it from the spinless situation and that may spoil spin-selective transparency. We will show that this is not the case.

In the following we will examine the system described by Eq. (3.6) in two limiting cases, for strong and weak impurity strengths. For the realistic case of repulsive interaction we have  $K_\rho < 1$ ,  $K_\sigma > 1$  and  $U_\sigma < U_\rho$ . Our steps will be to first determine the ground state without fluctuations from  $V_{\text{eff}}$ , see Eq. (3.6), and then to include fluctuations to check for the stability of that ground state. Before doing that, in the next section we consider the spinless case for completeness.

### 3.3 Resonant tunneling of spinless electrons

In this section we will present the theory of Kane and Fisher [20, 66] for resonant tunneling of spinless electrons in the case of two single impurities having the strength  $V$ . This is also a limiting case of our model (3.1) for strong magnetic fields which polarizes the system and leaves only a band with electrons of one spin direction. Similarly to Eq. (3.6), the effective action in terms of the fluctuating fields at the impurity positions  $\phi_1(\tau) = \varphi(-a/2, \tau)$  and  $\phi_2(\tau) = \varphi(a/2, \tau)$  can be derived and reads

$$\frac{S_{\text{eff}}^{(1)}}{\hbar} = \int \frac{d\omega}{2\pi} \frac{|\omega|}{\pi K} \left( |\phi_+(\omega)|^2 + \frac{1}{4} |\phi_-(\omega)|^2 \right) + \frac{1}{\hbar} \int d\tau V_{\text{eff}}^{(1)}, \quad (3.11)$$

where the effective potential energy  $V_{\text{eff}}^{(1)}$  reads

$$V_{\text{eff}}^{(1)}(\phi_+, \phi_-) = U\phi_-(\tau)^2 + \frac{2V}{\pi\alpha} \cos(2\phi_+(\tau)) \cos(\phi_-(\tau) - k_F a). \quad (3.12)$$

By  $\alpha$  we have denoted the short distance cutoff and  $U = \frac{\hbar\omega_F}{2\pi a K^2}$ . We have also introduced the fields

$$\phi_+ = \frac{1}{2}(\phi_1 + \phi_2), \quad (3.13)$$

$$\phi_- = \phi_2 - \phi_1, \quad (3.14)$$

and they measure the charge transferred across the two impurities and the charge on the island in between, respectively. We analyze the model (3.11) for weak and strong impurity strengths.

---

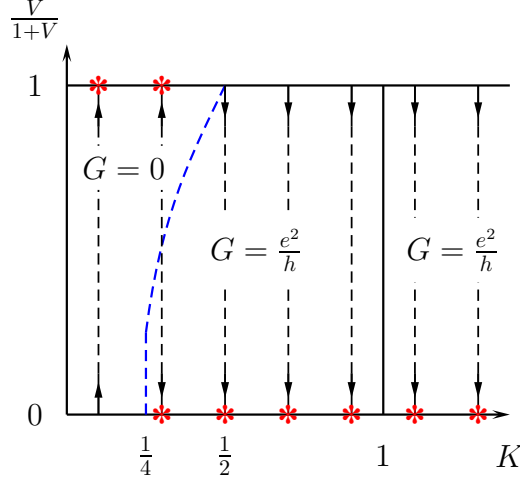


**Figure 3.1:** The renormalization group flow diagram for the impurity strength  $V$  as a function of the interaction  $K$  when the resonant condition  $\cos(k_F a) = 0$  is fulfilled [20]. For  $K > 1/2$  two equal point impurities are transparent, leading to the perfect conductance  $G = e^2/h$ .

In the weak impurity limit  $V/\alpha \ll U$ , the action (3.11) is minimized for  $\phi_1 = \phi_2$ , i.e. for  $\phi_- = 0$ . There the charging energy suppresses the change of the charge on the island. In that case of one can integrate out the (frozen) degrees of freedom  $\phi_-$  from the partition function in a cumulant expansion in powers of  $V/(\alpha U)$ . For the new scattering potential we get

$$V_{\text{eff}}^{(1)'} = \frac{2V}{\pi\alpha} \cos(k_F a) \cos(2\phi_+) + \frac{1}{2U} \left( \frac{V}{\pi\alpha} \right)^2 \sin(k_F a)^2 \cos(4\phi_+). \quad (3.15)$$

The resonant scattering occurs when the first term of the previous equation vanishes,  $\cos(k_F a) = 0$ . Then the most important term is the second one, and it is relevant in the renormalization group sense for  $K < 1/4$ . This leads to the interval of repulsive interactions  $1/4 < K < 1$  when the weak double impurity structure is transparent for electrons, oppositely to the single impurity case where any repulsion leads to the strong relevancy of a single impurity and insulating behavior.

In the strong impurity limit  $V/\alpha \gg U, E_F$ , the effective potential energy (3.12) can be minimized by minimizing the cosine terms first and then the charging energy. The former are minimal for

$$2\phi_p = \mp k_F a + \pi(1 + 2n_p), \quad (p = 1, 2) \quad (3.16)$$

where  $n_p$  are integers. Then, we get

$$V_{\text{eff}}^{(1)} = U\pi^2 \left( n + \frac{k_F a}{\pi} \right)^2 - \frac{2V}{\pi\alpha}, \quad (3.17)$$

where  $n = n_2 - n_1$  is an integer. Eq. (3.17) has a degenerate solution for  $n$  when  $\cos(k_F a) = 0$ . A physical interpretation for  $-n$  is that it corresponds to the number of electrons on the island. This means that the Coulomb blockade in that case does not play a role and does not penalize the change of charge on the island inside the interval  $[k_F a/\pi - 1/2, k_F a/\pi + 1/2]$ . In that case the analysis of the model (3.11) can be done in terms of small tunneling matrix elements  $t$  which describe hopping of electrons from outside to the island and vice versa. The island is described as a two-level system with two states, corresponding to the two possibilities for the number of electrons on the island. For small  $t$  the renormalization group equation obtained from the Coulomb gas representation reads

$$\frac{dt}{dl} = t \left( 1 - \frac{1}{2K} \right), \quad (3.18)$$

meaning for  $K > 1/2$  fluctuations tend to increase the value of  $t$ . Since the two impurities are local quantities, they are not expected to renormalize the interaction parameter  $K$  and since the conditions for the resonant tunneling in the weak and strong impurity case are identical, [20, 66] have concluded that the resonant tunneling occurs in the region of repulsive interactions, see Fig. 3.1. Then the system has the perfect conductance  $G = e^2/h$ . Here we should also mention that in the case of attractive interaction between electrons,  $K > 1$ , both a single impurity and two impurities are irrelevant perturbation and the system always has the perfect conductance.

### 3.4 Weak impurities

Now we are back to the original problem. In the limit of weak impurities,  $V_{\uparrow}, V_{\downarrow} \ll U_{\rho}, U_{\sigma}$ , the action (3.6) is minimized for  $\phi_{1s} = \phi_{2s}$ . Then the charging energy (3.10) is minimal,  $E_C = 0$ . A fixed phase at both impurities means no change of charge on the island, and hence the two barriers act as a single one. Integrating out these massive fluctuations contained in the fields  $\phi_{2s} - \phi_{1s}$  from the action (3.6), new scattering processes are generated. Apart from the one-electron backscattering terms present in Eq. (3.7), a newly generated scattering potential contains two-electron processes. For a repulsive interaction the only relevant such process is when two electrons of

---

different spins get simultaneously backscattered from the impurities. For the new scattering potential we obtain

$$V'_{\text{eff}} = \sum_s 2V_s \cos(k_{F_s}a) \cos(\phi_{1s} + \phi_{2s}) + V^{(2)} \sin(k_{F\uparrow}a) \sin(k_{F\downarrow}a) \cos(\phi_{1\uparrow} + \phi_{2\uparrow} + \phi_{1\downarrow} + \phi_{2\downarrow}), \quad (3.19)$$

where

$$V^{(2)} = V_{\uparrow}V_{\downarrow} \frac{U_{\sigma} - U_{\rho}}{2U_{\rho}U_{\sigma}}. \quad (3.20)$$

For a generic situation  $\cos(k_{F_s}a) \neq 0$ , the single electron backscattering processes, the first terms in Eq. (3.19), are the most important. To leading order in the impurity potential, the renormalization group flow equations is

$$\frac{dV_s}{dl} = V_s \left( 1 - \frac{K_{\rho} + K_{\sigma}}{2} \right), \quad (3.21)$$

from which we conclude that backward scattering terms  $V_s$  are relevant for  $K_{\rho} + K_{\sigma} < 2$ . Then the impurities tend to suppress the motion of electrons of both spins through them. The flow of  $V_{\downarrow}$  is shown in Fig. 3.3a in the region of small  $V_{\downarrow}$  values.

On the other hand, when  $\cos(k_{F\downarrow}a) = 0$  and  $\cos(k_{F\uparrow}a) \neq \{0, 1\}$ , the two-particle processes should be taken into account (only for spin- $\downarrow$  electrons since spin- $\uparrow$  already have backscattering as a leading term). From the renormalization group flow equation

$$\frac{dV^{(2)}}{dl} = V^{(2)}(1 - 2K_{\rho}), \quad (3.22)$$

we conclude that spin- $\downarrow$  electrons are effectively free at low energies for  $K_{\rho} > 1/2$ . This means that for not too strong repulsive interactions spin- $\downarrow$  electrons effectively do not scatter, while spin- $\uparrow$  electrons scatter off the impurities. This means that an asymmetry of the double barrier transparency is present at special points in the parameter space. The flow of  $V_{\downarrow}$  is shown in Fig. 3.3b in the region of small  $V_{\downarrow}$  values.

For other rather special cases, when  $|\cos(k_{F_s}a)|$  vanishes for  $s = \uparrow$  ( $s = \downarrow$ ) and reaches one for  $s = \downarrow$  ( $s = \uparrow$ ), one should take three-electron backscattering processes. We do not consider such a possibility here, since it requires tuning of two parameters and is of lesser importance.

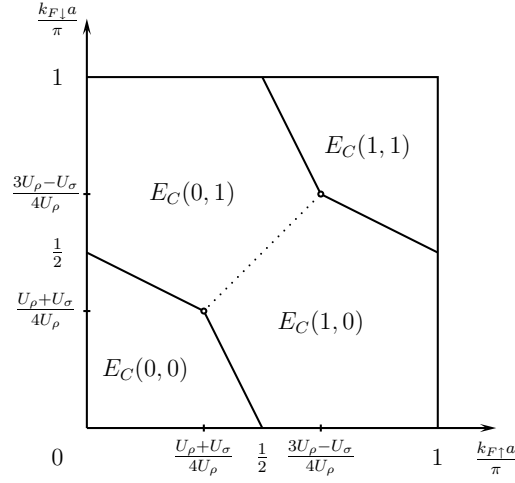


**Figure 3.2:** The ground state energy configurations of the charging energy  $E_C(n_\uparrow, n_\downarrow)$  in the limit of strong impurities, Eq. (3.24), for repulsive interaction  $U_\sigma < U_\rho$ . Points at boundaries between different ground state configurations correspond to the resonance points, special points where the ground state degeneracy is present. The boundaries drawn as solid lines describe resonances for either up or down spins, while the dotted line is a resonance for a spin exchange process at the island. The latter is the Kondo resonance and does not lead to the spin-polarized transport in our system.

### 3.5 Strong impurities

In the limit of very strong impurities,  $V_\uparrow, V_\downarrow \gg U_\rho, U_\sigma, E_F$ , the ground state of the system can be determined by subsequent minimization of the cosines and the charging energy, see Eqs. (3.7) and (3.10). The cosine terms are minimal for

$$2\phi_{ps} = \mp k_{Fs}a + \pi(1 + 2n_{ps}), \quad (p = 1, 2) \quad (3.23)$$

where  $n_{ps}$  are integers. Obviously, the ground state just with the cosine terms is highly degenerate. This degeneracy is broken by the charging energy. Plugging  $\phi_{ps}$  into  $E_C$  and defining  $n_s = n_{1s} - n_{2s}$  one gets

$$E_C(n_\uparrow, n_\downarrow) = \frac{\pi^2}{2}U_\rho \left( \frac{k_{F\uparrow}a}{\pi} + \frac{k_{F\downarrow}a}{\pi} - n_\uparrow - n_\downarrow \right)^2 + \frac{\pi^2}{2}U_\sigma \left( \frac{k_{F\uparrow}a}{\pi} - \frac{k_{F\downarrow}a}{\pi} - n_\uparrow + n_\downarrow \right)^2. \quad (3.24)$$

To characterize different nonequivalent minima of Eq. (3.24), it is useful to restrict the Fermi momenta and the impurity distance to satisfy the condition  $0 < k_{F\uparrow}a, k_{F\downarrow}a \leq \pi$ . Then,  $0 \leq n_\uparrow, n_\downarrow \leq 1$ . Allowing other values for  $k_{Fs}a$

just shifts  $n_s$ . A physical meaning of  $n_s$  is given by the fact that the (mean) particle number on the island is  $n_\uparrow + n_\downarrow$ . The ground states obtained after the minimization of the charging energy (3.24) for  $U_\sigma < U_\rho$  are shown in Fig. 3.2. For generic values of  $k_{F_s}a$ , the ground state is uniquely determined and has certain  $n_s$  values. However, at special lines different ground states meet. These lines define the resonance conditions. Boundaries between different ground states drawn as solid lines in Fig. 3.2 are important for our work: while the number of particles on the island with one spin direction fixed, the number of other spins is determined up to  $\pm 1$ . The Coulomb blockade is lifted just for one spin direction. This condition is needed for spin-selective barrier transparency.

We further solve the model along the boundary lines where  $E_C(1, 0) = E_C(1, 1)$ . Similar results hold for the other cases. While the electrostatic energy for changing the charge on the island is degenerate along these boundary lines, there is still a barrier strength which is nonzero and suppressed the electron flow. As we know from the solution of the single impurity problem [19], the barrier strength can be reduced by strong fluctuations (for attractive interaction in that particular case). Along the lines where  $E_C(1, 0) = E_C(1, 1)$  the fields  $\phi_{p\uparrow}$  are locked in deep cosine minima and have fixed  $n_\uparrow$ . Approximating the nonlinear cosine term by a quadratic term for  $\phi_{p\uparrow}$  one can integrate them out from the action (3.6). In the strong impurity limit one gets for the resulting action

$$\begin{aligned} \frac{S_r}{\hbar} = & \int \frac{d\omega}{2\pi} \frac{|\omega|}{2\pi K_{\text{eff}}} \left( |\phi_{1\downarrow}(\omega)|^2 + |\phi_{2\downarrow}(\omega)|^2 \right) \\ & + \frac{1}{\hbar} \int d\tau V_{\text{eff}} \left( -\frac{k_{F\uparrow}a + \pi}{2}, \frac{k_{F\uparrow}a + \pi}{2}, \phi_{1\downarrow}, \phi_{2\downarrow} \right), \end{aligned} \quad (3.25)$$

with

$$K_{\text{eff}} = \frac{2K_\rho K_\sigma}{K_\rho + K_\sigma}. \quad (3.26)$$

The same result could also be obtained by assuming a constant value for  $2\phi_{p\uparrow} = \mp(k_{F\uparrow}a + \pi)$  and eliminating these fields from Eq. (3.6) using the identity  $\int d\omega |\omega| |\phi(\omega)|^2 = \int d\tau d\tau' \frac{(\phi(\tau) - \phi(\tau'))^2}{(\tau - \tau')^2}$ . The action (3.25) describes resonant tunneling of spin- $\downarrow$  electrons in our model and is analogous to the case of spinless electrons [20]. The partition function is dominated by tunneling events connecting degenerate minima of the strong impurity potential. Using the Coulomb gas representation [20, 21, 66] one can produce the renormalization group equations for the tunneling transparency  $t_\downarrow$  of barriers for

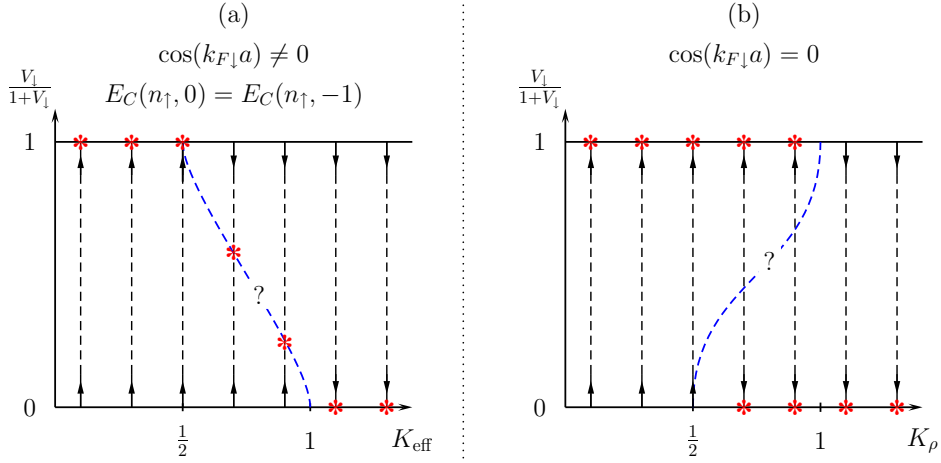


**Figure 3.3:** The renormalization group flow diagram for  $V_{\downarrow}$  as a function of interaction for parameters when the resonance is achieved only for strong impurities (a), and only for weak impurities (b). The middle region  $1/2 < K_{\text{eff}} < 1$  contains a line of fixed points in the case (a). The middle region  $1/2 < K_{\rho} < 1$  contains a phase transition line in the case (b). Precise form of these lines is unknown within our approach. The non-interacting point is achieved for  $K_{\rho} = K_{\sigma} = K_{\text{eff}} = 1$ .

spin- $\downarrow$  electrons. For strong impurity potential  $V_{\downarrow}$  it reads

$$\frac{dt_{\downarrow}}{dl} = t_{\downarrow} \left( 1 - \frac{1}{2K_{\text{eff}}} \right), \quad (3.27)$$

from which we get that for  $K_{\text{eff}} > \frac{1}{2}$  the transparency  $t_{\downarrow}$  is increased, or equivalently, the strength of  $V_{\downarrow}$  is reduced. The point  $K_{\text{eff}} = 1/2$  is inside the region where the interaction is repulsive.

Outside the special point  $2k_{F\downarrow}a = k_{F\uparrow}a = \pi$ , we already obtained in the previous section that an initially weak impurity is a relevant perturbation for any repulsive interaction. Since point impurities are local quantities they can not renormalize bulk quantities such as  $K_{\rho}, K_{\sigma}$ , and the flow of  $V_s$  is vertical [20, 34]. The flow diagram for  $V_{\downarrow}$  is shown in Fig. 3.3a. Since the two limiting cases (weak and strong impurity case) have opposite flows, it is highly plausible to have a line of fixed points somewhere in between. These attractive fixed points denote a new phase, where spins of one direction feel a finite-barrier strength at zero temperature, while electrons having the other spin direction are fully blocked and feel infinite-barrier strength, as we will show now.

We examine the model (3.6) for repulsive interactions in cases when the fields  $\phi_{p\downarrow}$  are freely fluctuating and completely frozen, an assumption which is appropriate close to the non-interacting point and in the strongly repulsive

region, respectively, see Fig. 3.3a. In the former case integrating out  $\phi_{p\downarrow}$  fields one gets an action that exactly matches the action of a single impurity in a Luttinger liquid, with the Luttinger parameter  $(K_\rho + K_\sigma)/2$ . In the latter case one arrives again to the same model, now with the Luttinger parameter  $K_{\text{eff}}$ . In both cases any repulsion ultimately renormalizes  $V_\uparrow$  to infinity, meaning massive fluctuations  $\phi_{p\uparrow}$  are justified, and also that spin- $\uparrow$  electrons are completely blocked.

Outside the resonance lines, see Fig. 3.2, a certain ground state is realized, and it has the  $n_s$  values fixed. There our model translates again into a single impurity problem with the Luttinger parameter  $K_{\text{eff}}$ , and the conclusions are similar to the single impurity case.

In Fig. 3.3b we show the flow of  $V_\downarrow$  for  $\cos(k_{F\downarrow}a) = 0$  and  $|\cos(k_{F\uparrow}a)| \neq 1$ . Again the flows of the two limiting cases are opposite, resulting in a separatrix in between the two resulting phases: perfectly conducting for spin down for small enough  $V_\downarrow$  and insulating for larger  $V_\downarrow$ . Outside the middle region, the flow of  $V_\downarrow$  is as in the single impurity case: toward zero for attractive interaction and toward infinity for very repulsive interactions. While the precise shapes of the separatrix and the line of fixed points can not be inferred from the present approach, it is plausible that they smoothly interpolate between insulating and conducting phases as the interaction strength is changed.

The condition for having strong impurities breaks down as the impurity strength is reduced towards the region where  $V_s \sim U_\ell$ . Then our minimization procedures for  $V_{\text{eff}}$  from sections 3.4 and 3.5 are not justified. We expect that the new line of fixed points is defined by that condition. Notice that  $U_\ell$  is interaction dependent (stronger for stronger repulsion) and that the new line follows this trend.

## 3.6 Transport

In this section we will calculate conductances of our system using the anticipated flow diagram, Fig. 3.3. Assuming the applied voltage to the island is  $V_G$  and to the ends of the wire is  $V_L$ , an additional term should be included in the action (3.6):

$$-\frac{eV_G\sqrt{2}}{\pi\hbar} \int d\tau \phi_{\rho^-} - \frac{eV_L\sqrt{2}}{\pi\hbar} \int d\tau \phi_{\rho^+}. \quad (3.28)$$

The voltage  $V_L$  pushes the electrons to advance in one direction along the wire, while the gate voltage  $V_G$  serves as a single tuning parameter. The above results are still valid, but one should take the shifted Fermi momenta

---

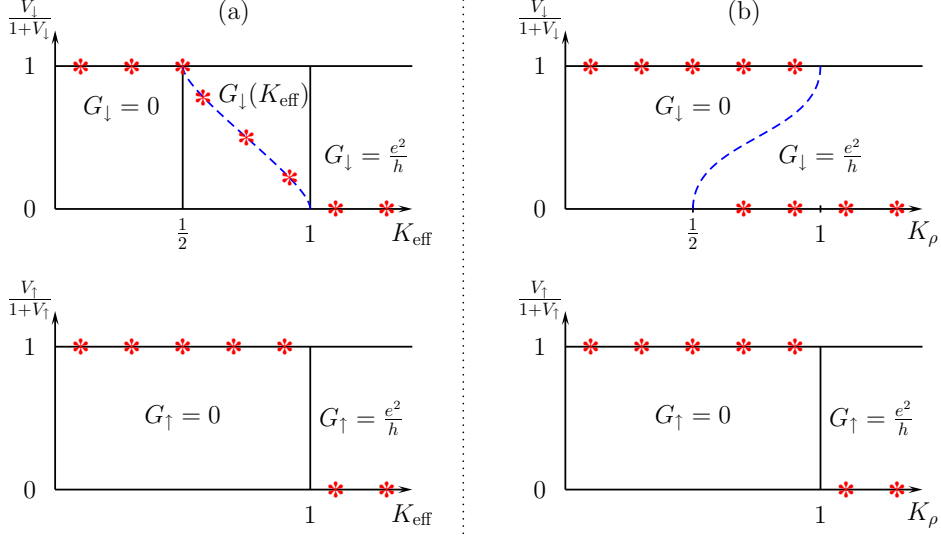


**Figure 3.4:** Zero temperature and low voltage conductances  $G_{\downarrow}$  and  $G_{\uparrow}$  at the resonance that correspond to the case shown in Fig. 3.3a (Fig. 3.3b) are shown on the left (a) (right (b)) side. The non-interacting point is  $K_{\rho} = K_{\text{eff}} = 1$ . By the asterisk symbol we denote the fixed point values of parameters. The spin-polarized transport occurs in regions where  $G_{\uparrow} \neq G_{\downarrow}$ .

due to nonzero  $V_G$

$$k'_{Fs} = k_{Fs} - \frac{eV_G K_{\rho}^2}{\hbar v_F}. \quad (3.29)$$

This means the resonant condition can be achieved by adjusting  $V_G$  for a fixed magnetic field and fixed distance between impurities.

Without impurities the system is described by Eq. (3.3) and has the perfect non-spin-polarized conductance  $2e^2/h$ , taking into account external leads [38, 39, 40]. The situation may drastically change when impurities are present. In the non-resonant case the conductance is suppressed at low  $V_L$  for repulsive interaction for both spin directions as  $\sim V_L^{2/K_{\text{eff}}-2}$ , similar to the single impurity case, since our model outside resonance translated into it with the Luttinger parameter  $K_{\text{eff}}$ .

On the resonance that corresponds to Fig. 3.3a, i.e. for strong impurities when the charge state for spin- $\downarrow$  electrons is degenerate on the island, one gets spin-polarized conductance. Inside the region where the new line of fixed points appears, different scattering is experienced by two spin orientations. While  $G_{\uparrow}$  is suppressed at low voltages as  $\sim V_L^{2/K_{\text{eff}}-2}$  near the point  $K_{\text{eff}} = 1/2$ , and as  $\sim V_L^{4/(K_{\rho}+K_{\sigma})-2}$  for  $K_{\rho} + K_{\sigma} \rightarrow 2^-$ ,  $G_{\downarrow}$  is not suppressed even at very low voltages. It is controlled by the fixed point which

determines the effective strength of impurity scattering. We can estimate it as  $G_{\downarrow}(K_{\text{eff}}) \sim \frac{e^2}{h} |t_{\downarrow}(K_{\text{eff}})|^2$  where  $t_{\downarrow}(K_{\text{eff}})$  is the tunneling matrix element between neighboring cosine minima which corresponds to the fixed point. Within our approach we are not able to determine its value.

On the resonance that corresponds to weak impurities, Fig. 3.3b, the system again has spin-polarized conductance which is controlled by the fixed points. In the lowest non-trivial order we have  $G_{\downarrow} = e^2/h$  for  $K_{\rho} > 1/2$  and  $G_{\uparrow} \sim V_L^{4/(K_{\rho}+K_{\sigma})-2}$ , for not too big initial values of impurity strengths. Otherwise the spin polarization is destroyed and the conductance behaves as in the non-resonant case. The conductances on the resonances are shown in Fig. 3.4.

So far we considered zero temperatures. At finite temperature the picture will be qualitatively unchanged until the electron thermal energy is much smaller than the charging energy and the Zeeman energy. In the opposite case, which is the high frequency limit  $|\omega| \gg v_{\ell}/a$ , or translated to temperature  $T \gg K_{\ell}U_{\ell}$ , for the starting action one would get Eqs. (3.6) and (3.7) with the replacements  $K_{\ell} \rightarrow K_{\ell}/2, U_{\ell} \rightarrow 0$ . This is exactly the action of a system of one-dimensional electrons with two impurities in series where coherent effects of impurities are missing. Such a system has essentially the same behavior as the single impurity case [20, 21].

## 3.7 Conclusions

In this chapter we have shown that a quantum wire with two impurities in an external magnetic field may have spin-filter properties for repulsive interactions. Our study is based on the resonance tunneling phenomenon which may be tuned by a single parameter, the gate voltage, for only one spin direction. The strength of the magnetic field is not important for our study, it is only required that electrons of different spin have different Fermi momenta. This leaves us with a region of parameters where the spin-polarized current appears at zero temperature. Sufficiently strong thermal effects destroy our picture and the system regains non-spin-polarized current. A qualitative study of low-temperature effects as well as details about the flow diagrams presented in Fig. 3.3 are left for a future study.

## 3.A Bosonization

In this appendix we present some details about the derivation of the bosonized action used in chapter 3. As a special case, our derivation also contains a

---

bosonized form of for the Luttinger liquid action used in chapters 2 and 4. Quite generally, we can write down the Hamiltonian of an interacting electronic system in one dimension in second quantization

$$H_{TL} = -i\hbar v_F \sum_s \int dx \left[ \psi_{Rs}^\dagger(x) \partial_x \psi_{Rs}(x) - \psi_{Ls}^\dagger(x) \partial_x \psi_{Ls}(x) \right] \quad (3.30)$$

$$+ \frac{1}{2} \sum_{s,s'} \int dx dx' W(x-x') \psi_s^\dagger(x) \psi_{s'}^\dagger(x') \psi_{s'}(x') \psi_s(x),$$

where the index  $s$  can take two values  $\uparrow$  and  $\downarrow$  for two spin projections,  $\psi_{Rs}(x), \psi_{Ls}(x)$  are the annihilation operators for right- and left-moving spin- $s$  electrons, and  $\psi_s = \psi_{Rs} + \psi_{Ls}$  is the annihilation operator for spin- $s$  electrons. This Hamiltonian takes into account linear dispersion of free electrons from the very beginning. For free electrons this is true only in the vicinity of the Fermi points. However, we are interested in deriving an effective Hamiltonian which properly captures low energy excitations, and this issue is unimportant for the rest of our derivation.

The low energy excitations occur in the vicinity of the Fermi points. Then the single particle field operator can be expressed as [8]

$$\begin{aligned} \psi_s(x) &= \psi_{Rs}(x) + \psi_{Ls}(x) \\ &= e^{ik_{Fs}x} R_s(x) + e^{-ik_{Fs}x} L_s(x), \end{aligned} \quad (3.31)$$

where the fields  $R_s(x), L_s(x)$  are slowly varying on the scale  $k_{Fs}^{-1}$ . In the bosonized representation they can be expressed in terms of bosonic displacement  $\varphi_s(x)$  and phase  $\theta_s(x)$  fields as

$$R_s(x) = \frac{\eta_s}{\sqrt{2\pi\alpha_s}} e^{i(\theta_s(x) - \varphi_s(x))}, \quad (3.32)$$

$$L_s(x) = \frac{\eta_s}{\sqrt{2\pi\alpha_s}} e^{i(\theta_s(x) + \varphi_s(x))}, \quad (3.33)$$

where  $\alpha_s$  is the short distance cutoff which is of the order of  $k_{Fs}^{-1}$ , and  $\eta_s$  are the Klein factors, introduced to insure proper anticommutation relations between the original fermionic operators. They anticommute  $\{\eta_s, \eta_{s'}\} = 2\delta_{s,s'}$  and satisfy  $\eta_s^\dagger = \eta_s$ . The bosonic fields satisfy the following commutation relation

$$[\varphi_s(x), \theta_{s'}(x')] = \frac{i\pi}{2} \text{sign}(x-x') \delta_{s,s'}. \quad (3.34)$$

The fermionic densities for right and left moving electrons are

$$R_s^\dagger(x) R_s(x) = -\frac{1}{2\pi} \partial_x (\varphi_s(x) - \theta_s(x)), \quad (3.35)$$

$$L_s^\dagger(x) L_s(x) = -\frac{1}{2\pi} \partial_x (\varphi_s(x) + \theta_s(x)). \quad (3.36)$$

The total electron density  $\rho_s(x) = \psi_s^\dagger(x)\psi_s(x)$  can now be written as a sum of the long-wavelength part  $\rho_s^{(0)}$  and the oscillating part  $\rho_s^{(2k_{F_s})}$ :

$$\begin{aligned}\rho_s(x) &= \rho_s^{(0)}(x) + \rho_s^{(2k_{F_s})}(x) \\ &= -\frac{1}{\pi}\partial_x\varphi_s(x) + \frac{1}{\pi\alpha_s}\cos(2\varphi_s(x) - 2k_{F_s}x).\end{aligned}\quad (3.37)$$

Notice that Eq. (3.37) does not contain a constant part,  $k_{F_s}/\pi$ , that is the part of the density coming from the filled Fermi sea.

Using the bosonic variables, the kinetic part ( $W(x) = 0$ ) of the Hamiltonian (3.30) becomes

$$H_{\text{kin}} = \sum_s \frac{\hbar v_s}{2\pi} \int dx \left[ \frac{1}{K_s}(\partial_x\varphi_s)^2 + K_s(\partial_x\theta_s)^2 \right], \quad (3.38)$$

where the dimensionless Luttinger parameter  $K_s = 1$  has been introduced, and  $v_s$  is the velocity of excitations, satisfying  $v_s = v_F/K_s$ .

Up to an additive constant, the interaction energy between electrons can be rewritten as

$$\begin{aligned}H_{\text{int}} &= \frac{1}{2} \sum_{s,s'} \int dx dx' \left( \underbrace{\psi_{R_s}^\dagger \psi_{R_s} + \psi_{L_s}^\dagger \psi_{L_s}}_{q \approx 0} + \underbrace{\psi_{R_s}^\dagger \psi_{L_s} + \psi_{L_s}^\dagger \psi_{R_s}}_{|q| \approx 2k_{F_s}} \right)_x \\ &\quad \times \left( \underbrace{\psi_{R_{s'}}^\dagger \psi_{R_{s'}} + \psi_{L_{s'}}^\dagger \psi_{L_{s'}}}_{q \approx 0} + \underbrace{\psi_{R_{s'}}^\dagger \psi_{L_{s'}} + \psi_{L_{s'}}^\dagger \psi_{R_{s'}}}_{|q| \approx 2k_{F_{s'}}} \right)_{x'} W(x - x'),\end{aligned}\quad (3.39)$$

where by  $q$  we have denoted the momentum transfer of a scattering process. The low energy part of the interaction energy (3.39) is encoded in scattering processes which have small overall momentum transfer. They occur when either one has terms  $q \approx 0$  simultaneously at  $x$  and  $x'$ , or  $q \approx 2k_{F_s}$  at  $x$  and  $q \approx -2k_{F_{s'}}$  at  $x'$ , or  $q \approx -2k_{F_s}$  at  $x$  and  $q \approx 2k_{F_{s'}}$  at  $x'$ .

We can distinguish forward and backward scattering parts of the interaction,  $H_{\text{int}} = H_{\text{int}}^f + H_{\text{int}}^b$ . The former one, using the bosonic representation for the fermionic operators, Eqs. (3.31)-(3.33), reads

$$\begin{aligned}H_{\text{int}}^f &= \frac{1}{2} \sum_{s,s'} \int dx dx' W(x - x') \rho_s^{(0)}(x) \rho_{s'}^{(0)}(x') \\ &= \frac{\widetilde{W}(0)}{2\pi^2} \sum_{s,s'} \int dx (\partial_x\varphi_s)(\partial_x\varphi_{s'}) + \dots,\end{aligned}\quad (3.40)$$

where we have expanded in the last line the density  $\rho_s^{(0)}(x')$  around  $x$  using the fact that  $W(x - x')$  is the short-ranged interaction and that fields  $\varphi_s$  are

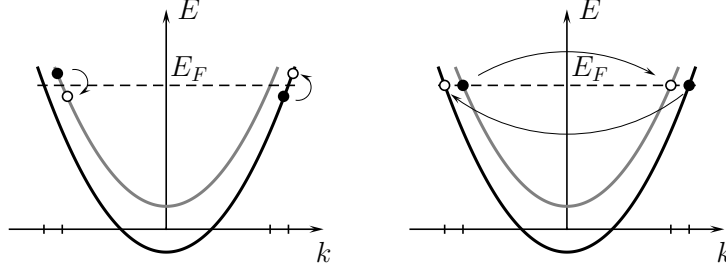


**Figure 3.5:** Inter-subband scattering processes: left is shown forward scattering and right backward scattering.  $E_F$  denotes the Fermi energy.

slowly varying on scales where  $W(x-x')$  appreciably decays. The condition that  $\varphi_s$  is slowly varying on scales  $k_{Fs}^{-1}$  gives us a condition that  $W(x-x')$  should have a range  $\sim k_{Fs}^{-1}$ . By  $\widetilde{W}$  we have denoted a Fourier transform.

For the situation that we consider, where electrons of different spins have different Fermi momenta, the forward scattering part of the interaction, (3.40), consists of two different scattering processes: between electrons of equal spins  $s = s'$  and between electrons of different spin  $s \neq s'$ . These processes are called intra-subband and inter-subband scattering processes, respectively [67]. The inter-subband scattering processes are shown in Fig. (3.5).

Using the bosonic representation of fermionic operators, Eqs. (3.31)-(3.33), the backward interaction can be cast in the form

$$H_{\text{int}}^b = \frac{1}{8\pi^2 \alpha_{\uparrow} \alpha_{\downarrow}} \sum_{s,s'} \int dx dx' W(x') \left( e^{i2x(k_{Fs'} - k_{Fs})} e^{-ix'(k_{Fs} + k_{Fs'})} \right. \quad (3.41)$$

$$\left. e^{i2(\varphi_s(x+x'/2) - \varphi_{s'}(x-x'/2))} + h.c. \right).$$

For the intra-subband part  $s = s'$ , we should expand the fields. To do this safely, the fields should be normal-ordered [8]. Using the formula

$$\cos(\varphi_s) = \langle \cos(\varphi_s) \rangle : \cos(\varphi_s) :, \quad (3.42)$$

where  $\langle \dots \rangle$  is an average over the Hamiltonian (3.38),  $: \dots :$  denotes normal ordering, and the expression

$$\langle (\varphi_s(x) - \varphi_s(x'))^2 \rangle = \ln \frac{|x - x'|}{\alpha_s}, \quad (3.43)$$

for the intra-subband part of interaction we get

$$H_{\text{int}}^{b,\text{intra}} = -\frac{\widetilde{W}(2k_{Fs})}{2\pi^2} \sum_s \int dx (\partial_x \varphi_s)^2. \quad (3.44)$$

For the inter-subband part  $s \neq s'$  we get

$$H_{\text{int}}^{b,\text{inter}} = \frac{\widetilde{W}(k_{F\uparrow} + k_{F\downarrow})}{2\pi^2\alpha_{\uparrow}\alpha_{\downarrow}} \int dx \cos [2\varphi_{\uparrow}(x) - 2\varphi_{\downarrow}(x) + 2(k_{F\downarrow} - k_{F\uparrow})x]. \quad (3.45)$$

The total interaction is given as a sum  $H_{\text{int}} = H_{\text{int}}^f + H_{\text{int}}^{b,\text{intra}} + H_{\text{int}}^{b,\text{inter}}$ .

Including only intra-subband interaction in the kinetic energy, for the low energy effective Hamiltonian we get Eq. (3.38) with

$$K_s = \left( 1 + \frac{\widetilde{W}(0) - \widetilde{W}(2k_{Fs})}{\pi\hbar v_F} \right)^{-1/2}. \quad (3.46)$$

For repulsive interaction we have  $K_s < 1$ . Had we considered spinless electrons from the very beginning, for the low energy Hamiltonian we would have obtained Eq. (3.38) without the sum over  $s$ , with the Luttinger parameter given by (3.46). This is a standard Luttinger liquid Hamiltonian given in terms of bosonic fields [8].

Taking into account inter-subband interaction, under the assumption  $K_{\uparrow} = K_{\downarrow} = K$  that is justified for a small difference between  $k_{F\uparrow}$  and  $k_{F\downarrow}$ , we get

$$H_0 = \sum_{\ell=\rho,\sigma} \frac{\hbar v_{\ell}}{2\pi} \int dx \left[ \frac{1}{K_{\ell}} (\partial_x \varphi_{\ell})^2 + K_{\ell} (\partial_x \theta_{\ell})^2 \right], \quad (3.47)$$

with

$$K_{\ell} = K \left( 1 \pm \frac{K^2 \widetilde{W}(0)}{\pi\hbar v_F} \right)^{-1/2}, \quad (3.48)$$

$$\varphi_{\rho} = \frac{1}{\sqrt{2}} (\varphi_{\uparrow} + \varphi_{\downarrow}), \quad (3.49)$$

$$\varphi_{\sigma} = \frac{1}{\sqrt{2}} (\varphi_{\uparrow} - \varphi_{\downarrow}), \quad (3.50)$$

and similarly for  $\theta_{\rho}, \theta_{\sigma}$ . The inter-subband backward interaction  $H_{\text{int}}^{b,\text{inter}}$  is an irrelevant operator for any repulsive interaction (and also because it contains under the cosine an oscillating term that makes this term also irrelevant) and is neglected in Eq. (3.47). Therefore, the effective low-energy Hamiltonian of a quantum wire is a sum of two free Luttinger liquid Hamiltonians, for spin and for charge degrees of freedom, Eq. (3.47). The corresponding imaginary-time action used in the main text is given by formula (3.3).

---

## 3.B Bosonized model

In this appendix we will derive the full form of the Hamiltonian (3.1) in the bosonized representation, showing that the effect of the forward scattering part  $\rho_s^{(0)}$  of the electron density that couples to the impurity potential  $V(x)$  is to renormalize the Fermi wavevector. The starting Hamiltonian (3.1) is a sum

$$H = H_0 + H_V, \quad (3.51)$$

where the part without impurity potential is given by Eq. (3.47), and the impurity part is

$$H_V = \sum_s \int dx V(x) \rho_s(x). \quad (3.52)$$

Using Eq. (3.37), it can be rewritten in the bosonized form as

$$\begin{aligned} H_V &= H_V^{(0)} + H_V^{(2k_F)} \\ &= -\frac{\sqrt{2}}{\pi} \int dx V(x) \partial_x \varphi_\rho(x) + \sum_s \int dx \frac{V(x)}{\pi \alpha_s} \cos(2\varphi_s(x) - 2k_{F_s}x). \end{aligned} \quad (3.53)$$

Introducing the new fields

$$\varphi'_s(x) = \varphi_s(x) - \frac{K_\rho}{\hbar v_\rho} \int_0^x dy V(y), \quad (3.54)$$

$$\theta'_s(x) = \theta(x), \quad (3.55)$$

which satisfy the commutation relation (3.34), the first part of Eq. (3.53),  $H_V^{(0)}$ , can be diagonalized by a square completion with the corresponding term from  $H_0$ , and up to an unimportant additive constant we get

$$\begin{aligned} H &= \sum_{\ell=\rho,\sigma} \frac{\hbar v_\ell}{2\pi} \int dx \left[ \frac{1}{K_\ell} (\partial_x \varphi'_\ell)^2 + K_\ell (\partial_x \theta'_\ell)^2 \right] \\ &\quad + \sum_s \int dx \frac{V(x)}{\pi \alpha_s} \cos \left( 2\varphi'_s(x) - 2k_{F_s}x + \frac{2K_\rho}{\hbar v_\rho} \int_0^x dy V(y) \right). \end{aligned} \quad (3.56)$$

Taking the impurity potential to be

$$V(x) = V (\delta(x + a/2) + \delta(x - a/2)), \quad (3.57)$$

we finally obtain

$$\begin{aligned}
H = & \sum_{\ell=\rho,\sigma} \frac{\hbar v_\ell}{2\pi} \int dx \left[ \frac{1}{K_\ell} (\partial_x \varphi'_\ell)^2 + K_\ell (\partial_x \theta'_\ell)^2 \right] \\
& + \sum_s \frac{V}{\pi \alpha_s} \int dx [\cos(2\varphi'_s(-a/2) + k'_{Fs}a) + \cos(2\varphi'_s(a/2) - k'_{Fs}a)],
\end{aligned} \tag{3.58}$$

where

$$k'_{Fs} = k_{Fs} - \frac{VK_\rho}{\hbar v_\rho a}. \tag{3.59}$$

We have proved that the effect of the forward scattering of electrons on two impurities is unimportant taking into account the renormalization of the Fermi wavevector and a new definition of the displacement field. In the main text of chapter 3 we use the notation without primes, keeping in mind that that fields and the wavevector have the meaning derived in this appendix.

We would also like to stress here, that the question of a term in the Hamiltonian which arises from the forward scattering of electrons on a single or double impurity is often neglected in literature, or even not mentioned [19, 20, 21, 68]. Here we have shown that it is justified to neglect it even in the case with magnetic field, when one has a bit more complicated problem with four Fermi points. As a special case, our proof also applies to the case without magnetic field.

# The effect of randomness in one-dimensional fermionic systems

*In this chapter we study the competition between the Mott and the Anderson-insulating state in a one-dimensional disordered fermionic system. The notorious difficulties associated with strong coupling phases are avoided by using a new description in terms of the kink energies (or instanton surface tension) of the electronic displacement pattern. Tracing back both a finite compressibility and a nonzero ac conductivity to vanishing kink energy we exclude the existence of an intermediate Mott-glass phase in systems with short range interaction.*

## 4.1 Introduction

Quantum-mechanical interference effects lead to the localization of non-interacting electrons in even weakly disordered solids in one and two space dimensions [16, 17, 23, 69]. This type of (Anderson) insulator is characterized by both a finite ac conductivity at low frequencies and a finite compressibility [70]. Interaction between electrons reduces the effect of disorder and may lead to metallic behavior in two dimensions [71]. In Mott insulators, on the other hand, insulating behavior results from the blocking of sites by repulsive interaction between electrons [72] and hence is dominated by correlation effects. The Mott-insulating phase is incompressible and has a finite gap in the ac conductivity. A natural question is then: what happens in systems when both disorder and interactions are non-negligible? Is there, depending on the strength of interaction or disorder, a single transition between these two phases, or is the scenario more complex, including more phases? Are there more than just these two types of insulators?

A particularly interesting case to consider these questions is that of elec-

---

trons in one space dimension where both interaction and disorder effects are strong, destroying Fermi liquid behavior [8]. Systems of this type have been considered in a number of studies. Early work by Ma [73] using real-space renormalization group for the disordered one-dimensional Hubbard model suggests a direct transition from the Anderson-insulating to the Mott-insulating phase. This result contrasts with more recent work (see, for example, Refs. [23, 69, 74, 75] and references therein) where a new type of order, different from the Mott-insulating and Anderson-insulating phase, was found. In particular in Refs. [23, 69, 75], the existence of a new Mott-glass phase was postulated which was supposed to be incompressible but had no gap in the optical conductivity. Analytical investigations are hampered by the strong coupling nature of the phases which does not allow a renormalization group study. Alternative approaches, like the variational method used in Refs. [23, 69], are difficult to control when applied to scalar fields as in the present case.

In this chapter we tackle this problem by relating both the compressibility and the ac conductivity to the kink energy of the bosonic displacement field  $\varphi(x)$  describing electrons in one dimension [8]. The approach has some similarities with the treatment of the flat phase of a surface undergoing a roughening transition [76] and may be useful for other strong coupling problems as well. Adding (removing) a charge at a site  $x$  corresponds to the insertion of a  $\delta\varphi(x) = \pm\pi$  kink in the bosonic field. The compressibility of the systems is determined by adding kinks (or antikinks) to the classical ground state of the system. If the kink energy is finite, the system is incompressible. Similarly, the optical conductivity follows from transitions between the ground state and the first excited state which involves kink-antikink pairs. For vanishing kink energy, the level splitting between the ground and the excited state is exponentially small in the kink-antikink distance. A decreasing energy  $\hbar\omega$  will then drive transitions between levels of pairs of ever increasing distance, and hence the ac conductivity remains finite for small  $\omega$ . This is no longer the case when the kink energy is finite: the energy of the kink-antikink pair is the lower bound for the level splitting, and hence the optical conductivity shows a gap of this size. Thus, as long as there is no true long range interaction between charges, incompressibility and a gap in the optical conductivity require each other. Thus, there is no Mott-glass phase for systems with short range interaction only.

This chapter is organized as follows. In section 4.2 we introduce a model of interacting fermions in one dimension in the presence of both disordered and commensurate potentials. In section 4.3 we introduce the rigidities of our system and discuss its ac conductivity. Renormalization group equations and the phase diagram are discussed in section 4.4. We consider the question of

---

the Mott glass phase existence in section 4.5, which is followed by discussions and conclusions.

## 4.2 Model

The electron density  $\rho(x)$  of the electrons is related to their displacement field  $\varphi(x)$  as [8]

$$\rho(x) = \frac{k_F}{\pi} - \frac{1}{\pi} \partial_x \varphi + \frac{k_F}{\pi} \cos(2\varphi - 2k_F x) + \dots, \quad (4.1)$$

where  $k_F$  is the Fermi momentum. For simplicity throughout this chapter we use  $e = \hbar = 1$ . The ground state energy of the system follows from

$$E_0 = - \lim_{T \rightarrow 0} T \ln \int \mathcal{D}\varphi e^{-S[\varphi]}, \quad (4.2)$$

where the action is [8, 23, 69]

$$S = \frac{1}{2\pi K} \int_0^{L\Lambda} dx \int_0^{\lambda_T \Lambda} d\tau \left[ (\partial_\tau \varphi)^2 - (\partial_x \varphi + \mu(x))^2 \right. \\ \left. + (\zeta(x)e^{-i2\varphi} + h.c.) - w \cos(2\varphi) - \frac{2\pi\kappa}{\Lambda^2} F\varphi \right]. \quad (4.3)$$

Here we have introduced dimensionless space and imaginary time coordinates by the transformation  $\Lambda x \rightarrow x$  and  $\Lambda v\tau \rightarrow \tau$  where  $v$  is the plasmon velocity and  $\Lambda$  a large momentum cutoff.  $\lambda_T = v/T$  and  $L$  denote the thermal de Broglie wavelength of the plasmons and the system size, respectively.  $w$  denotes the strength of the umklapp scattering term (or the strength of a commensurate potential),  $F$  the external driving force and  $\kappa$  the compressibility [50, 77].  $\mu(x)$  and  $\zeta(x)$  result from the coupling of the random impurity potential to the long wavelength and the periodic part of electron density (4.1), respectively, with

$$\langle \zeta(x)\zeta^*(x') \rangle = u^2 \delta(x - x'), \quad (4.4)$$

$$\langle \mu(x)\mu(x') \rangle = \sigma \delta(x - x'), \quad (4.5)$$

all other correlators vanish. As a difference with respect to chapters 2 and 3 here we consider a system that contains many weak, densely spaced impurities. In that case the scale of variation of the physical quantities is much larger than the distance between the impurities. This type of disorder is called the Gaussian disorder and there impurities act collectively [8]. This is, for example, seen in the renormalization of the Luttinger parameter and the plasmon velocity, in contrast to the single impurity case.

---

### 4.3 Rigidities and ac conductivity

We begin with a discussion of the rigidities, which are related to the (inverse) compressibility and conductivity of the system. If the rigidities diverge (as in the strong coupling phases), the appropriate description is that in terms of the kink energies  $\Sigma_{x/\tau}$ . We first consider the application of a fixed strain  $\vartheta$  by imposing the boundary conditions  $\varphi(0, \tau) = 0$  and  $\varphi(L, \tau) = \pi\vartheta L\Lambda$ . The boundary condition in the  $\tau$ -direction is assumed to be periodic. For  $\vartheta \ll 1$  and  $L \rightarrow \infty$  the corresponding increase  $\Delta E_0(\vartheta, 0) = E_0(\vartheta, 0) - E_0(0, 0)$  of the ground state energy  $E_0(\vartheta, 0)$  is clearly an even but not necessarily analytic function of  $\vartheta$ . Thus

$$\left. \frac{\Delta E_0(\vartheta, 0)}{L} \right|_{L \rightarrow \infty} \approx \begin{cases} \vartheta^2/(2\kappa), & \Sigma_x = 0, \\ \Sigma_x |\vartheta|, & \kappa = 0. \end{cases} \quad (4.6)$$

The right hand side of this relation has to be understood as follows: if  $\Sigma_x = 0$  then the stiffness  $1/\kappa$  describes the response to the twisted boundary conditions; the change of  $\varphi$  is spread over the whole sample. If however the system becomes incompressible, then the kink energy  $\Sigma_x$  is nonzero; the change of  $\varphi$  from 0 to  $\pi$  occurs in a narrow kink region of width  $\xi$  much smaller than  $L$ . The position of the kink is chosen such that the energy is minimal. A nonzero kink energy resembles the step free energy of a surface below the roughening transition [76]. If we apply instead of the fixed boundary conditions an external stress to the system, then  $\Sigma_x$  is of the order of the critical stress to generate the first kink.

In a similar manner we can apply non-trivial boundary conditions in the  $\tau$ -direction by choosing  $\varphi(x, 0) = 0$  and  $\varphi(x, L_\tau) = \pi j L_\tau / v$ . This corresponds to imposing an external current  $j = \langle \partial_\tau \varphi \rangle / \pi$  at  $x = 0$  and  $x = L$ :

$$\left. \frac{\Delta E_0(0, j)}{L} \right|_{L \rightarrow \infty} \approx \begin{cases} j^2/(2D), & \Sigma_\tau = 0, \\ \Sigma_\tau |j|, & D = 0. \end{cases} \quad (4.7)$$

Here  $D = \kappa v^2$  denotes the charge stiffness and determines the Drude peak of the conductivity  $\sigma(\omega) = D\delta(\omega) + \sigma_{\text{reg}}(\omega)$  [8, 78]. In Lorentz invariant systems we have  $\Sigma_x = v\Sigma_\tau$ .

So far we have assumed that  $\Sigma_x$  is self-averaging if  $L \rightarrow \infty$ . In the same way we may introduce local rigidities by applying twisted boundary conditions over a large but finite interval  $[x, x + L_x\Lambda]$ ,  $\Lambda^{-1} \ll L_x \ll L$ . The result for  $\Sigma_x$  will then depend in general on the size  $L_x$  of the interval, i.e.  $\Sigma_x$  should be replaced by  $\Sigma_x(L_x)$ .

In cases where  $D$  vanishes, the frequency dependent conductivity  $\sigma(\omega)$  may still be nonzero, provided  $\omega$  is finite. For low kink energy  $\Sigma_x$ , spontaneous tunneling processes between metastable states and their instanton

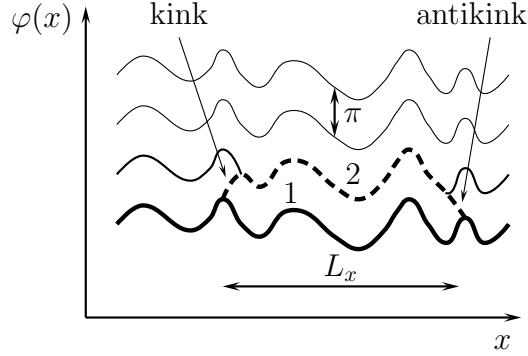


**Figure 4.1:** Kink and antikink in the displacement profile  $\varphi(x)$ . The thin lines represent the minima of the potential energy in the absence of the driving force, the bold line one metastable state and the dashed line the instanton configuration, respectively. Applying a fixed strain to the system only kinks (or antikinks) are enforced in the system.

configurations (configurations 1 and 2 in Fig. 4.1) will occur. Metastable states are here the classical ground states of Eq. (4.3) in the absence of the driving force [50, 77]. Different metastable states follow from each other by a shift of  $\varphi$  by a multiple of  $\pi$ . The instanton configuration connects two neighboring metastable states. Spontaneous tunneling leads to a level splitting of the two states of the order

$$\delta E \approx \sqrt{4\Sigma_x^2(L_x) + C(v\Lambda)^2 e^{-2L_x\Sigma_\tau}}, \quad (4.8)$$

which has to match the energy  $\omega$  of the external field. Here,  $1/\Sigma_\tau \sim K\xi$  plays the role of the tunneling length, while  $C > 0$  is a numerical factor. This mechanism was first considered for non-interacting electrons by Mott [70] and extended to the interacting case in Refs. [79, 80, 81]. Thus, to get a non-zero  $\sigma(\omega)$  for arbitrary low frequency  $\omega$ ,  $2\Sigma_x(L_x) < \omega \rightarrow 0$  which requires  $2\Sigma_x(L_x) \rightarrow 0$  for a finite density of kink positions, which implies a finite compressibility.

## 4.4 Fixed points and phases

We come now to the discussion of the possible phases of model (4.3) by attributing them to their renormalization group fixed points (denoted by superscript \*). Bare values will get a subscript  $_0$ . For small  $u$  and  $w$  the

lowest order renormalization group equations read:

$$\frac{dK}{dl} = -K(au^2 + bw^2), \quad (4.9)$$

$$\frac{d\sigma}{dl} = \sigma(1 - 2bw^2), \quad (4.10)$$

$$\frac{dw}{dl} = w \left( 2 - K - \frac{2}{\pi}\sigma \right), \quad (4.11)$$

$$\frac{du^2}{dl} = u^2(3 - 2K) + \frac{1}{\pi}\sigma w^2, \quad (4.12)$$

$$\frac{d\kappa}{dl} = -b\kappa w^2. \quad (4.13)$$

As far as there is an overlap, the flow equations agree with those found in Refs. [82, 83].  $l$  is the logarithm of the length scale and  $a, b$  are positive non-universal constants of order one that depend on the renormalization procedure. The dynamical critical exponent has been chosen  $z = 1$  corresponding to the Luttinger liquid fixed point.

The Luttinger liquid phase is characterized by  $u_L^* = w_L^* = 0$  and hence  $\Sigma_x = \Sigma_\tau = 0$ .  $K_L^* > 0$  and  $\kappa_L^* = K_L^*/(\pi v_L^*) > 0$ . The fixed point is reached for sufficiently large values of  $K$ . The long time and large scale behavior of the system is that of a clean Luttinger liquid characterized both by a finite compressibility  $\kappa_L^*$  and a finite charge stiffness  $D_L = \kappa_L^* v_L^{*2}$ . The dynamical conductivity is given by  $\sigma_{\text{reg}} = iD_L/(\pi\omega)$ . The presence of the forward scattering term  $\sim \mu(x)\partial_x\varphi$  does not change these results since it can be always removed by the transformation

$$\varphi(x) \rightarrow \varphi(x) + \int_0^x dx' \mu(x'). \quad (4.14)$$

The Mott insulator is characterized by  $K_M^* = \kappa_M^* = u_M^* = \sigma_M^* = 0$  but  $w_M^* \gg 1$ . Clearly the fixed point  $w_M^*$  is outside the applicability range of Eqs. (4.9)-(4.13), but nevertheless some general properties of this phase can be concluded. The system is in the universality class of the two-dimensional classical sine Gordon model which describes, among other things, the Mott insulator to Luttinger liquid transition and the roughening transition of a two-dimensional classical crystalline surface [76]. In the Mott insulating phase  $\kappa$  vanishes. The system is characterized by a finite kink energy  $\Sigma_x \sim (\kappa_0 \xi_M)^{-1}$ , where  $\xi_M$  denotes the correlation length of the Mott-insulating phase [76]. According to Eq. (4.8), the ac conductivity vanishes for  $\omega \lesssim 2\Sigma_x$ .

The Anderson insulator is characterized by  $w_A^* = K_A^* = 0$  but  $u_A^* \gg 1$ .  $\kappa_A^* \approx \kappa_0$  is finite which is the result of the so-called statistical tilt symmetry [84]: the boundary condition  $\varphi(L, y) = \pi\vartheta L$  can be made periodic by the transformation  $\varphi = \tilde{\varphi} + \pi\vartheta x$  and  $\alpha = \tilde{\alpha} - \pi\vartheta x$  with the same statistical properties of  $\tilde{\alpha}$  and  $\alpha$ .  $\alpha$  is defined as  $\zeta = |\zeta|e^{i\alpha}$ . The twist in boundary conditions appears then in the elastic energy  $(2\kappa\pi^2)^{-1}\langle(\partial_x\varphi - \pi\vartheta)^2\rangle$  and hence  $\Sigma_x = 0$ . The transition to the Luttinger liquid phase occurs at  $K \geq 3/2$ .

Next, we look at  $\Sigma_x(L_x)$  at a finite length scale  $\xi_A \ll L_x \ll L$ , such that the parameters are close to their fixed point values.  $\xi_A$  is the correlation length which diverges at the transition to the Luttinger liquid phase. To find the classical ground state of the system under periodic boundary conditions we have first to choose  $2\varphi_i + \alpha_i = 2\pi n_i$  with  $n_i$  integer, and secondly the elastic term has to be minimized with respect to the  $n_i$ . The subscript  $i$  refers to the sites of the lattice with spacing  $\xi_A$  and  $\zeta_i = |\zeta_i|e^{i\alpha_i}$ . The solution is  $n_i = \sum_{j \leq i} [(\alpha_j - \alpha_{j-1})/2\pi]_G$ , see Refs. [50, 77].  $[x]_G$  denotes the closest integer to  $x$ . The ground state is uniquely determined by the  $\alpha_j$  apart from the pairs of sites (of measure zero) at which  $\alpha_j - \alpha_{j-1} = \pm\pi$ . At such pairs the ground state bifurcates since two solutions are possible. For pairs at which  $\alpha_j - \alpha_{j-1} = \pm\pi + \epsilon$ ,  $|\epsilon| \ll 1$  we can go over to an excited state by creating a kink which costs at most the energy  $\Sigma_x \approx \epsilon/(\kappa_0\xi_A)$ . Those ‘‘almost’’ bifurcating sites correspond to states close to the Fermi energy. The smallest  $\epsilon$  found with probability of order one in a sample of length  $L_x$  is of the order  $\xi_A/L_x$  and hence  $\Sigma_x \approx 1/(L_x\kappa_0)$ , i.e. the kink energy vanishes for  $L_x \rightarrow \infty$  and hence the system is compressible. Twisted boundary conditions in the  $\tau$ -direction gives  $\Sigma_\tau \sim (K_0\xi_A)^{-1}$  [50, 77].

As explained already, a vanishing  $\Sigma_x$  is also crucial for the existence of the low frequency conductivity  $\sigma(\omega) \sim \omega^2 \ln^2 \omega$  as has been discussed in detail in Refs. [79, 80, 81]. This result can be understood in terms of tunneling processes between rare positions at which the kink energies  $\Sigma_x$  are much smaller than  $1/(\kappa_0 L_x)$ .

## 4.5 Mott-glass phase

This new hypothetical phase was proposed in Refs. [23, 69] to be characterized by a vanishing compressibility,  $\kappa_G^* = 0$ , but a nonzero optical conductivity at low frequencies. Since the phase is considered to be glassy, both fixed point values are expected to be nonzero,  $w_G^*, u_G^* \gg 1$ . Similarly to the Anderson insulator, the ground state can be found by minimizing first the two backward scattering terms followed by minimization of the elastic energy. Although the ground state solution is now more involved than for

---

the Mott-insulating and Anderson-insulating case, for  $F = 0$  it is clearly periodic with period  $\pi$ . As before, kinks (or antikinks) with  $\delta\varphi = \pm\pi$  allow the accommodation of twisted boundary conditions and the formation of instantons. A vanishing compressibility corresponds to a finite kink energy  $\Sigma_x \geq \mathcal{C} > 0$  which, according to (4.8), leads to a gap in the ac conductivity. Thus, in a system with a nonzero  $\sigma(\omega)$  for small  $\omega$  also the compressibility has to be nonzero, contrary to the claims in Refs. [23, 69].

So far, we have assumed that all interactions are short range. In the case of an Anderson insulator with additional long range Coulomb interaction, the bare compressibility  $\kappa_0$  is diminished by a factor  $[1 + \mathcal{D} \ln(k_F L_x)]^{-1}$  where  $\mathcal{D} = 2\pi^2 \kappa_0 / \varepsilon_s$  [50, 77].  $\varepsilon_s$  denotes the dielectric constant. Thus, for  $L_x \rightarrow \infty$ , the Anderson insulator becomes incompressible. The effect of Coulomb interaction on  $\sigma(\omega)$  is known for  $K = 1$  only [85], where  $\sigma(\omega)$  is increasing by a factor  $\{\varepsilon_s \xi_A |\omega| \ln[v_F / (\xi_A \omega)]\}^{-1}$ . Thus the Anderson insulator is transformed to a Mott-glass phase, but there are again only two phases.

We come now to the discussion of the phase diagram of our model (4.3). From Eqs. (4.9)-(4.13) follows that the random backward scattering term is generated by forward scattering and the commensurate pinning potential. Since  $\sigma(l) = \sigma_0 e^l$  the two eigenvalues  $\lambda_1 = 3 - 2K$  and  $\lambda_2 = 4 - 2K - 4\sigma/\pi$  describing the renormalization group flow of  $u^2$  and  $w^2$  around the the Luttinger liquid fixed point  $u^* = w^* = 0$  have opposite sign:  $u(l)$  increases whereas  $w(l)$  decreases. Thus the hypothetical Mott-glass phase, if it existed, could not reach up to the point  $u = w = 0$ , in contrast to the findings in Refs. [23, 69]. From this we conclude that for not too large values of  $w_0$  the Anderson insulator phase is stable, as is shown in Fig. 4.2. To find the phase boundary to the Mott-insulating phase we consider the stability of the Mott-insulating phase with respect to the formation of a kink by the disorder. To lowest order in the disorder we get for the kink energy in the Mott-insulating phase

$$\Sigma_x \sim \frac{\sqrt{w_0}}{\kappa_0} \left[ 1 - \frac{1}{2} \left( \frac{\sigma_0^2}{w_0} \right)^{1/4} - \frac{u_0}{\pi^2 w_0^{3/4}} \right], \quad (4.15)$$

which gives from  $\Sigma_x = 0$  for the phase boundary between the Mott-insulating and the Anderson-insulating phase as depicted in Fig. 4.2. A similar result follows from the self-consistent harmonic approximation.

So far we considered only typical disorder fluctuations. If  $|\zeta(x)|$  and  $\mu(x)$  are Gaussian distributed and rare events are taken into account, then Eq. (4.15) remains valid with the replacements  $\sigma_0 \rightarrow \sigma_0 \ln(L\Lambda)$  and  $u_0^2 \rightarrow u_0^2 \ln(L\Lambda)$ . Thus the size of the Mott-insulating phase is reduced but finite unless we have  $L \rightarrow \infty$ .

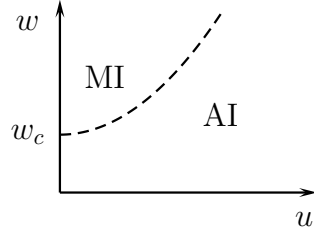


**Figure 4.2:** Schematic phase diagram with  $w_c \sim \sigma^2$ . MI (AI) denotes that the Mott insulator (Anderson insulator) is realized in indicated region of parameters.

These findings are supported by the observation that the forward scattering term in Eq. (4.3) can be removed from the action by transformation (4.14) [86]. On sufficiently large scales  $\gtrsim 1/(\sigma_0\Lambda)$  this transformation leaves only a random backward scattering term of strength  $\sqrt{u_0^2 + w_0^2}/(4\sigma_0)$  in the action, which results for sufficiently small  $K$  in the Anderson-insulating phase.

## 4.6 Discussions and conclusions

Now we briefly comment on the variational approach and replica symmetry breaking which have been used in Refs. [23, 69] where the Mott glass phase has been found. In the variational approach the full Hamiltonian is replaced by a harmonic one; this leads to the decoupling of Fourier components  $\varphi_q$  with different wavevector  $q$ . Without replica symmetry breaking one obtains from this approach the results of perturbation theory which is valid only on small scales. Replica symmetry breaking gives the possibility of a further reduction of the free energy. The results obtained in this way are exact only in cases when the coupling between different Fourier components is irrelevant and the physics is dominated by the largest length scale. Thus replica symmetry breaking is not an intrinsic property of the true solution of the problem, but a property of the variational approach. An illustrative example is the related problem of the interface roughening transition in a random potential [87]. The variational approach with replica symmetry breaking gives three phases: a flat, a rough and a glassy flat phase [88], where the rough phase has Flory like exponents. The functional renormalization group (which takes the coupling of different Fourier modes into account) gives however only two phases: the flat and the rough phase, but at the transition a logarithmically diverging interface width [87]. A similar situation may exist also in the present case.

To conclude, in this chapter we have shown for a one-dimensional disordered Mott insulator (4.3), tracing back both the compressibility and the ac

conductivity to the kink energy  $\Sigma_x$  of the electronic displacement field, that an incompressible system has also a vanishing optical conductivity. Thus we exclude the possibility of the existence of a Mott-glass phase in systems with short range interaction.

# Vortex configurations in a superconducting film with a magnetic dot

*In this chapter we consider a thin superconducting film with a magnetic dot, having permanent magnetization normal to the film surface, placed on the film. For sufficiently high dot magnetization a single vortex is created in the film. A further increase of the magnetization is accompanied by the appearance of more vortices and antivortices in the ground state.*

## 5.1 Introduction

Type-II superconductors in an external homogeneous magnetic field are comprehensively studied and well understood [24, 89]. They accommodate regularly distributed flux tubes–vortices for external fields between the lower and the upper critical field [90]. A similar scenario occurs in type-II superconducting films in perpendicular fields [26, 91]. A difference is that the first critical field for films vanishes for macroscopically large samples [91, 92].

An interesting class of systems which have attracted a great attention only recently are ferromagnet–superconductor hybrid systems. There one examines the influence of a material with heterogeneous magnetization on a superconductor [30]. Direct contact between the magnetic material and the superconductor is avoided usually by a thin insulating layer which suppresses the proximity effect. These hybrid systems can be fabricated under the full control of their parameters [31]. The inhomogeneous magnetization of ferromagnets generates an inhomogeneous magnetic field that penetrates the superconductor. As a response to that field, supercurrents and vortices are induced in the film. The magnetic field generated by the supercurrents interacts with the magnetic subsystem. By tuning the parameters of the latter we examine different phenomena of the composite system. Hybrid systems offer a number of realizations of new interesting phenomena, which include

---

pinning of magnetization induced vortices, commensurability effects between the external magnetic field and the periodic structure of magnetic material on the superconductor resistivity and others [30, 31, 93, 94].

In this chapter we are focused on the simplest ferromagnet–superconductor hybrid system. It consists of a single magnetic dot grown on top of a type-II superconducting film. The magnetic dot is assumed to have permanent magnetization normal to the film surface. Despite its simplicity, this system deserves attention since many different ground states can be realized in the parameter space. Dots having sufficiently small magnetization produce only supercurrents in the film. There is a critical dot magnetization above which the appearance of a single vortex is energetically favorable. Further increase of magnetization is accompanied with the appearance of different configurations of vortex states in the ground state (GS) [95, 96, 97, 98, 99, 100]. This is in striking contrast with respect to films in homogeneous fields, where any external magnetic field induces vortices [91, 92].

Our main goal is to define regions in the parameter space with different ground state configurations of vortices. A possible question that is under debate in literature is whether antivortices may also be induced in the film. One finds different statements about the presence of antivortices: while their existence is claimed in [97, 100, 101], they are not found in [98, 99]. Rough estimates [97], calculations with magnetic dipole [101] or studies inside the nonlinear Ginzburg–Landau theory with restriction to zero total vorticity states [100] seems to be insufficient. We give an independent and detailed study of this problem in this chapter. We will determine conditions for the appearance of different vortex–antivortex states and their spacial configurations.

The dot magnetization produces the magnetic field in the film, which is parallel to the magnetization under the dot, but antiparallel for distances larger than the dot radius. This magnetic field favors the creation of vortices under the dot and of antivortices outside the dot region. Which vortex–antivortex configuration has the smallest energy depends on the parameters of the system.

A vortex has a spatial structure. The superconducting order parameter vanishes, roughly speaking, at distances smaller than  $\xi$  around the center of the vortex. Here  $\xi$  denotes the coherence length of a superconductor [24]. The nonlinear Ginzburg–Landau approach takes into account the finite size of the vortex core. However, except from numerical treatments one can hardly derive any analytic results [100]. Our approach is rather based on the London–Maxwell equations [98, 102]. Although it treats vortices as point objects, it is a useful approach since one may derive analytic expressions for relevant quantities which become asymptotically exact when all lengths in

---

the problem are larger than the spatial vortex extension.

It is interesting to mention that the vortex nucleation in superconducting microtriangles and squares occurs in such a way that the symmetry of the superconductor is preserved [103, 104]. For example, in the case of a triangle, the state having the total vorticity two is realized when three vortices are placed around a single antivortex in the center of the triangle. This means that  $C_3$  symmetry is preserved. Our system, consisting of the infinite superconducting film and with magnetic dot on top of it, has rotational  $C_\infty$  symmetry around the dot center. This symmetry is reduced in the presence of vortices and antivortices, contrary to the above mentioned example. For the most possible symmetric states with the total vorticity zero, the rotational symmetry is either reduced to a discrete  $C_N$  symmetry (when the number of vortices and antivortices is  $N \geq 2$ ) or does not exist at all (for a vortex–antivortex pair). When two and more (we have checked up to four) vortices and antivortices are present in the zero vorticity state, vortices are distributed in a symmetric fashion around the dot center, while antivortices are placed outside the dot in the same manner, like homothetically transformed vortices. In the case of a single vortex–antivortex pair, the dot’s center, vortex and antivortex are collinear. Other states with nonzero vorticity are less symmetric. When the number of antivortices is five and more, they may form shells around a central vortex in zero vorticity states [100]. We do not consider such situation in our study.

The rest of the chapter is organized as follows. In section 5.2 we introduce a theoretical model to describe the system. We calculate the interaction energy between a cylindrical magnetic dot and vortices in the film. In section 5.3 we determine the conditions for the ground state configurations that consist of a single vortex and a vortex–antivortex pair. We also find separatrices between those ground states and the positions of vortices. In section 5.4 we calculate the magnetic field in the whole space and the supercurrents in the film when a single vortex is present in the system. In section 5.5 we present numerical results for the phase diagram with diversity of vortex–antivortex configurations. Section 5.6 contains numerical estimates of the relevant parameters and our conclusions. Some technical details are relegated to the appendices.

## 5.2 Model

We consider a circular magnetic dot of a radius  $R$  and a thickness  $a_t$  placed at a distance  $d$  above an infinite superconducting film, with its basis parallel to the film surface. The dot magnetization  $M$  is assumed to be constant and

---

normal to the film surface, see Fig. 5.1. Apart from the supercurrents, the dot may also induce vortices and antivortices in the film. We will study these vortex configurations. Since our problem has many parameters there are many regions in the parameter space which may have different ground state configurations (GSC). The GSC denotes a configuration of vortices in the film having the lowest energy among all other configurations; the trivial GSC has no vortices. This is expected for sufficiently small  $M$ . With increasing  $M$  creation of vortices becomes energetically favorable.

We assume quite generally that our system consists of  $N$  vortices of vorticities  $n_i$  placed at positions  $\boldsymbol{\rho}_i$  for a given magnetization of the dot  $M$ . The energy of the system in that case reads

$$E_{n_1, \dots, n_N} = \sum_{i=1}^N n_i^2 U_v + \sum_{i < j}^N n_i n_j U_{vv}(\rho_{ij}, 1, 1) + \sum_{i=1}^N n_i U_{mv}(\rho_i, 1), \quad (5.1)$$

where  $\rho_{ij} = |\boldsymbol{\rho}_i - \boldsymbol{\rho}_j|$  and  $\rho_i = |\boldsymbol{\rho}_i|$ .  $U_v$  is the single vortex energy,  $U_{vv}$  is the vortex–vortex interaction, and  $U_{mv}$  is the vortex–magnet interaction. For a given magnetization of the dot, the system will be in the state where  $E_{n_1, \dots, n_N}$  is minimal. Expression (5.1) assumes that the system in the trivial ground state has zero energy,  $E_0 = 0$ .

Expressions for  $U_{mv}$  and  $U_{vv}$  can be calculated by using the approach developed in Refs. [98, 102] based on the London–Maxwell equations. The details are presented in appendix 5.A. For the interaction energy between the dot and a vortex of vorticity  $n$  placed at the distance  $\rho$  from the dot’s center we get

$$U_{mv}(\rho, n) = -nMR\phi_0 \int_0^\infty dk J_0(k\rho) J_1(kR) \frac{e^{-kd} - e^{-k(d+a_t)}}{k(1 + 2\lambda k)}, \quad (5.2)$$

where  $J_0$  and  $J_1$  are the Bessel functions of the first kind.  $\lambda$  is the effective penetration depth and is equal  $\lambda_L^2/d_s$ , where  $\lambda_L$  is the London penetration depth and  $d_s$  the film thickness. The film thickness is assumed to satisfy  $d_s \ll \lambda_L$ , when the variation of the vector potential and the phase of the order parameter may be neglected across the thickness of the film, see appendix 5.A. Expression (5.2) can be evaluated asymptotically in some regions, see

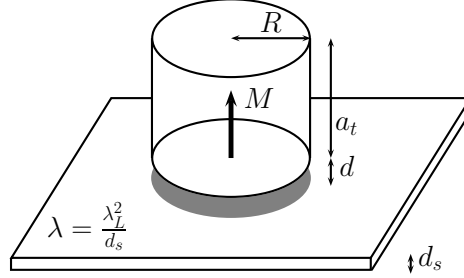


**Figure 5.1:** Magnetic dot with perpendicular permanent magnetization  $M$  upon infinite superconducting film.

appendix 5.B, and has the following behavior (we take  $d = 0$  for simplicity):

$$U_{mv}(\rho, n) = -nMa_t\phi_0\frac{R}{4\lambda} \begin{cases} 2 - \frac{\rho^2}{2R^2}, & \rho \ll a_t \ll R \ll \lambda, \\ \frac{R}{2a_t} + \frac{R}{a_t} \ln \frac{2a_t}{R} - \frac{\rho^2}{2Ra_t}, & \rho \ll R \ll a_t \ll \lambda, \\ \frac{R}{2\lambda} \left( \frac{2\lambda}{\rho} + \ln \frac{\rho}{4\lambda} + \gamma \right), & a_t, R \ll \rho \ll \lambda, \\ \frac{4\lambda^2 R}{\rho^3}, & a_t, R \ll \lambda \ll \rho. \end{cases} \quad (5.3)$$

The interaction between the two vortices of vorticities  $n_1$  and  $n_2$  separated by a distance  $\rho$  is given by

$$U_{vv}(\rho, n_1, n_2) = \frac{n_1 n_2 \phi_0^2}{16\pi\lambda} \left[ H_0 \left( \frac{\rho}{2\lambda} \right) - Y_0 \left( \frac{\rho}{2\lambda} \right) \right], \quad (5.4)$$

and has the asymptotic form

$$U_{vv}(\rho, n_1, n_2) = n_1 n_2 \begin{cases} 2U_v, & \rho \ll \xi \ll \lambda, \\ \frac{\phi_0^2}{8\pi^2\lambda} \left( \ln \frac{4\lambda}{\rho} - \gamma \right), & \xi \ll \rho \ll \lambda, \\ \frac{\phi_0^2}{4\pi^2} \frac{1}{\rho}, & \lambda \ll \rho. \end{cases} \quad (5.5)$$

In the previous expressions  $\phi_0$  is the magnetic flux quantum,  $H_0$  is the Struve function of order zero and  $Y_0$  is the Bessel function of the second kind of order zero [105].  $U_v$  is the single vortex energy [106], and reads

$$U_v = \frac{\phi_0^2}{16\pi^2\lambda} \left( \ln \frac{4\lambda}{\xi} - \gamma \right), \quad (5.6)$$

where  $\gamma \approx 0.577$  is the Euler constant. Two vortices which centers are at distances smaller than  $\xi$  are considered in our model as a double vortex. Its total energy is  $4U_v$ : from the two single vortices comes  $2U_v$  as well as

from their interaction. In the same way a vortex–antivortex pair at distances smaller than  $\xi$  does not exist, i.e. it is annihilated. Here we mention that Eqs. (5.4) and (5.6) are valid for films with lateral dimensions larger than the effective penetration depth. In the opposite case the lateral system size enters expressions (5.4) and (5.6) instead of  $\lambda$ . This change does not complicate further considerations and we do not consider such situation. We would like also to point out that the core energy of a vortex should be, in principle, also included in Eq. (5.1), but it can be taken into account through the small renormalization of the term in brackets in Eq. (5.6) for  $U_v$ .

In the following we will use the energy expression (5.1) which will be minimized in the parameter space and which determines the structure of vortex configurations in the GS.

### 5.3 Ground states with vortices

To determine the GSCs of the system with respect to different parameters, we consider the asymptotic forms of Eqs. (5.2) and (5.4). For simplicity we will just consider the case of thin magnetic dots ( $a_t < R$ ) placed on the film surface ( $d = 0$ ). The other cases may be straightforwardly done having calculated the asymptotic forms of  $U_{mv}$ , Eq. (5.3).

The necessary condition for the appearance of an extra vortex with respect to the trivial GSC is  $E_1 \leq E_0$ . Using Eq. (5.3) in the lowest order in  $\lambda/R$  we obtain

$$\mathcal{M} \geq \frac{2\lambda}{R}, \tag{5.7}$$

where we have introduced

$$\mathcal{M} = \frac{Ma_t\phi_0}{U_v}. \tag{5.8}$$

This result agrees with the one from Ref. [98]. Here we have taken into account that the strongest attraction energy between single vortex and magnet occurs at  $\rho = 0$ . The phase boundary is a linear function of  $\lambda/R$  for  $R < \lambda$ . For large dot radii  $R$ , result (5.7) shows that any nonzero magnetization induces a vortex in the film. This resembles the result for vanishing of the first critical field for thin films in an external homogeneous magnetic field [91, 92].

Apart from the trivial GSC and the single vortex state, there are other states for higher  $\mathcal{M}$ . We will now determine a portion of the parameter space where a vortex–antivortex pair appears in the GS. The energy  $E_{1,-1}$  of

---

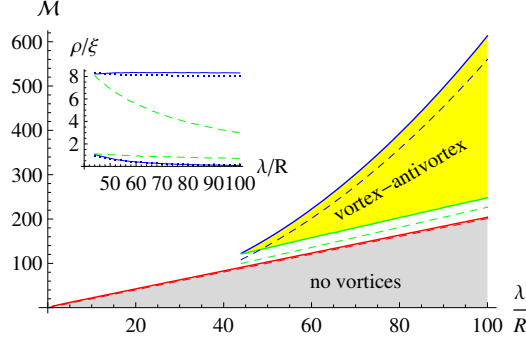


**Figure 5.2:** Phase diagram of a magnetic dot for  $L_g = 6$  and  $a_t/R = 0.01$ : the vortex–antivortex state appears for large enough dot magnetization and large enough  $\lambda/R$ . The solid lines are obtained numerically, while the dashed are analytic formulae (5.7), (5.11) and (5.12) with  $A = 1.7$ . Inset: the upper(lower) curves show the antivortex(vortex) positions. The solid (dashed) lines correspond to the upper (lower) phase boundary of the vortex–antivortex pair. The dotted lines are plotted using analytic formulae (5.14) and (5.15).

a vortex–antivortex pair separated by a distance  $\rho$  ( $\rho \ll 2\lambda$ ) with the vortex under the dot center reads

$$\frac{E_{1,-1}(\rho)}{U_v} = 2 + \frac{U_{mv}(0,1)}{U_v} + \frac{\mathcal{M}R^2}{4\lambda\rho} - \left( \frac{2}{L_g} + \frac{\mathcal{M}R^2}{8\lambda^2} \right) \left( L_g - \ln \frac{\rho}{\xi} \right), \quad (5.9)$$

where

$$L_g = \ln \frac{4\lambda}{\xi} - \gamma \quad (5.10)$$

is the logarithmic factor in the vortex self energy. We may notice from Eq. (5.9) that the main contribution from the magnetic dots on the antivortex is the energy cost, and it scales with the distance from the dot as  $1/\rho$ , while the energy gain due to the vortex–antivortex attraction scales logarithmically. This different behavior ( $1/\rho$  vs.  $\ln \rho$ ) may lead to a stable potential minimum for some parameters. For that energy minimum we find  $\rho^* = 2\lambda / (1 + \frac{2}{L_g} \frac{8\lambda^2}{\mathcal{M}R^2})$  which should be supplemented with the self consistency condition  $\rho^* \ll \lambda$  where Eq. (5.9) is valid, and also with  $\rho^* > a_t, R$ . The implicit equation  $E_{1,-1}(\rho^*) = 0$  defines the phase boundary for the creation of a vortex–antivortex pair. In addition, if the conditions  $E_{1,-1}(\rho^*) < E_1$  and  $E_{1,-1} < 0$  are satisfied, the vortex–antivortex pair forms the GS. The condition  $E_{1,-1} \leq E_1$  gives

$$\mathcal{M} \leq \frac{\lambda^2}{R^2} \frac{32}{L_g \left[ \exp \left( 1 + \gamma + \frac{L_g}{2} \right) - 2 \right]}, \quad (5.11)$$

which is the upper dashed line for the vortex–antivortex phase boundary in Fig. 5.2. The other phase boundary we get from the condition that the antivortex is placed outside the dot,  $\rho^* \geq AR$ , which gives

$$\mathcal{M} \geq \frac{8}{L_g} \frac{\lambda}{R} A, \quad (5.12)$$

where  $A$  is a positive number of order one.

From the last two inequalities we obtain the condition on  $\lambda/R$  when the vortex–antivortex forms the GS (in the case  $a_t < R, d = 0$ ):

$$\frac{\lambda}{R} \geq \frac{A}{4} \left[ \exp \left( 1 + \gamma + \frac{L_g}{2} \right) - 2 \right]. \quad (5.13)$$

For simplicity, in Eq. (5.9) we have assumed that the vortex position is under the dot,  $\rho_1 = 0$ . Having in mind relatively flat magnet–vortex interaction (5.3) for  $\rho < R$  the system can gain even more energy allowing  $\rho_1 > 0$  toward the antivortex, since the energy loss in the vortex–magnet interaction may be overcompensated by the vortex–antivortex attraction. A similar calculation to the previous one gives for the vortex displacement

$$\frac{\rho_1}{R} = \frac{64\lambda^2}{\mathcal{M}^2 R^2 L_g^2}, \quad (5.14)$$

while for the antivortex

$$\frac{\rho}{2\lambda} = \frac{1}{1 + \frac{2}{L_g} \frac{8\lambda^2}{\mathcal{M}R^2}} - \frac{2R}{\mathcal{M}L_g\lambda}, \quad (5.15)$$

and the center of the dot, vortex and antivortex are collinear. Physically, the stronger the magnetization of the dot is, the closer the vortex to the dot’s center is. We also see that the symmetry of the single vortex GSC is broken for the range of parameters where the antivortex appears.

## 5.4 Magnetic field

The magnetic dot on top of the superconducting film induces circular supercurrents in the film. These currents generate magnetic field in and outside the film. The total magnetic field in space is a sum of three terms: due to the supercurrents, due to the dot and due to vortices. In this section we calculate the magnetic field. The details of calculation are given in appendix 5.A.

---

A vortex of vorticity  $n$  produces normal to the film surface (axial) and parallel the film surface (radial) magnetic field which respectively read [107]

$$B_z^v(\rho, z) = \frac{n\phi_0}{2\pi} \int_0^\infty dk \frac{k \exp(-k|z|)}{1 + 2\lambda k} J_0(k\rho), \quad (5.16)$$

$$B_{\parallel}^v(\rho, z) = \frac{n\phi_0}{2\pi} \frac{|z|}{z} \int_0^\infty dk \frac{k \exp(-k|z|)}{1 + 2\lambda k} J_1(k\rho). \quad (5.17)$$

The previous expressions at the film surface  $z = 0$  have the following asymptotic forms:

$$B_z^v(\rho, 0) = \frac{n\phi_0}{8\pi\lambda^2} \begin{cases} \frac{2\lambda}{\rho}, & \rho \ll \lambda, \\ \left(\frac{2\lambda}{\rho}\right)^3, & \lambda \ll \rho, \end{cases} \quad (5.18)$$

$$B_{\parallel}^v(\rho, z \rightarrow 0) = \frac{n\phi_0}{8\pi\lambda^2} \frac{|z|}{z} \begin{cases} \frac{2\lambda}{\rho}, & \rho \ll \lambda, \\ \left(\frac{2\lambda}{\rho}\right)^2, & \lambda \ll \rho. \end{cases} \quad (5.19)$$

The parallel magnetic field outside the film (remember that in our calculations the film is just in the  $z = 0$  plane) changes the sign going from one side of the film to the other. This is due to the fact that the vortex induces the supercurrents in the film which circulate around it, and the jump in  $B_{\parallel}^v$  crossing the film surface is the condition for the jump of parallel magnetic field at boundaries due to surface currents [1]. The normal magnetic field is continuous across the film. The surface current density  $K_v$  produced by the vortex is given by

$$\mathbf{K}_v = \frac{c}{4\pi} \hat{\mathbf{z}} \times (\mathbf{B}_{\parallel}^v(\rho, 0^+) - \mathbf{B}_{\parallel}^v(\rho, 0^-)), \quad (5.20)$$

which agrees with the (integrated over  $z$ ) expression for the current density around a vortex, Eq. (5.42).

The magnetic field due to the dot is given by the two integrals:

$$B_z^d(\rho, z) = -2\pi MR \int_0^\infty dk J_0(k\rho) J_1(kR) \left\{ \frac{\exp(-k(|z| + d))}{1 + 2\lambda k} \right. \quad (5.21)$$

$$\times [1 - \exp(-ka_t)] + \text{sign}(d - z) [1 - \exp(-k|d - z|)] -$$

$$\left. \text{sign}(d + a_t - z) [1 - \exp(-k|d + a_t - z|)] \right\},$$

$$B_{\parallel}^d(\rho, z) = -2\pi MR \int_0^\infty dk J_1(k\rho) J_1(kR) \left\{ \text{sign}(z) \frac{\exp(-k(|z| + d))}{1 + 2\lambda k} \right. \quad (5.22)$$

$$\times [1 - \exp(-ka_t)] + \exp(-k|d - z|) - \exp(-k|d + a_t - z|) \left. \right\}.$$

Eq. (5.21)(Eq. (5.22)) we write as a sum  $B_{z(\parallel)}^d = B_{z(\parallel)}^{dm} + B_{z(\parallel)}^{df}$  of the fields due to the dot  $B_{z(\parallel)}^{dm}$  and due to the supercurrents  $B_{z(\parallel)}^{df}$ .  $B_{z(\parallel)}^{dm}$  is mathematically defined by setting  $\lambda \rightarrow \infty$  in Eq. (5.21)(Eq. (5.22)), which physically means the system with the dot but without the film. We evaluate (5.21) and (5.22) for  $d = 0$  and at the film surface. The purely magnetic terms are given by

$$B_z^{dm}(\rho, 0) = -\pi MR^2 a_t \frac{1}{\rho^3}, \quad (5.23)$$

$$B_{\parallel}^{dm}(\rho, 0) = -\pi MR^2 a_t \frac{3a_t}{2\rho^4}, \quad (5.24)$$

to the leading order for  $\rho \gg a_t, R$ . The previous result can be understood as the magnetic dipolar field [1]. The part due to the supercurrents is

$$B_z^{df}(\rho, 0) = -\pi MR^2 a_t \begin{cases} \frac{1}{4\lambda\rho^2}, & a_t, R \ll \rho \ll \lambda, \\ \mathcal{O}\left(\frac{1}{\rho^4}\right), & a_t, R \ll \lambda \ll \rho, \end{cases} \quad (5.25)$$

$$B_{\parallel}^{df}(\rho, z \rightarrow 0) = -\pi MR^2 a_t \frac{|z|}{z} \begin{cases} \frac{1}{\lambda\rho^2}, & a_t, R \ll \rho \ll \lambda, \\ \frac{6\lambda}{\rho^4}, & a_t, R \ll \lambda \ll \rho. \end{cases} \quad (5.26)$$

Again, the parallel field  $B_{\parallel}^{df}$  jumps across the film surface due to the surface currents. The surface current density  $K_m$  in the film due to the presence of the dot is given by

$$\mathbf{K}_m = \frac{c}{4\pi} \hat{\mathbf{z}} \times (\mathbf{B}_{\parallel}^{df}(\rho, 0^+) - \mathbf{B}_{\parallel}^{df}(\rho, 0^-)). \quad (5.27)$$

As first proposed in Ref. [98] the presence of a single vortex in the film can be proved by observing the change of sign of the total field  $B_z$  near the film. We can now calculate that it happens when  $B_z^d(\rho_{sz}, 0) + B_z^v(\rho_{sz}, 0) = 0$ , which gives  $\rho_{sz} = 2\pi\sqrt{MR^2 a_t \lambda / \phi_0}$  provided a single vortex appears in the GS. Using the condition for the single vortex appearance, Eq. (5.7), we obtain  $\rho_{sz} \approx \sqrt{L_g R \lambda / 2}$ . We can also formulate a similar condition for the presence of a single vortex for the parallel field, which also changes the sign for at the distance  $\rho_{s\parallel}$  from the dot.  $\rho_{s\parallel}$  is defined as a solution of the equation  $B_{\parallel}^d(\rho_{s\parallel}, 0) + B_{\parallel}^v(\rho_{s\parallel}, 0) = 0$ . The solution of the resulting cubic equation is  $\rho_{s\parallel} \approx (6\pi^2 MR^2 a_t^2 \lambda / \phi_0)^{1/3}$  above the film ( $z \rightarrow 0^+$ ), which using Eq. (5.7) becomes  $\rho_{s\parallel} \approx (3L_g R a_t \lambda / 4)^{1/3}$ .

Qualitatively different behavior of the normal and parallel magnetic field is summarized in Fig. 5.3 when a single vortex is present in the GS. Sufficiently close to the dot dominates the dipolar field from the dot, while at larger distances the vortex part of the field is a leading term.

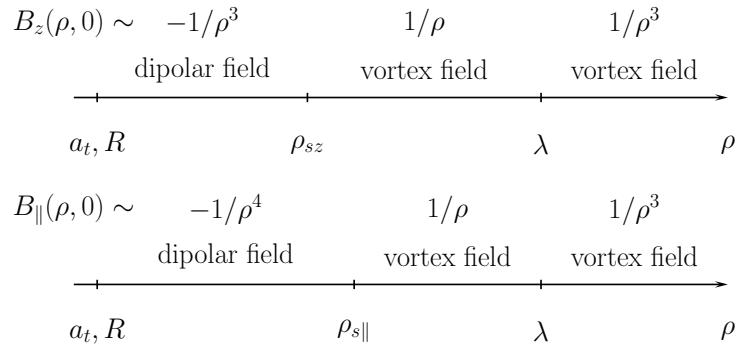


**Figure 5.3:** Behavior of the magnetic field near the upper film surface. The magnetization of the dot is assumed to be directed as in Fig. 5.1, such that a single vortex appears under the dot. The magnetic field changes the sign at some distance from the dot due to the presence of the vortex.

So far we have only considered a single vortex under the dot. Since there may be many other vortex–antivortex states in the film, the magnetic field (the vortex part only) of such configurations will behave differently than in Eqs. (5.18) and (5.19). It will also have the angular dependence. In that case the total magnetic field close enough to the dot will be dominated by the dipolar field from the dot, while at larger distances the anisotropic vortex part of the magnetic field will prevail. One should be able to use the measurement of the magnetic field near the film for detection of vortex states induced by the dot.

## 5.5 Numerical study of ground states with low number of vortices

In section 5.3 we have shown analytically that a vortex–antivortex pair can be present in the GS. That was the simplest GSC containing the antivortex. Certainly there are other more complicated states for a range of parameters. The analytic study of these states is in principle straightforward using already introduced expressions, but tedious. In this section we study numerically GSCs. For a given configurations uniquely determined by  $n_1, n_2, \dots$  we use expression (5.1) to obtain the energy minimum and the positions of vortices and antivortices. The GSC for given  $\lambda/R, a_t/R, L_g$  and  $\mathcal{M}$  has the energy minimum over of all possible vortex–antivortex configurations. In our calculations we took into account just states with low numbers of vortices, since they cover significant part of the parameter space as well as the other states are computationally demanding. The dot–magnet distance is set to

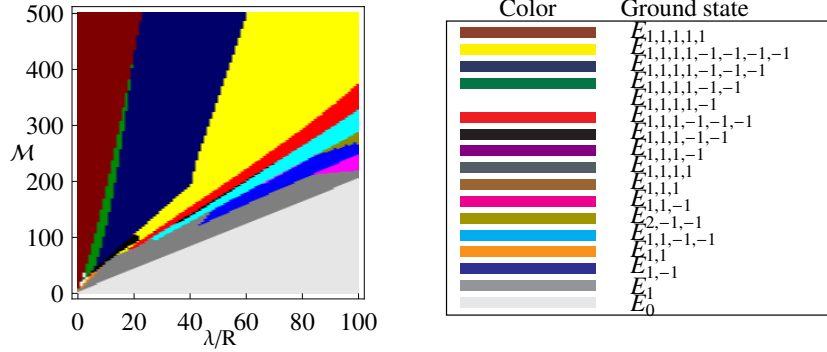


**Figure 5.4:** Phase diagram of a magnetic dot for  $L_g = 6$  and  $a_t/R = 0.01$  with different vortex-antivortex configurations.

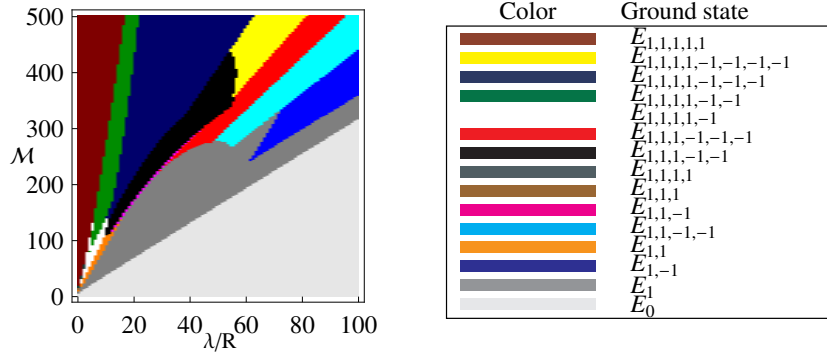


**Figure 5.5:** Phase diagram of a magnetic dot for  $L_g = 6$  and  $a_t/R = 1$  with different vortex-antivortex configurations.

$d = 0$ . We have examined all states which have up to four vortices with antivortices, while for the states with five vortices we took into account vortices without antivortices. This is certainly not correct since antivortices appear in states with five vortices as well, but such states are located in a particular region of the parameter space and do not affect states containing up to three vortices (see further in the text).

The states with six and more vortices are not taken into account. This is not crucial for our study since the vortex state of vorticity  $n$  will appear in the phase diagram for  $\mathcal{M} \geq 2n\lambda/R$ , which is either for large magnetization or large magnetic dots (with respect to  $\lambda$ ). On the other hand, the boundary line for  $n$  single vortices (and antivortices) is moved a little bit toward smaller  $\mathcal{M}$  for a given  $\lambda/R$ .

In Fig. 5.4 we show the GSCs for the case of a magnetic dot with  $a_t/R = 0.01$  and  $L_g = 6$ . For low values of  $\mathcal{M}$  there are no vortices in the GS for any  $\lambda/R$ . With increasing  $\mathcal{M}$  the state  $E_1$  appears. Further increase of  $\mathcal{M}$  is

ultimately followed with the appearance of antivortices. To be specific, let us consider  $\lambda/R = 50$ . After  $E_1$ , the state with antivortex  $E_{1,-1}$  appears which is the GSC for some region of  $\mathcal{M}$ . Then the states  $E_{1,1,-1,-1}$ ,  $E_{1,1,1,-1,-1,-1}$ ,  $E_{1,1,1,-1,-1,-1,-1}$ ,  $E_{1,1,1,1,-1,-1,-1,-1}$  appear for larger  $\mathcal{M}$ . Further states might have included the states with five vortices with antivortices if we had taken them into account. The states that evolve from each other have one vortex and/or one antivortex more/less than its neighbors. We believe that this should mean that the states with three vortices will not be affected by the states with five vortices.

Also the net vorticity of the GSCs is small ( $0, \pm 1$ ), in general, just near the origin it is higher. However, for small  $\lambda/R$  the dot radius is pretty large for realistic films and a further analysis with finer resolution of  $\lambda/R$  is necessary. We are here mainly concentrated in the region where  $R < \lambda$  since it is the most interesting experimentally.

The distances between the center of the dot and vortices and antivortices are shown in Fig. 5.6 and Fig. 5.7 respectively. We see that they abruptly change at the boundaries between different GSCs. We also see that the antivortices when are present, are placed at distances of a few  $R$ . Inside the same GSC, for fixed  $\lambda/R$ , the antivortices spread with increasing  $\mathcal{M}$ , while the vortices shrink. This is plausible, since very large magnetization of the dot would expel antivortices to very large distances. The interaction energy can not be then compensated by the attractive vortex–antivortex attraction. On the other hand, vortices are attracted at smaller distances toward the potential minimum of the vortex–magnet interaction. These results are also confirmed by the analytic formulae (5.14) and (5.15) from the study of a single pair. We also find that in the states of zero total vorticity that contain two, three and four vortices, the positions of antivortices are obtained as homothetically transformed positions of vortices, and they form line, equilateral triangle and square, respectively.

The GSCs without antivortices are shown in Fig. 5.8. The relative energy difference due to the presence of antivortices is shown in Fig. 5.9. The relative energy gain is quite significant, which means that states without and with antivortices have quite different energies.

We see at Fig. 5.9 that the vortex states containing single vortices appear for smaller values of magnetization, while the state with a double vortex,  $E_2$ , is present for higher  $\mathcal{M}$ . A simple analytical check translated the condition  $E_{1,1} \leq E_2$  into

$$\mathcal{M} \leq \frac{1}{L_g} \exp(2L_g + 1 - 2\gamma) \frac{R}{\lambda}, \quad (5.28)$$

which for  $L_g = 6$  becomes  $\mathcal{M} \leq 23200R/\lambda$ . This also gives one expla-

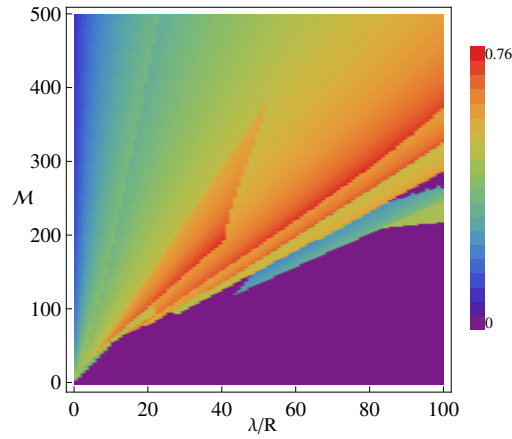


**Figure 5.6:** Vortex distances (in units of the dot radius  $R$ ) from the dot center for  $L_g = 6$  and  $a_t/R = 0.01$  which correspond to the ground state configurations given in Fig. 5.4.

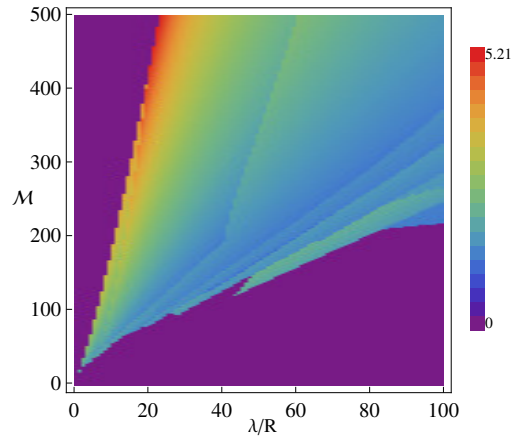


**Figure 5.7:** Antivortex distances (in units of the dot radius  $R$ ) from the dot center for  $L_g = 6$  and  $a_t/R = 0.01$  which correspond to the ground state configurations given in Fig. 5.4.

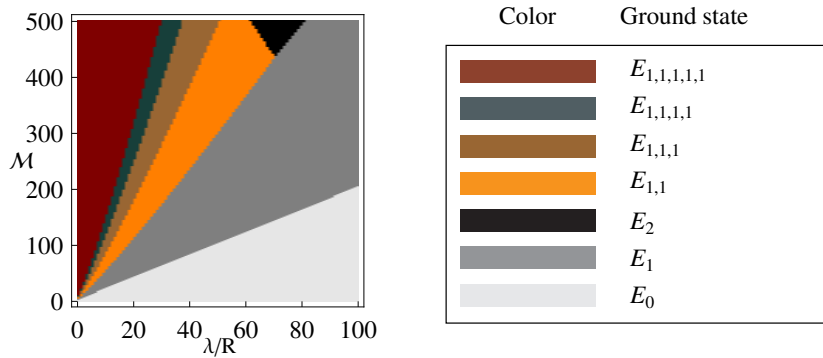


**Figure 5.8:** Phase diagram of a magnetic dot for  $L_g = 6$  and  $a_t/R = 0.01$  when antivortices are excluded from the energy minimization procedure.

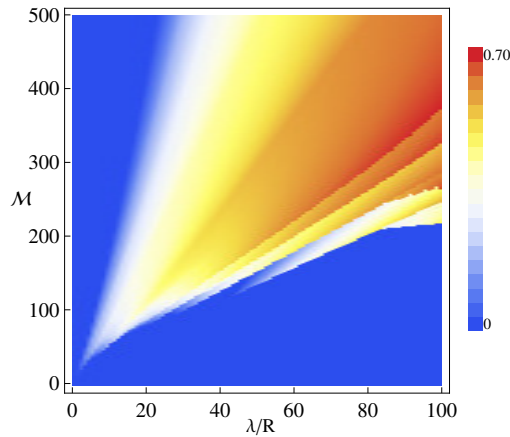


**Figure 5.9:** Relative energy change in the ground state when antivortices are included for  $L_g = 6$  and  $a_t/R = 0.01$ .

nation why the only ground state that has giant vortices (vortices having the vorticity larger than one) in Fig. 5.4 is  $E_{2,-1,-1}$ . It appears around  $\lambda/R = 100, \mathcal{M} = 250$ , which is in agreement with the rough estimate of Eq. (5.28). The other states with giant vortices may appear only for higher  $\mathcal{M}\lambda/R$  ratios.

For comparison with thicker magnetic dots, we have calculated the GSCs for  $a_t/R = 1$  and they are shown in Fig. 5.5. The single vortex appears now for larger  $\mathcal{M}$ , which is obvious from Eq. (5.7). The state  $E_{1,-1}$  now occurs for larger  $\lambda/R$ . However, a global picture with diversity of vortex–antivortex states again holds. A GSC here is shifted toward higher  $\lambda/R$  and  $\mathcal{M}$  values with respect to the corresponding GSC for thinner dots.

## 5.6 Discussions and conclusions

Now we comment about the applicability of the London approximation to our system. The ratio between the dot radius  $R$  and the coherence length  $\xi$  as a function  $\lambda/R$  is given as  $R/\xi = R \exp(L_g + \gamma)/(4\lambda)$ . We may conclude that for  $\lambda/R < 100$  and  $L_g = 6$  the dot radius is always larger than the coherence length. On the other hand, a necessary condition for the London approach to be valid is that the all lengths are (much) larger than the coherence length. We see that this is well satisfied when  $\lambda/R$  approaches smaller values. We expect that our results with different GSCs are valid even qualitatively for  $\lambda/R \lesssim 50$ , while the general picture with antivortices and low vorticity GSCs holds even for smaller dot radii. However, it is expected that for smaller  $R/\xi$  ratios, giant vortices are favorable. We have already mentioned such tendency. Let us mention that a certainly better numerical way would be the nonlinear Ginzburg–Landau theory. For the case of mesoscopic superconducting discs, a comparison of these two methods shows that they give similar results for  $R = 6\xi$  and for states that have up to five vortices [108].

Let us consider numerical values of parameters for realistic systems. For thin Nb films close to the critical temperature  $T/T_c = 0.98$ , the values for the London penetration depth and the coherence length are  $\lambda_L \cong 560$  nm and  $\xi \cong 58$  nm [109]. Then  $L_g = 6$  corresponds to a film of the thickness  $d_s \cong 30$  nm having the effective penetration depth  $\lambda \cong 10.5 \mu\text{m}$ . The condition for the  $E_{1,-1}$  state (5.13) can be rewritten as  $R < \lambda_L \sqrt{\xi/(9d_s)}$ , or  $R < 260$  nm in our case. The condition for the applicability of the London theory,  $\xi < R$  is still satisfied, so the results should be also valid. Larger magnetic dots may have other vortex–antivortex configurations, and the London theory is expected to be applicable there.

In this chapter we have considered infinite films. We expect this not to be a severe limitation as soon as the dot radius is much smaller than the system size, since the antivortices when appear are placed at distances of the order of  $R$  and the boundaries of the film should not affect them. For films with lateral dimensions smaller than  $\lambda$ , the single vortex energy given by Eq. (5.6) will have under the logarithm the lateral system dimension instead of  $4\lambda$ . For small dot radii one should repeat the same procedure as we described, just with a new value for the single vortex energy  $U_v$ .

To conclude, in this chapter we have considered a thin superconducting film with a cylindrical magnetic dot with permanent magnetization placed on the top of it. Inside the Maxwell–London approach we have calculated the vortex–magnet interaction and its asymptotic limits. Using these results we have shown analytically that a vortex–antivortex pair appears in the ground

---

state of the system for some range of dot's radii and its magnetization. The necessary magnetization for that is comparable to the magnetization for the appearance of a single vortex. The magnetic field everywhere in space is also calculated. Near the film surface, it has different scaling forms with respect to the distance from the center of the dot. This fact may be used for the experimental detection of vortices. In addition to that, we have calculated the phase diagram numerically, taking into accounts the states that have up to four vortices and antivortices.

## 5.A Derivation of the model

In this appendix we will calculate several quantities used in the main text of this chapter. We consider the system which consists of a superconducting film and a single magnetic dot, as shown in Fig. 5.1. Magnetic field everywhere in space  $\mathbf{B}(\boldsymbol{\rho}, z)$  is determined by the total current density  $\mathbf{j}(\boldsymbol{\rho}, z)$  via Ampère's law,  $\nabla \times \mathbf{B}(\boldsymbol{\rho}, z) = 4\pi\mathbf{j}(\boldsymbol{\rho}, z)/c$ . The total current density is a sum of the superconducting current density and the current density due to the presence of magnetic dot, which reads  $c\nabla \times \mathbf{M}(\boldsymbol{\rho}, z)$ .

The supercurrent density is determined by the second Ginzburg–Landau equation. In a three-dimensional superconductor with the order parameter  $\psi(\mathbf{r}) = |\psi(\mathbf{r})|e^{i\varphi(\mathbf{r})}$  it reads [24]

$$\mathbf{j}_s(\mathbf{r}) = \frac{\hbar e^*}{m^*} |\psi(\mathbf{r})|^2 \left( \nabla \varphi(\mathbf{r}) - \frac{e^*}{\hbar c} \mathbf{A}(\mathbf{r}) \right), \quad (5.29)$$

where  $e^*$  and  $m^*$  are the effective charge and mass of a pair of electrons and  $\mathbf{A}(\mathbf{r})$  is the vector potential. In the London approximation  $|\psi(\mathbf{r})|$  is regarded as a constant except in the small core regions around vortices. Then, the previous equation can be written as

$$\mathbf{j}_s(\mathbf{r}) = \frac{c}{4\pi\lambda_L^2} \left( \frac{\phi_0}{2\pi} \nabla \varphi(\mathbf{r}) - \mathbf{A}(\mathbf{r}) \right), \quad (5.30)$$

where  $\lambda_L$  is the London penetration depth, which is given by

$$\lambda_L^2 = \frac{m^* c^2}{4\pi e^{*2} |\psi(\mathbf{r})|^2}, \quad (5.31)$$

and the flux quantum is  $\phi_0 = hc/e^* = hc/(2e)$ .

For a superconducting film placed in the  $x$ - $y$  plane one integrates Eq. (5.30) over a film thickness  $d_s$  along the  $\hat{\mathbf{z}}$  direction. If the film is much thinner than  $\lambda_L$  we may assume that  $\varphi(\mathbf{r})$  and  $\mathbf{A}(\mathbf{r})$  remain constant across the thickness

---

of the film. If we imagine that all current is concentrated in a delta-function sheet in the plane  $z = 0$ , the three-dimensional superconducting current density (5.30) can be written as

$$\mathbf{j}_s(\boldsymbol{\rho}, z) = \frac{c}{4\pi\lambda} \left( \frac{\phi_0}{2\pi} \nabla\varphi(\boldsymbol{\rho}) - \mathbf{A}_{2d}(\boldsymbol{\rho}) \right) \delta(z), \quad (5.32)$$

where we have introduced the effective penetration depth of the film

$$\lambda = \frac{\lambda_L^2}{d_s}. \quad (5.33)$$

$\mathbf{A}_{2d}(\boldsymbol{\rho})$  is the vector potential in the two-dimensional film. Expressing the magnetic field as  $\mathbf{B} = \nabla \times \mathbf{A}$ , the Ampère's law becomes

$$\begin{aligned} \nabla \times (\nabla \times \mathbf{A}(\boldsymbol{\rho}, z)) &= -\frac{1}{\lambda} \mathbf{A}_{2d}(\boldsymbol{\rho}) \delta(z) + \frac{1}{\lambda} \frac{\phi_0}{2\pi} \nabla\varphi(\boldsymbol{\rho}) \delta(z) \\ &+ 4\pi \nabla \times \mathbf{M}(\boldsymbol{\rho}, z). \end{aligned} \quad (5.34)$$

We have got the London-Maxwell equation which determines currents and interaction energies in our system. Due to linearity of the London-Maxwell equation the vector potential may be written as a sum  $\mathbf{A} = \mathbf{A}_v + \mathbf{A}_m$ , where  $\mathbf{A}_v$  and  $\mathbf{A}_m$  are determined as solutions of the corresponding London-Maxwell equations generated by vortices and by the dot magnetization, respectively.

We will first solve the vortex part of the Eq. (5.34) which reads

$$\nabla \times (\nabla \times \mathbf{A}_v(\boldsymbol{\rho}, z)) = -\frac{1}{\lambda} \mathbf{A}_{v2d}(\boldsymbol{\rho}) \delta(z) + \frac{1}{\lambda} \frac{\phi_0}{2\pi} \nabla\varphi(\boldsymbol{\rho}) \delta(z). \quad (5.35)$$

For a single vortex of vorticity  $n$  the gradient of its phase is given by the expression

$$\nabla\varphi(\boldsymbol{\rho}) = n \frac{\hat{\mathbf{z}} \times \boldsymbol{\rho}}{\rho^2}. \quad (5.36)$$

Introducing the Fourier-transform of the vortex vector potential

$$\mathbf{A}_v(\mathbf{k}_\rho, k_z) = \int d^2k_\rho \int dk_z e^{-i\mathbf{k}_\rho \boldsymbol{\rho}} e^{-ik_z z} \mathbf{A}_v(\boldsymbol{\rho}, z) \quad (5.37)$$

and

$$\mathbf{A}_{v2d}(\mathbf{k}_\rho) = \int d^2k_\rho e^{-i\mathbf{k}_\rho \boldsymbol{\rho}} \mathbf{A}_{v2d}(\boldsymbol{\rho}) \quad (5.38)$$

and using the Coulomb gauge  $\nabla \cdot \mathbf{A}_v = 0$ , Eq. (5.35) becomes

$$\mathbf{A}_v(\mathbf{k}_\rho, k_z) + \frac{1}{\lambda(k_\rho^2 + k_z^2)} \mathbf{A}_{v2d}(\mathbf{k}_\rho) = \frac{in\phi_0}{\lambda(k_\rho^2 + k_z^2)} \frac{\mathbf{k}_\rho \times \hat{\mathbf{z}}}{k_\rho^2}. \quad (5.39)$$

Taking into account that the three-dimensional vector potential at  $z = 0$  must match the two-dimensional one  $\mathbf{A}_v(\boldsymbol{\rho}, z = 0) = \mathbf{A}_{v2d}(\boldsymbol{\rho})$ , after some elementary algebra we get [107]

$$\mathbf{A}_v(\mathbf{k}_\rho, k_z) = \frac{2in\phi_0}{(k_\rho^2 + k_z^2)(1 + 2\lambda k_\rho)} \frac{\mathbf{k}_\rho \times \hat{\mathbf{z}}}{k_\rho}. \quad (5.40)$$

Using Eq. (5.40) and inverse Fourier transforming the expression  $\mathbf{B}_v(\mathbf{k}_\rho, k_z) = i\mathbf{k} \times \mathbf{A}_v(\mathbf{k}_\rho, k_z)$ , where  $\mathbf{k} = \mathbf{k}_\rho + k_z \hat{\mathbf{z}}$ , one gets the expressions for the magnetic field produced by the vortex, Eqs. (5.16) and (5.17).

The current density produced by a single vortex of vorticity  $n$  placed at origin can be calculated from the Fourier transformed Ampère's law

$$\begin{aligned} \mathbf{j}_s(\mathbf{k}_\rho, k_z) &= \frac{c}{4\pi} i\mathbf{k} \times (i\mathbf{k} \times \mathbf{A}_v(\mathbf{k}_\rho, k_z)) \\ &= \frac{c}{4\pi} (k_\rho^2 + k_z^2) \mathbf{A}_v(\mathbf{k}_\rho, k_z). \end{aligned} \quad (5.41)$$

We get

$$\begin{aligned} \mathbf{j}_s(\boldsymbol{\rho}, z) &= \frac{\hat{\mathbf{z}} \times \boldsymbol{\rho}}{\rho} \delta(z) \frac{n\phi_0 c}{4\pi^2} \int_0^\infty dk_\rho \frac{k_\rho J_1(k_\rho \rho)}{1 + 2\lambda k_\rho} \\ &= \frac{\hat{\mathbf{z}} \times \boldsymbol{\rho}}{\rho} \delta(z) \frac{n\phi_0 c}{32\lambda^2 \pi} \left[ H_1\left(\frac{\rho}{2\lambda}\right) - Y_1\left(\frac{\rho}{2\lambda}\right) - \frac{2}{\pi} \right]. \end{aligned} \quad (5.42)$$

The force acting on a vortex of vorticity  $n_1$  separated by a distance  $\rho$  from the vortex of vorticity  $n$  at origin is [24]

$$\mathbf{F} = \int dz \mathbf{j}_s(\boldsymbol{\rho}, z) \times \frac{n_1 \phi_0}{c} \hat{\mathbf{z}}. \quad (5.43)$$

On the other hand, the force is determined as a negative gradient of the interaction energy between these two vortices

$$\mathbf{F} = -\nabla U_{vv}(\rho, n, n_1). \quad (5.44)$$

Combining the last two equations, for the interaction energy between the two vortices we get

$$U_{vv}(\rho, n, n_1) = nn_1 \frac{\phi_0^2}{16\pi\lambda} \left[ H_0\left(\frac{\rho}{2\lambda}\right) - Y_0\left(\frac{\rho}{2\lambda}\right) \right]. \quad (5.45)$$

Next, we will solve the London–Maxwell equation for the magnetic part. It reads

$$\nabla \times (\nabla \times \mathbf{A}_m(\boldsymbol{\rho}, z)) = -\frac{1}{\lambda} \mathbf{A}_{m2d}(\boldsymbol{\rho}) \delta(z) + 4\pi \nabla \times \mathbf{M}(\boldsymbol{\rho}, z). \quad (5.46)$$

Fourier transforming Eq. (5.46) we get

$$k^2 \mathbf{A}_m(\mathbf{k}_\rho, k_z) - \mathbf{k}(\mathbf{k} \cdot \mathbf{A}_m(\mathbf{k}_\rho, k_z)) = -\frac{1}{\lambda} \mathbf{A}_{m2d}(\mathbf{k}_\rho) + 4\pi i \mathbf{k} \times \mathbf{M}(\mathbf{k}_\rho, k_z), \quad (5.47)$$

which in the axial gauge  $A_{mz} = 0$  has the solution [98]

$$A_{m\rho}(\mathbf{k}_\rho, k_z) = 4\pi i \frac{\mathbf{M}(\mathbf{k}_\rho, k_z)}{k_z} \cdot \frac{\mathbf{k}_\rho \times \hat{\mathbf{z}}}{k_\rho}, \quad (5.48)$$

$$A_{m\varphi}(\mathbf{k}_\rho, k_z) = -\frac{A_{m2d\varphi}(\mathbf{k}_\rho)}{\lambda(k_\rho^2 + k_z^2)} + \frac{4\pi i \mathbf{M}(\mathbf{k}_\rho, k_z)}{k_\rho(k_\rho^2 + k_z^2)} \cdot (k_z \mathbf{k}_\rho - k_\rho^2 \hat{\mathbf{z}}). \quad (5.49)$$

For a cylindric magnetic dot with magnetization along  $\hat{\mathbf{z}}$ , see Fig. 5.1 for parameters of the dot, one obtains the vector potential  $\mathbf{A}_m$  with components  $A_{m\rho} = A_{mz} = 0$  and

$$A_{m\varphi}(\mathbf{k}_\rho, k_z) = \frac{4\pi i k_\rho M(\mathbf{k}_\rho)}{k_\rho^2 + k_z^2} \left[ \frac{e^{-k_\rho d} - e^{-k_\rho(d+at)}}{a_t k_\rho (1 + 2\lambda k_\rho)} - M(k_z) \right], \quad (5.50)$$

where the Fourier transform of the dot magnetization is given by  $\mathbf{M}(\mathbf{k}_\rho, k_z) = M(\mathbf{k}_\rho) M(k_z) \hat{\mathbf{z}}$  with

$$M(\mathbf{k}_\rho) = \frac{2\pi MRa}{k_\rho} J_1(k_\rho R), \quad (5.51)$$

$$M(k_z) = \frac{i}{k_z a_t} [e^{-ik_z(d+at)} - e^{-ik_z d}]. \quad (5.52)$$

Using Eq. (5.50) one can calculate the magnetic field produced by the dot everywhere in space. The final expressions are given in Eqs. (5.21) and (5.22).

To determine the interaction energy vortex–dot we need an expression for the current density produced by the dot in the film. Using the Fourier transformed Ampère’s law,

$$\begin{aligned} \mathbf{j}_m(\mathbf{k}_\rho, k_z) &= \frac{c}{4\pi} i \mathbf{k} \times (i \mathbf{k} \times \mathbf{A}_m(\mathbf{k}_\rho, k_z)) \\ &= \frac{c}{4\pi} (k_\rho^2 + k_z^2) A_{m\varphi}(\mathbf{k}_\rho, k_z) \frac{\hat{\mathbf{z}} \times \mathbf{k}_\rho}{k_\rho}, \end{aligned} \quad (5.53)$$

for the current density in the film sheet produced by the magnetic dot, we obtain

$$\mathbf{j}'_m(\boldsymbol{\rho}, z) = \delta(z) c M R a_t \frac{\boldsymbol{\rho} \times \hat{\mathbf{z}}}{\rho} \int_0^\infty dk_\rho J_1(k_\rho \rho) J_1(k_\rho R) \frac{e^{-k_\rho d} - e^{-k_\rho(d+a_t)}}{a(1+2\lambda k_\rho)}. \quad (5.54)$$

The force acting on a vortex of vorticity  $n$  separated by a distance  $\rho$  from the dot's center is

$$\mathbf{F} = \int dz \mathbf{j}'_m(\boldsymbol{\rho}, z) \times \frac{n\phi_0}{c} \hat{\mathbf{z}}. \quad (5.55)$$

On the other hand, this force is determined as a negative gradient of the interaction energy between the dot and vortex

$$\mathbf{F} = -\nabla U_{mv}(\rho, n). \quad (5.56)$$

Combining the last two equations for the interaction energy we obtain

$$U_{mv}(\rho, n) = -n M R \phi_0 \int_0^\infty dk_\rho J_0(k_\rho \rho) J_1(k_\rho R) \frac{e^{-k_\rho d} - e^{-k_\rho(d+a_t)}}{k_\rho(1+2\lambda k_\rho)}. \quad (5.57)$$

## 5.B Calculation of $U_{mv}$

In this appendix we calculate asymptotically the integrals that appear in the interaction energy (5.2). To do that it is sufficient to calculate the integral of the form

$$I(a, b, c) = \int_0^\infty dx J_0(ax) J_1(x) \frac{e^{-cx}}{x(1+2bx)}. \quad (5.58)$$

In the limit  $a \gg c$  and  $a \gg 1$  this integral will be cut by the oscillations of the Bessel functions and the main contribution comes from the region  $x < 1/a \ll 1$ . Then we can expand  $J_1(x) \exp(-cx) \approx x(1-cx)/2$ . Using the tabulated integrals [110]

$$\int_0^\infty dx \frac{J_0(\alpha x)}{1+x} = \frac{\pi}{2} [H_0(\alpha) - Y_0(\alpha)], \quad (5.59)$$

$$\int_0^\infty dx J_0(\alpha x) = \frac{1}{\alpha}, \quad (5.60)$$

we easily obtain

$$I(a, b, c) = \frac{2b+c\pi}{8b^2} \frac{\pi}{2} \left[ H_0\left(\frac{a}{2b}\right) - Y_0\left(\frac{a}{2b}\right) \right] - \frac{c}{4ab}. \quad (5.61)$$

Using the expansion [105]

$$\frac{\pi}{2} [Y_0(x) - H_0(x)] = \begin{cases} \gamma + \log \frac{x}{2} - x, & x \ll 1 \\ -x^{-1} + x^{-3}, & x \gg 1 \end{cases} \quad (5.62)$$

where  $\gamma \approx 0.577$  is the Euler constant, one can further simplify the asymptotic expressions for  $I(a, b, c)$ .

In the limit  $a \ll c$  and  $a \ll 1$  integral (5.58) is cut by the exponential function at  $x \approx 1/c$ , which means the argument of  $J_0$  function  $ax \approx a/c \ll 1$  and we expand  $J(0, ax) \approx 1 - a^2x^2/4$ . We obtain

$$I(a, b, c) = \int_0^\infty dx J_1(x) \exp(-cx) \left( -\frac{a^2}{8b} + \frac{1}{x} + \frac{\frac{a^2}{8b} - 2b}{1 + 2bx} \right). \quad (5.63)$$

Then using the tabulated integrals [110]

$$\int_0^\infty dx \frac{J_1(\alpha x)}{1+x} = 1 + \frac{1}{\alpha} + \frac{\pi}{2} [Y_1(\alpha) - H_1(\alpha)], \quad (5.64)$$

$$\int_0^\infty dx J_1(\alpha x) \frac{\exp(-\gamma x)}{x} = -\gamma + \sqrt{1 + \gamma^2}, \quad (5.65)$$

$$\int_0^\infty dx J_1(\alpha x) \exp(-\gamma x) = 1 - \frac{\gamma}{\sqrt{1 + \gamma^2}}, \quad (5.66)$$

and the expansion for  $x \ll 1$  [105]

$$\frac{\pi}{2} [H_1(x) - Y_1(x)] = \frac{1}{x} + \frac{x}{4} \left( 1 - 2\gamma + \log \frac{4}{x^2} \right) \quad (5.67)$$

we obtain for  $a \ll c \ll 1 \ll b$

$$I(a, b, c) = \frac{1}{8b} \left( 1 - 2\gamma + c(a^2 - 4) - a^2\sqrt{1 + c^2} + \log \frac{16}{b^2} \right) + c - \frac{c}{\sqrt{1 + c^2}}. \quad (5.68)$$

In the above expressions  $J_0$  and  $J_1$  are the Bessel functions of the first kind,  $Y_0$  and  $Y_1$  are the Bessel functions of the second kind, while  $H_0$  and  $H_1$  are the Struve functions of order zero and one, respectively [105].

---

# Superconducting film with randomly magnetized dots

*In this chapter we consider a thin superconducting film with randomly magnetized dots on top of it. We show that for dots with permanent and random magnetization normal or parallel to the film surface, our system is an experimental realization of the two-dimensional XY model with random phase shifts. The low-temperature superconducting phase, that exists without magnetic dots, survives in the presence of magnetic dots for sufficiently small disorder.*

## 6.1 Introduction

Since the pioneering papers by Berezinskii [111] and Kosterlitz and Thouless [27] finite temperature phase transitions in two-dimensional (2D) systems, which have a continuous symmetry specified by a phase, have become a very active research field. It turned out that two-dimensional superfluids [112] as well as thin superconducting films [28, 29, 113, 114] have a Berezinskii–Kosterlitz–Thouless transition at a finite temperature  $T_{2D}$ . The low-temperature phase is superfluid (superconducting) and has quasi-long range order, while the disordered high-temperature is normal liquid (metallic) for superfluids (superconductors). These systems are successfully described by the two-dimensional XY model, see Eq. (6.1) with  $A_{ij} \equiv 0$ . Theoretical predictions were confirmed experimentally: a universal jump in the superfluid density at  $T_{2D}$  [115] and different current-voltage characteristics of superconducting films below and above  $T_{2D}$  [116].

Introducing the disorder through the random phase shifts in the two-dimensional XY model physics becomes more complex. The Hamiltonian of the two-dimensional XY model with random phase shifts reads [117, 118]

$$H = -\frac{\varepsilon_0}{\pi} \sum_{i,j} \cos(\phi_i - \phi_j - A_{ij}), \quad (6.1)$$

where the sum runs over all nearest neighboring sites on a square lattice.

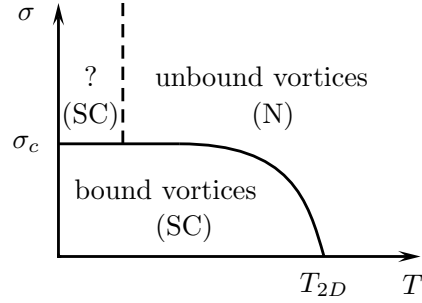


**Figure 6.1:** Phase diagram of the two-dimensional XY model with random phase shifts. At low temperature and weak disorder  $\sigma < \sigma_c$  a superconducting phase (SC) occurs where vortices are bound in pairs. Above  $T_{2D}$  vortices are unbound and the phase is non-superconducting (N). According to some studies, see Refs. [124, 125, 126], at low temperatures and for strong enough disorder appears another superconducting phase.

$\phi_i$  denotes the phase of the order parameter, while  $A_{ij}$  are quenched random phase shifts on bonds of the square lattice produced by some kind of disorder. We assume that  $A_{ij}$  are Gaussian distributed, uncorrelated, have the mean value zero  $\langle A_{ij} \rangle = 0$ , and the variance  $\langle A_{ij}^2 \rangle = \sigma$ . The pure two-dimensional XY model contains two different kinds of excitations which are decoupled. The spin-wave excitations describe small changes of the phase  $\phi$  and do not drive any phase transitions. Another kind of excitations are vortices, topological excitations, and they are essential for the existence of a Berezinskii–Kosterlitz–Thouless transition in the two-dimensional XY model at  $T_{2D}$ . Vortices are bound in pairs in the low-temperature phase, and unbound at high temperatures. Introducing the disorder in the form of random phase shifts, the low-temperature superconducting phase survives for weak enough disorder; this has been shown first analytically [118, 119, 120, 121] and then numerically [122, 123]. The phase diagram of the model (6.1) is given in Fig. 6.1.

The Hamiltonian (6.1) describes the thermodynamic behavior of several disordered systems, including two-dimensional ferromagnets with random Dzyaloshinskii–Moriya interaction [117], Josephson junction arrays with positional disorder [127] and vortex glasses [128]. In this chapter we will consider another system and show that it also belongs to the class of systems that can be described by the model (6.1). It is a ferromagnet-superconductor hybrid system. The system consists of a thin superconducting film covered by magnetic dots with permanent, but random magnetization. For more details about hybrid systems see recent reviews [30, 31]. We will show that our system can be described by the Hamiltonian (6.1) under some conditions defined below. Knowing the solution of the model (6.1) we can establish the possible phases of the system.

Placed on top of the film, a single magnetic dot with sufficiently large magnetization, normal to the film surface, induces and pins vortices and antivortices around it [96, 97, 100]. We have also shown it in chapter 5. A regular lattice of magnetic dots with constant and equal magnetization is the source of a periodic pinning potential for vortices in the film. The magnetic dots induce periodic arrays of vortices and antivortices in the film, provided the dot magnetization is high enough [129, 130]. The periodic pinning is absent in the case of a random dot magnetization, and there magnetic dots are a source of disordered pinning potential for vortices. Lyuksyutov and Pokrovsky [30, 96] considered a superconducting film with a magnetic dots array with random, sufficiently strong magnetic moments and concluded that the dot array induces the resistive state in the film. They have not considered the case when magnetic moments are weak. In this chapter we will show that the superconducting state survives provided the disorder is not too strong. Hybrid systems with a regular lattice of magnetic dots with random magnetization [131], and without a lattice, but homogeneously distributed dots on top of a thin superconducting film [132] have been recently experimentally realized.

In the rest of the chapter in section 6.2 we introduce a model for our hybrid system and give its solution by mapping it to the model (6.1). Section 6.3 contains discussions and conclusions. Some technical details are postponed to the appendix.

## 6.2 Model and its solution

We consider a thin superconducting film characterized by the London penetration depth  $\lambda_L$ , the coherence length  $\xi$ , a thickness  $d_s$  and a typical lateral dimension  $L$ . The London penetration depth is in general temperature dependent and we assume that our film has the effective penetration depth  $\lambda = \lambda_L^2/d_s$  that exceeds film's lateral dimension  $L$ . This limit is valid for "dirty" superconducting films [28]. In addition, provided the bulk critical temperature is larger than a critical temperature  $T_{2D}$  for vortex unbinding, the film has a Berezinskii–Kosterlitz–Thouless transition at  $T_{2D}$  [28, 113].

We consider dots with permanent random magnetization placed on top of the film. They produce a random potential  $V$  for vortices in the film. Assuming vortices of vorticities  $n_i$  are placed on a quadratic lattice with the lattice constant  $a$  (which is of the order of the coherence length), the effective

---

lattice Hamiltonian for the system may be written as

$$H_v = \sum_i [n_i^2(E_c + U_v) + n_i V_i] + \frac{1}{2} \sum_{i \neq j} n_i n_j U_{vv}(\rho_{ij}), \quad (6.2)$$

where the sum runs over all lattice sites,  $\varepsilon_0 = \phi_0^2/(16\pi^2\lambda)$ , the flux quantum is  $\phi_0 = hc/(2e)$ ,  $V_i$  is the random potential at site  $i$ , while  $E_c$  is the single vortex core energy which is of the order  $\varepsilon_0$ .  $U_v$  and  $U_{vv}(\rho_{ij})$  are the single vortex energy and the interaction energy of two vortices separated by a distance  $\rho_{ij}$ , respectively. For  $L < \lambda$  they read [106, 133]

$$U_v = \varepsilon_0 \ln \frac{L}{a}, \quad (6.3)$$

$$U_{vv}(\rho_{ij}) = 2\varepsilon_0 \ln \frac{L}{\rho_{ij}}. \quad (6.4)$$

Using expressions (6.3) and (6.4) it is useful to rewrite the Hamiltonian (6.2) in the form

$$H_v = \sum_i (n_i^2 E_c + n_i V_i) - \varepsilon_0 \sum_{i \neq j} n_i n_j \ln \frac{\rho_{ij}}{a} + N^2 U_v, \quad (6.5)$$

where we have introduced the total vorticity of the system  $N = \sum_i n_i$ . In the limit  $L \gg a$  ( $a \sim \xi$ ) the last term of Eq. (6.5) penalizes the total energy for nonzero total vorticities, so we consider in the following only configurations of vortices with the total vorticity  $N = 0$ . Without the disorder potential,  $V_i = 0$ , a superconducting film described by the model (6.5) has a Berezinskii–Kosterlitz–Thouless transition at the temperature  $T_{2D} = \varepsilon_0(T_{2D})/2$ , where  $\varepsilon_0(T_{2D})$  denoted that one should take value  $\lambda(T_{2D})$  renormalized by the presence of vortices [27, 28, 113].

Next, we consider effects of the random potential. First we consider the case when the dots have random magnetization parallel to the film surface. We model the magnetic dots as magnetic dipoles placed on top of the film at lattice sites. To characterize statistical properties of the dots, we assume that the  $x$ - and  $y$ - components of the magnetic moment at site  $i$  are Gaussian distributed, have zero mean value and are uncorrelated from site to site:

$$\langle m_{i\alpha} \rangle = 0, \quad \langle m_{i\alpha} m_{j\beta} \rangle = \mu^2 \delta_{ij} \delta_{\alpha\beta}, \quad \alpha, \beta = x, y \quad (6.6)$$

where  $\langle \dots \rangle$  denotes an average over disorder. Since the dots have random magnetic moments, we can say that  $\mu$  is the measure for a typical magnetic moment of a magnetic dot at some lattice site.

The interaction energy between a single dot having the magnetic moment  $\mathbf{m}$  parallel to the film surface and a vortex of vorticity  $n$  placed at a relative distance  $\boldsymbol{\rho}$  from the dot can be calculated using the approach from chapter 5, appendix 5.A, and reads

$$\begin{aligned} U_{mv}^{\parallel}(n, \rho) &= \frac{\mathbf{m} \cdot \boldsymbol{\rho}}{\rho} \frac{n\phi_0}{2\pi} \int_0^{\infty} dk \frac{k J_1(k\rho)}{1 + 2\lambda k} \\ &= \frac{\mathbf{m} \cdot \boldsymbol{\rho}}{\rho} \frac{n\phi_0}{16\lambda^2} \left[ H_1\left(\frac{\rho}{2\lambda}\right) - Y_1\left(\frac{\rho}{2\lambda}\right) - \frac{2}{\pi} \right], \end{aligned} \quad (6.7)$$

where  $J_1$  is the Bessel function of the first kind,  $H_1$  is the Struve function and  $Y_1$  is the Bessel function of the second kind [105]. Notice that the interaction energy between the magnetic dipole and the vortex can be simply written in the form  $-\mathbf{m} \cdot \mathbf{B}_v$ , where  $\mathbf{B}_v$  is the magnetic field produced by the vortex (Eq. (5.17)) at the dipole position [134]. In the limit  $\rho \ll \lambda$  the interaction energy (6.7) reads

$$U_{mv}^{\parallel}(n, \rho) = \frac{\mathbf{m} \cdot \boldsymbol{\rho}}{\rho} \frac{n\phi_0}{4\pi\lambda\rho}. \quad (6.8)$$

The random site potential  $V_i$  is given as a sum over the lattice

$$V_i = \sum_{j \neq i} \frac{U_{mv}^{\parallel}(n_j, \rho_{ij})}{n_j} = \frac{\phi_0}{4\pi\lambda} \sum_{j \neq i} \frac{\mathbf{m}_j \cdot \boldsymbol{\rho}_{ij}}{\rho_{ij}^2}. \quad (6.9)$$

By summing over  $j \neq i$  in the previous expression we avoid the short scale cutoff divergence of the interaction energy (6.7) at  $\rho = 0$ , which exists because the dots are placed at the top of the film in our model. In reality magnetic dipoles are separated from the film surface by some small distance  $\sim a$ . Since  $V_i$  is a sum of many independent random variables it is Gaussian distributed (notice here that the assumption about Gaussian distribution for  $m_{i\alpha}$  is not necessary condition for  $V_i$  to be Gaussian distributed; it is sufficient that dots have a distribution with a finite variance). Its mean, variance and site to site correlations can be calculated and read

$$\langle V_i \rangle = 0, \quad (6.10)$$

$$\langle V_i^2 \rangle = 2\pi \frac{\mu^2 \varepsilon_0}{\lambda a^2} \ln \frac{L}{a} + \mathcal{O}(1), \quad (6.11)$$

$$\langle (V_i - V_j)^2 \rangle = 4\pi \frac{\mu^2 \varepsilon_0}{\lambda a^2} \ln \frac{\rho_{ij}}{a} + \mathcal{O}(1). \quad (6.12)$$

The model (6.5) with the disorder potential (6.9) which has properties (6.10), (6.11) and (6.12) exactly matches the vortex part of the two-dimensional XY

---

model with random phase shifts [117, 135]. From the solution of the model (6.1), see Refs. [118, 121, 135], we know its phase diagram, see Fig. 6.1. At zero temperature there is a critical value for the typical magnetic moment per unit length  $\mu_c/a = \phi_0/(8\pi\sqrt{2\pi})$ . Below that value the system has no free vortices, while above that value the disorder spontaneously induces unbound vortices. The connection between  $\sigma$  introduced as the disorder strength in Eq. (6.1) and the typical magnetic moment  $\mu$  introduced in Eq. (6.6) is  $\sigma = \left(\frac{4\pi^2\mu}{\phi_0 a}\right)^2$ , while the random phase is  $\mathbf{A}_i = \frac{4\pi^2}{\phi_0 a} \hat{\mathbf{z}} \times \mathbf{m}_i$  where the  $x$ - ( $y$ -)component of  $\mathbf{A}_i$  corresponds to the disorder  $A_{ij}$  on horizontal (vertical) bond at site  $i$ .

In the case that the dot magnetization is normal to the film surface, similar to Eq. (6.7), for the interaction energy between a dot of magnetization  $m$  and a vortex of vorticity  $n$  separated by a distance  $\rho$  we get

$$\begin{aligned} U_{mv}^\perp(n, \rho) &= m \frac{n\phi_0}{2\pi} \int_0^\infty dk \frac{kJ_0(k\rho)}{1 + 2\lambda k} \\ &= m \frac{n\phi_0}{16\lambda^2} \left[ Y_0\left(\frac{\rho}{2\lambda}\right) - H_0\left(\frac{\rho}{2\lambda}\right) - \frac{4\lambda}{\pi\rho} \right]. \end{aligned} \quad (6.13)$$

The previous expression simplifies for  $\rho \ll \lambda$  and reads

$$U_{mv}^\perp(n, \rho) = m \frac{n\phi_0}{4\pi\lambda\rho}. \quad (6.14)$$

By assuming that the film is covered by magnetic dots with random magnetization normal to the film surface (along the  $\hat{\mathbf{z}}$  direction), satisfying

$$\langle m_{iz} \rangle = 0, \quad \langle m_{iz} m_{jz} \rangle = \mu^2 \delta_{ij}, \quad (6.15)$$

for the site random potential we get

$$V'_i = \sum_{j \neq i} \frac{U_{mv}^\perp(n_j, \rho_{ij})}{n_j} = \frac{\phi_0}{4\pi\lambda} \sum_{j \neq i} \frac{m_{jz}}{\rho_{ij}}, \quad (6.16)$$

which, as we show in the appendix, is equivalent to  $V_i$ ; it has statistical properties (6.10)-(6.12). We may conclude that the system with magnetic moments normal to the film has the same phase diagram as in the case of moments parallel to the film surface.

### 6.3 Discussions and conclusions

Having shown the equivalence between our system and the vortex part of the two-dimensional XY model with random phase shifts, we may infer some

---

properties of the former. The phase diagram is given in Fig. 6.1. The low temperature and low disorder phase is superconducting. There vortices and antivortices are bound in pairs. The current–voltage characteristic for  $T \rightarrow T_{2D}$  and  $T < T_{2D}$  and for weak disorder is expected to be very similar to the one of Halperin and Nelson [29] for the pure case,  $V \sim I^3$ , possibly with a small correction due to the disorder. This phase has zero linear resistivity. The high temperature phase is metallic and has a nonzero linear resistivity. There free vortices dissipate energy and produce the linear current–voltage characteristic  $V \sim I$ .

In Ref. [96] the conclusion about the resistive state of the film when the dots with normal magnetization are present relies on the assumption that the randomly magnetized dots pin vortices of vorticity  $\pm 1$ . These pinned vortices serve as a source of the random potential for other bound vortices, which unbind and fill deep valleys of the random potential. These unbound vortices lead to the resistive state of the film. We agree that this scenario occurs for sufficiently strong disorder when the dots can induce and pin vortices. A single dot can induce and pin quite different configurations of vortices and antivortices regarding its magnetic moment, as we have shown in chapter 5. We expect that a random lattice of dots can also pin, from site to site, quite a different number of vortices and antivortices which produce different potential than one assumed in Ref. [96]. However, our conclusion, that the resistive state in films occurs when the disorder is sufficiently strong, agrees with the one from Ref. [96]. Moreover, we give the strength of the disorder above which the resistive state occurs.

By making a comparison between  $\mu_c$  and the magnetic moment  $m_{1c}$  of a single magnetic dot with normal magnetization necessary to induce and pin an extra vortex in the film, we obtain  $m_{1c} \approx \mu_c \sqrt{8\pi} (b/a) \ln(L/a)$ , where  $b$  is the distance between the dipole and the film surface. In addition, knowing that the value  $\mu_c$  corresponds not to typical but rare magnetic moments from the tail of distribution [118, 136], we may conclude that even a very rare magnetic dot in the film that has the magnetic moment  $\mu_c$  is not able to induce and pin vortices. Such pinned vortices served as a source of random potential in [96].

In this chapter we have considered the dots as magnetic dipoles. This fact is unimportant as long as the dot size is not too big with respect to the lattice constant. What is crucial for any kind of magnetic dots is their interaction with a vortex which decays as  $1/\rho$ , which is universal for any geometrical shape of dots, when the vortex is sufficiently far from the dot. The magnetic field produced by a vortex decays as  $1/\rho$  and the interaction energy dot–vortex universally decays, regardless of the shape of the dot. This form of the interaction produces logarithmically diverging, with the system size,

---

variance of the disorder potential that is characteristic for the Hamiltonian (6.1).

Recently, the question of a possible third phase for strong disorder and at low temperatures has been raised in numerical studies of the model (6.1) with uniformly random phase  $A_{ij}$  in the interval  $[-r\pi, r\pi]$  with  $0 \leq r \leq 1$ , with conflicting results about its existence [124, 126, 137]. While for  $r < r_c \approx 0.37$  [123] it is accepted that the superconducting phase survives at low temperature, the case  $r > r_c$  is still under debate. An experimental study of Josephson junction arrays with positional disorder [125] supports the existence the third phase. The new phase is superconducting according to the experiments of Ref. [125] and numerical investigations of Ref. [124]. In the limit  $\sigma \rightarrow \infty$  the model (6.1) and the so-called gauge glass limit,  $r = 1$ , are equivalent, and we expect that the conjectures about the phase diagram for the case of uniformly distributed phase apply as well to the Gaussian distribution of the phase. The existence of the third phase is a challenging question that could be experimentally resolved by using magneto-superconducting hybrid systems as a realization for the model (6.1).

To conclude, we have shown that a thin superconducting film covered by magnetic dots with random magnetization provides an experimental realization for the two-dimensional XY model with random phase shifts. The phase diagram of the latter model helped us to conclude that a low-temperature superconducting phase of a superconducting film without dots survives when the dots are placed on top of the film, provided their magnetization is not too large.

## 6.A Equivalence between random potentials

In this appendix we prove that expressions for the disorder potential with magnetic moments parallel to the film surface (6.9) and normal to the film surface (6.16) are equivalent. Rewriting the expression  $\mathbf{m}_j \cdot \boldsymbol{\rho}_{ij}/\rho_{ij}^2$  from Eq. (6.9) as  $m_j \cos(\alpha_j - \alpha_\rho)/\rho_{ij}$ , where  $\cos \alpha_j = \mathbf{m}_j \cdot \hat{\mathbf{x}}/m_j$  and  $\cos \alpha_\rho = \boldsymbol{\rho}_{ij} \cdot \hat{\mathbf{x}}/\rho_{ij}$ , we will in the following show that the distribution of the random variable  $m_{rj} = m_j \cos(\alpha_j - \alpha_\rho)$  (which is the projection of  $\mathbf{m}_j$  onto  $\boldsymbol{\rho}_{ij}$ ) is Gaussian distributed with zero mean and the variance  $\mu^2$ .

By assumption (6.6), the components of the magnetic moment  $m_{jx}$  and  $m_{jy}$  are Gaussian distributed and have the distribution function

$$p(t) = \frac{1}{\sqrt{2\pi}\mu} \exp\left(-\frac{t^2}{2\mu^2}\right), \quad t = m_{jx}, m_{jy}. \quad (6.17)$$

Then the distribution function of the magnetic moment  $m_j = \sqrt{m_{jx}^2 + m_{jy}^2}$

is

$$\begin{aligned}
 p(m_j) &= \int_{-\infty}^{\infty} dm_{jx} \int_{-\infty}^{\infty} dm_{jy} p(m_{jx}) p(m_{jy}) \delta\left(m_j - \sqrt{m_{jx}^2 + m_{jy}^2}\right) \\
 &= \frac{m_j}{\mu^2} \exp\left(-\frac{m_j^2}{2\mu^2}\right),
 \end{aligned} \tag{6.18}$$

while the angle  $\alpha_j$  between  $m_{jx}$  and  $m_j$  is uniformly distributed in the interval  $[0, 2\pi)$  and has the distribution  $p(\alpha_j) = 1/(2\pi)$ . The distribution of the random variable  $m_{rj}$  is

$$p(m_{rj}) = \int_0^{\infty} dm_j \int_0^{2\pi} d\alpha_j p(m_j) p(\alpha_j) \delta(m_{rj} - m_j \cos(\alpha_j - \alpha_\rho)). \tag{6.19}$$

The previous expression can be most easily evaluated first by taking the Fourier transform of  $p(m_{rj})$

$$\begin{aligned}
 \tilde{p}_k &= \int_0^{\infty} dm_j \int_0^{2\pi} d\alpha_j \frac{m_j}{2\pi\mu^2} \exp\left(-\frac{m_j^2}{2\mu^2}\right) \exp[ikm_j \cos(\alpha_j - \alpha_\rho)] \\
 &= \exp\left(-\frac{k^2\mu^2}{2}\right),
 \end{aligned} \tag{6.20}$$

and then taking the inverse Fourier transform of the previous expression. It leads to

$$p(m_{rj}) = \frac{1}{\sqrt{2\pi}\mu} \exp\left(-\frac{m_{rj}^2}{2\mu^2}\right). \tag{6.21}$$

In that way we have proved that the random potential (6.9)

$$V_i = \frac{\phi_0}{4\pi\lambda} \sum_{j \neq i} \frac{\mathbf{m}_j \cdot \boldsymbol{\rho}_{ij}}{\rho_{ij}^2} = \frac{\phi_0}{4\pi\lambda} \sum_{j \neq i} \frac{m_{rj}}{\rho_{ij}} \tag{6.22}$$

matches the random potential (6.16). We conclude that frozen magnetic dipoles parallel to the film create the same random potential for vortices in the film as magnetic dipoles normal to the film, provided both are Gaussian distributed.

---

This page intentionally left blank

## Bibliography

- [1] J. D. Jackson, *Classical Electrodynamics* (John Wiley and Sons, New York, 1975), 2nd ed.
  - [2] P. Nozieres and D. Pines, *Theory of Quantum Liquids* (Westview Press, Boulder, 1999).
  - [3] C. J. Pethick and H. Smith, *Bose-Einstein Condensation in Dilute Gases* (Cambridge University Press, 2002).
  - [4] P. C. Hohenberg, Phys. Rev. **158**, 383 (1967).
  - [5] N. D. Mermin and H. Wagner, Phys. Rev. Lett. **17**, 1133 (1966).
  - [6] T. Nattermann, *Disordered systems, script* (unpublished, 2004).
  - [7] O. M. Auslaender, H. Steinberg, A. Yacoby, Y. Tserkovnyak, B. I. Halperin, K. W. Baldwin, L. N. Pfeiffer, and K. W. West, Science **308**, 88 (2005).
  - [8] T. Giamarchi, *Quantum Physics in One Dimension* (Clarendon Press, Oxford, 2003).
  - [9] M. Tzolov, B. Chang, A. Yin, D. Straus, J. M. Xu, and G. Brown, Phys. Rev. Lett. **92**, 075505 (2004).
  - [10] J. Cumings and A. Zettl, Phys. Rev. Lett. **93**, 086801 (2004).
  - [11] A. N. Aleshin, J. Y. Lee, S. W. Chu, S. W. Lee, B. Kim, S. J. Ahn, and Y. W. Park, Phys. Rev. B **69**, 214203 (2004).
  - [12] W. Kang, H. L. Stormer, L. N. Pfeiffer, K. W. Baldwin, and K. W. West, Nature(London) **403**, 59 (2000).
  - [13] O. M. Auslaender, A. Yacoby, R. de Picciotto, K. W. Baldwin, L. N. Pfeiffer, and K. W. West, Science **295**, 825 (2002).
  - [14] T. Stöferle, H. Moritz, C. Schori, M. Köhl, and T. Esslinger, Phys. Rev. Lett. **92**, 130403 (2004).
-

- 
- [15] D. E. Feldman and Y. Gefen, Phys. Rev. B **67**, 115337 (2003).
- [16] P. W. Anderson, Phys. Rev. **109**, 1492 (1958).
- [17] E. Abrahams, P. W. Anderson, D. C. Licciardello, and T. V. Ramakrishnan, Phys. Rev. Lett. **42**, 673 (1979).
- [18] B. I. Shklovskii and A. L. Efros, *Electronic properties of doped semiconductors* (Springer, Heidelberg, 1984).
- [19] C. L. Kane and M. P. A. Fisher, Phys. Rev. Lett. **68**, 1220 (1992).
- [20] C. L. Kane and M. P. A. Fisher, Phys. Rev. B **46**, 15233 (1992).
- [21] A. Furusaki and N. Nagaosa, Phys. Rev. B **47**, 4631 (1993).
- [22] K. Gottfried and T.-M. Yan, *Quantum Mechanics: Fundamentals* (Springer-Verlag, New York, 2003).
- [23] T. Giamarchi, P. Le Doussal, and E. Orignac, Phys. Rev. B **64**, 245119 (2001).
- [24] M. Tinkham, *Introduction to superconductivity* (McGraw-Hill, 1996).
- [25] D. R. Nelson, *Defects and Geometry in Condensed Matter Physics* (Cambridge University Press, 2002).
- [26] J. Pearl, Appl. Phys. Lett. **5**, 65 (1964).
- [27] J. M. Kosterlitz and D. J. Thouless, J. Phys. C **6**, 1181 (1973).
- [28] M. R. Beasley, J. E. Mooij, and T. P. Orlando, Phys. Rev. Lett. **42**, 1165 (1979).
- [29] B. I. Halperin and D. R. Nelson, J. Low Temp. Phys. **36**, 599 (1979).
- [30] I. F. Lyuksyutov and V. L. Pokrovsky, Adv. in Phys. **54**, 67 (2005).
- [31] M. Vélez, J. I. Martín, J. E. Villegas, A. Hoffmann, E. M. González, J. L. Vicent, and I. K. Schuller, J. Magn. Magn. Mater. **320**, 2547 (2008).
- [32] A. O. Caldeira and A. J. Leggett, Phys. Rev. Lett. **46**, 211 (1981).
- [33] U. Weiss, *Quantum Dissipative Systems* (World Scientific, 1999).
- [34] M. P. A. Fisher and W. Zwerger, Phys. Rev. B **32**, 6190 (1985).
-

- 
- [35] G. Schön and A. D. Zaikin, Phys. Rep. **198**, 237 (1990).
- [36] A. H. C. Neto and M. P. A. Fisher, Phys. Rev. B **53**, 9713 (1996).
- [37] G. Refael, E. Demler, Y. Oreg, and D. S. Fisher, Phys. Rev. B **68**, 214515 (2003).
- [38] D. Maslov and M. Stone, Phys. Rev. B **52**, R5539 (1995).
- [39] V. V. Ponomarenko, Phys. Rev. B **52**, R8666 (1995).
- [40] I. Safi and H. J. Schulz, Phys. Rev. B **52**, R17040 (1995).
- [41] R. Egger and H. Grabert, Phys. Rev. Lett. **79**, 3463 (1997).
- [42] M. A. Cazalilla, F. Sols, and F. Guinea, Phys. Rev. Lett. **97**, 076401 (2006).
- [43] K. A. Matveev, D. Yue, and L. I. Glazman, Phys. Rev. Lett. **71**, 3351 (1993).
- [44] F. D. M. Haldane, Phys. Rev. Lett. **47**, 1840 (1981).
- [45] J. P. Hirth and J. Lothe, *Theory of Dislocations* (John Wiley and Sons, New York, 1982).
- [46] B. Joós, Q. Ren, and M. S. Duesbery, Phys. Rev. B **50**, 5890 (1994).
- [47] L. Radzihovsky, Phys. Rev. B **73**, 104504 (2006).
- [48] A. Schmid, Phys. Rev. Lett. **51**, 1506 (1983).
- [49] A. I. Larkin and Yu. N. Ovchinnikov, Sov. Phys. JETP **59**, 420 (1984).
- [50] S. V. Malinin, T. Nattermann, and B. Rosenow, Phys. Rev. B **70**, 235120 (2004).
- [51] T. Vuletić, B. Korin-Hamzić, S. Tomić, B. Gorshunov, P. Haas, M. Dressel, J. Akimitsu, T. Sasaki, and T. Nagata, Phys. Rev. B **67**, 184521 (2003).
- [52] J. Friedel, Nuovo Cimento Suppl. **7**, 287 (1958).
- [53] R. Egger and H. Grabert, Phys. Rev. Lett. **75**, 3505 (1995).
- [54] R. Egger and H. Grabert, Phys. Rev. Lett. **77**, 538 (1996).
-

- 
- [55] H. J. Schulz, Phys. Rev. Lett. **71**, 1864 (1993).
- [56] A. O. Caldeira and A. J. Leggett, Annals of Physics **149**, 374 (1983).
- [57] K. Gottfried and T.-Y. Yan, *Quantum mechanics: fundamentals* (Springer-Verlag, New York, 2003).
- [58] T. Hikihara, A. Furusaki, and K. A. Matveev, Phys. Rev. B **72**, 035301 (2005).
- [59] K. Kamide, Y. Tsukada, and S. Kurihara, Phys. Rev. B **73**, 235326 (2006).
- [60] T. Kimura, K. Kuroki, and H. Aoki, Phys. Rev. B **53**, 9572 (1996).
- [61] D. Schmeltzer, Phys. Rev. B **65**, 193303 (2002).
- [62] D. Schmeltzer, A. R. Bishop, A. Saxena, and D. L. Smith, Phys. Rev. Lett. **90**, 116802 (2003).
- [63] V. Gritsev, G. Japaridze, M. Pletyukhov, and D. Baeriswyl, Phys. Rev. Lett. **94**, 137207 (2005).
- [64] J. Sun, S. Gangadharaiah, and O. A. Starykh, Phys. Rev. Lett. **98**, 126408 (2007).
- [65] J. E. Birkholz and V. Meden, Phys. Rev. B **79**, 085420 (2009).
- [66] C. L. Kane and M. P. A. Fisher, Phys. Rev. B **46**, 7268 (1992).
- [67] O. A. Starykh, D. L. Maslov, W. Häusler, and L. I. Glazman, in *Low-Dimensional Systems*, edited by T. Brandeis (Springer, New York, 2000), p. 37.
- [68] A. Furusaki and N. Nagaosa, Phys. Rev. B **47**, 3827 (1993).
- [69] E. Orignac, T. Giamarchi, and P. Le Doussal, Phys. Rev. Lett. **83**, 2378 (1999).
- [70] N. Mott, Philos. Mag. **17**, 1259 (1968).
- [71] A. Finkel'stein, Z. Phys. B **56**, 189 (1984).
- [72] N. F. Mott, *Metal-Insulator Transitions* (Taylor and Francis, London, 1990).
- [73] M. Ma, Phys. Rev. B **26**, 5097 (1982).
-

- 
- [74] H. Pang, S. Liang, and J. F. Annett, Phys. Rev. Lett. **71**, 4377 (1993).
- [75] Y. Suzumura and M. Isobe, J. Phys. Soc. Jpn. **73**, 3092 (2004).
- [76] P. Nozieres, in *Solids Far from Equilibrium*, edited by C. Godreche (Cambridge University Press, Cambridge, 1992).
- [77] T. Nattermann, T. Giamarchi, and P. Le Doussal, Phys. Rev. Lett. **91**, 056603 (2003).
- [78] W. Kohn, Phys. Rev. **133**, A171 (1964).
- [79] M. V. Feigel'man and V. M. Vinokur, Phys. Lett. A **87**, 53 (1981).
- [80] M. M. Fogler, Phys. Rev. Lett. **88**, 186402 (2002).
- [81] B. Rosenow and T. Nattermann, Phys. Rev. B **73**, 085103 (2006).
- [82] S. Fujimoto and N. Kawakami, Phys. Rev. B **54**, R11018 (1996).
- [83] I. F. Herbut, Phys. Rev. B **57**, 13729 (1998).
- [84] U. Schulz, J. Villain, E. Brézin, and H. Orland, J. Stat. Phys. **51**, 1 (1988).
- [85] B. I. Shklovskii and A. L. Efros, Sov. Phys. JETP **54**, 218 (1981).
- [86] M. P. A. Fisher, P. B. Weichman, G. Grinstein, and D. S. Fisher, Phys. Rev. B **40**, 546 (1989).
- [87] T. Emig and T. Nattermann, Phys. Rev. Lett. **81**, 1469 (1998).
- [88] J.-P. Bouchaud and A. Georges, Phys. Rev. Lett. **68**, 3908 (1992).
- [89] G. Blatter, M. V. Feigel'man, V. B. Geshkenbein, A. I. Larkin, and V. M. Vinokur, Rev. Mod. Phys. **66**, 1125 (1994).
- [90] A. A. Abrikosov, Sov. Phys. JETP **5**, 1174 (1957).
- [91] A. L. Fetter and P. C. Hohenberg, Phys. Rev. **159**, 330 (1967).
- [92] D. S. Fisher, Phys. Rev. B **22**, 1190 (1980).
- [93] J. I. Martín, M. Vélez, J. Nogués, and I. K. Schuller, Phys. Rev. Lett. **79**, 1929 (1997).
- [94] D. J. Morgan and J. B. Ketterson, Phys. Rev. Lett. **80**, 3614 (1998).
-

- 
- [95] I. K. Marmoros, A. Matulis, and F. M. Peeters, *Phys. Rev. B* **53**, 2677 (1996).
- [96] I. F. Lyuksyutov and V. L. Pokrovsky, *Phys. Rev. Lett.* **81**, 2344 (1998).
- [97] R. Sasik and T. Hwa, arxiv:cond-mat/0003462 (2000).
- [98] S. Erdin, A. M. Kayali, I. F. Lyuksyutov, and V. L. Pokrovsky, *Phys. Rev. B* **66**, 014414 (2002).
- [99] S. Erdin, *Phys. Rev. B* **72**, 014522 (2005).
- [100] M. V. Milošević and F. M. Peeters, *Phys. Rev. B* **68**, 024509 (2003).
- [101] M. V. Milošević, S. V. Yampolskii, and F. M. Peeters, *Phys. Rev. B* **66**, 174519 (2002).
- [102] S. Erdin, in *Frontiers in Superconducting Materials*, edited by A. Narlikar (2005), p. 425.
- [103] L. F. Chibotaru, A. Ceulemans, V. Bruyndoncx, and V. V. Moshchalkov, *Nature (London)* **408**, 833 (2000).
- [104] L. F. Chibotaru, A. Ceulemans, V. Bruyndoncx, and V. V. Moshchalkov, *Phys. Rev. Lett.* **86**, 1323 (2001).
- [105] M. Abramowitz and I. A. Stegun, *Handbook of Mathematical Functions* (Dover, New York, 1972).
- [106] J. Pearl, in *Low Temperature Physics-LT9*, edited by J. G. Daunt, D. O. Edwards, F. J. Milford, and M. Yagub (1965), p. 566.
- [107] A. A. Abrikosov, *Introduction to the theory of metals* (North-Holland, 1988).
- [108] B. J. Baelus, L. R. E. Cabral, and F. M. Peeters, *Phys. Rev. B* **69**, 064506 (2004).
- [109] A. Hoffmann, P. Prieto, and I. K. Schuller, *Phys. Rev. B* **61**, 6958 (2000).
- [110] A. P. Prudnikov, Y. A. Brychkov, and O. I. Marichev, *Integrals and Series* (Gordon and Breach Science Publishers, Amsterdam, 1986).
- [111] V. L. Berezinskii, *Sov. Phys. JETP* **34**, 610 (1972).
-

- 
- [112] D. R. Nelson and J. M. Kosterlitz, Phys. Rev. Lett. **39**, 1201 (1977).
- [113] S. Doniach and B. A. Huberman, Phys. Rev. Lett. **42**, 1169 (1979).
- [114] L. A. Turkevich, J. Phys. C **12**, L385 (1979).
- [115] D. J. Bishop and J. D. Reppy, Phys. Rev. Lett. **40**, 1727 (1978).
- [116] D. J. Resnick, J. C. Garland, J. T. Boyd, S. Shoemaker, and R. S. Newrock, Phys. Rev. Lett. **47**, 1542 (1981).
- [117] M. Rubinstein, B. Shraiman, and D. R. Nelson, Phys. Rev. B **27**, 1800 (1983).
- [118] T. Nattermann, S. Scheidl, S. E. Korshunov, and M. S. Li, J. Phys. I France **5**, 565 (1995).
- [119] M.-C. Cha and H. A. Fertig, Phys. Rev. Lett. **74**, 4867 (1995).
- [120] G. S. Jeon, S. Kim, and M. Y. Choi, Phys. Rev. B **51**, 16211 (1995).
- [121] D. Carpentier and P. Le Doussal, Phys. Rev. Lett. **81**, 2558 (1998).
- [122] J. Maucourt and D. R. Grempel, Phys. Rev. B **56**, 2572 (1997).
- [123] J. M. Kosterlitz and M. V. Simkin, Phys. Rev. Lett. **79**, 1098 (1997).
- [124] P. Holme, B. J. Kim, and P. Minnhagen, Phys. Rev. B **67**, 104510 (2003).
- [125] Y.-J. Yun, I.-C. Baek, and M.-Y. Choi, Europhys. Lett. **76**, 271 (2006).
- [126] Q.-H. Chen, J.-P. Lv, and H. Liu, Phys. Rev. B **78**, 054519 (2008).
- [127] E. Granato and J. M. Kosterlitz, Phys. Rev. B **33**, 6533 (1986).
- [128] C. Ebner and D. Stroud, Phys. Rev. B **31**, 165 (1985).
- [129] M. V. Milošević and F. M. Peeters, Phys. Rev. Lett. **93**, 267006 (2004).
- [130] D. J. Priour and H. A. Fertig, Phys. Rev. Lett. **93**, 057003 (2004).
- [131] J. E. Villegas, K. D. Smith, L. Huang, Y. Zhu, R. Morales, and I. K. Schuller, Phys. Rev. B **77**, 134510 (2008).
- [132] Y. T. Xing, H. Micklitz, T. G. Rappoport, M. V. Milošević, I. G. Solórzano-Naranjo, and E. Baggio-Saitovitch, Phys. Rev. B **78**, 224524 (2008).
-

- [133] P. M. Chaikin and T. M. Lubensky, *Principles of condensed matter physics* (Cambridge University Press, 1995).
  - [134] G. Carneiro, Phys. Rev. B **69**, 214504 (2004).
  - [135] L.-H. Tang, Phys. Rev. B **54**, 3350 (1996).
  - [136] S. E. Korshunov and T. Nattermann, Physica B **222**, 280 (1996).
  - [137] H. G. Katzgraber, Phys. Rev. B **67**, R180402 (2003).
-

## Acknowledgements

- I would like to thank Prof. Thomas Nattermann for supervising this thesis and sharing his ideas and views of physics and life with us, his students.
  - I would like to thank Prof. George Japaridze for many discussions in connection with chapter 3.
  - I would like to thank Prof. Valery Pokrovsky for helpful discussions on the topic studied in chapters 5 and 6.
  - I owe special thanks to Friedmar Schütze for a friendly atmosphere, many discussions and a critical reading of parts of this thesis.
  - I would also like to thank Dr. Gianmaria Falco for critical comments on some parts of the thesis and his nice stories.
  - I thank Dr. Leiming Chen and Dr. Christophe Deroulers for a nice ambiance and pleasant lunch breaks.
  - I thank Dr. Pera for patience, innumerable discussions and everything else.
  - Finally, I am grateful to my parents for all things they have done for me.
-

This page intentionally left blank

# Abstract

The subject of this thesis is order and transport in interacting disordered low-dimensional systems, namely Luttinger liquids and thin superconducting films. The disorder is produced by point impurities in Luttinger liquids and by magnetic dots in thin films.

In the second chapter we consider the influence of dissipation on the transport properties of a Luttinger liquid. In the presence of a single impurity we find an exponential suppression of the conductance as a function of applied voltage and temperature at sufficiently low voltages and temperatures.

In the third chapter we study a Luttinger liquid in the presence of two impurities and of an external magnetic field. The magnetic field splits the electrons with respect to their spin. We show that this system exhibits spin-filtering effect due to the resonance tunneling effect, which can also be achieved in this particular case, similarly to the case without the field. By tuning a single parameter, one may reach the resonance points when the transmission of spins with one spin-direction is dominating at low temperatures and voltages.

The fourth chapter is related to the question of the competition of a periodic and random potential in a Luttinger liquid. The periodic potential alone produces a Mott-insulating state at sufficiently small amount of quantum fluctuations, measured by the interaction parameter  $K$ . The random potential alone leads to the Anderson-insulating state for small values of  $K$ . In the presence of both potentials and when the interaction is short-ranged, we do not find an intermediate Mott-glass phase, contrary to some studies.

The fifth chapter deals with a thin superconducting film with a magnetic dot placed on top of it. We calculate the configurations of vortex-antivortex ground states for such system, finding a diversity of vortex-antivortex states as a function of parameters of the dot.

The sixth chapter studies a thin superconducting film covered by magnetic dots of random magnetization. We show that this system is a realization of the two-dimensional XY model with random phase shifts. The latter model helps us to determine the phase diagram of our system.

---

This page intentionally left blank

## Zusammenfassung

Gegenstand der vorliegenden Arbeit sind Ordnung und Transport in ungeordneten niedrigdimensionalen Systemen mit Wechselwirkung, wobei der Schwerpunkt auf ungeordneten Luttingerflüssigkeiten und dünnen supraleitenden Filmen liegt. In Luttingerflüssigkeiten ist die Unordnung durch Punktstörstellen realisiert, in dünnen supraleitenden Filmen betrachten wir magnetische Verunreinigungen.

Im zweiten Kapitel studieren wir den Einfluß von Dissipation auf die Transporteigenschaften einer Luttingerflüssigkeit. Bei hinreichend niedrigen Temperaturen und äußeren Feldern finden wir, in Gegenwart einer einzelnen Verunreinigung, eine exponentielle Unterdrückung des Leitwertes als Funktion der angelegten Spannung und der Temperatur.

Im dritten Kapitel betrachten wir eine Luttingerflüssigkeit in Gegenwart zweier Störstellen und eines zusätzlichen externen magnetischen Feldes. Das Magnetfeld unterteilt die Elektronen hinsichtlich ihres Spins. Wir zeigen, daß dieses System einen Spinfiltereffekt aufweist, der sich aus dem Resonanz-Tunneleffekt ergibt. Durch Abstimmen eines einzelnen Parameters kann man die Resonanzpunkte treffen, an denen bei tiefen Temperaturen und Spannungen die Transmission von Spins einer vorgegebenen Ausrichtung dominiert.

Das vierte Kapitel bezieht sich auf die Frage nach dem Gegenspiel eines periodischen und eines Unordnungspotentials in einer Luttingerflüssigkeit. Das periodische Potential allein führt zu einem Mottisolator, wenn die Quantenfluktuationen hinreichend schwach sind. Ein Maß hierfür ist der dimensionslose Luttingerparameter  $K$ . Liegt nur ein Unordnungspotential vor, so ergibt sich für kleine Werte von  $K$  ein Andersonisolator. In Gegenwart beider Potentiale schließen wir für kurzreichweitige Wechselwirkungen die intermediäre Mottglass-Phase aus, die in anderen Arbeiten postuliert wurde.

Mit dünnen supraleitenden Filmen, auf deren Oberseite ein magnetischer Punkt platziert ist, befassen wir uns im fünften Kapitel. Wir berechnen die Konfigurationen von Vortex-Antivortex-Grundzuständen in einem solchen System und finden eine Vielzahl an Vortex-Antivortex-Zuständen in Abhängigkeit der Parameter des Magnetpunktes.

Das sechste Kapitel ist dem Studium dünner supraleitender Filme gewidmet, auf denen Magnetpunkte zufälliger Magnetisierung verteilt sind. Es

---

wird gezeigt, daß solche Systeme Realisierungen des zweidimensionalen XY-Modells mit stochastischer Phase darstellen. Dieses Modell erweist sich als hilfreich bei der Bestimmung des Phasendiagramms für unser System.

---

# Erklärung

Ich versichere, dass ich die von mir vorgelegte Dissertation selbständig angefertigt, die benutzten Quellen und Hilfsmittel vollständig angegeben und die Stellen der Arbeit - einschließlich Tabellen, Karten und Abbildungen -, die anderen Werken im Wortlaut oder dem Sinn nach entnommen sind, in jedem Einzelfall als Entlehnung kenntlich gemacht habe; dass diese Dissertation noch keiner anderen Fakultät oder Universität zur Prüfung vorgelegen hat; dass sie - abgesehen von unten angegebenen Teilpublikationen - noch nicht veröffentlicht worden ist sowie, dass ich eine solche Veröffentlichung vor Abschluss des Promotionsverfahrens nicht vornehmen werde. Die Bestimmungen der Promotionsordnung sind mir bekannt. Die von mir vorgelegte Dissertation ist von Prof. Dr. Thomas Nattermann betreut worden.

Köln, 27. April, 2009

Zoran Ristivojevic

## Teilpublikationen

1. "Absence of the Mott Glass Phase in 1D Disordered Fermionic Systems",  
T. Nattermann, A. Petković, Z. Ristivojevic, and F. Schütze, *Phys. Rev. Lett.* **99**, 186402 (2007).
  2. "Transport in a Dissipative Luttinger Liquid",  
Z. Ristivojevic and T. Nattermann, *Phys. Rev. Lett.* **101**, 016405 (2008). Also in *Vir. J. Nan. Sci. Tech.* **18**, 13 (2008).
  3. "Ground state configurations of vortices in superconducting film with magnetic dot",  
Z. Ristivojevic, (2008), arxiv:0812.2695
  4. "Superconducting film with randomly magnetized dots: a realization of the 2D XY model with random phase shifts",  
Z. Ristivojevic, (2009), arxiv:0903.5514
-

This page intentionally left blank

# Curriculum vitae

## Personal data

Date of birth 29. January 1979  
Place of birth Kruševac, Serbia  
Nationality Serbian  
Marital status Single

## Education

- 1986–1994** Elementary school, Kupci, Serbia.  
GPA: 5.00 (out of 5)
- 1994–1998** Mathematical Gymnasium, Belgrade, Serbia.  
GPA: 5.00 (out of 5)
- 1998–2003** Undergraduate studies, section Theoretical and Experimental Physics, Faculty of Physics, University of Belgrade, Belgrade, Serbia.  
GPA:10.00 (out of 10)  
Diploma thesis: “Entropy behavior in nonconservative electron transport”. Thesis advisor: Prof. Dr. Zoran Lj. Petrović.
- 2003–2005** Master studies in Physics, Department for gaseous electronics, Institute of Physics, University of Belgrade, Belgrade, Serbia.  
Master thesis: “Development and verification of a hybrid model for gas discharges” (undefended). Thesis advisor: Prof. Dr. Zoran Lj. Petrović.
- 2006–2009** Doctoral studies, Institute of Theoretical Physics, University of Cologne, Cologne, Germany.  
PhD thesis: “Order and transport in interacting disordered systems”. Thesis advisor: Prof. Dr. Thomas Nattermann.
-

### Significant awards and scholarships

- Feb 2003** Serbian Royal Family Karadjordjevic Award for one of 100 best university students in Serbia, Montenegro and Republic of Srpska.
- Sep 2000** Royal Norwegian Government Award for one of 500 best students in Serbia.
- 2003–2005** Scholarship from Ministry of Science and Technology, Government of Republic of Serbia.
- 2000–2003** Scholarship from Republic Foundation for Development of Scientific and Art Youth.
- 1992–1998** several awards at Republic and Federal competitions in physics and mathematics (problem solving).

### Employment

- Oct 2009–** Argonne National Laboratory, Argonne, USA.
- 2006–Sep 2009** Institute of Theoretical Physics, University of Cologne, Germany.
- Sep–Dec 2005** Institute of Physics, Belgrade, Serbia.
- 2004–2006** Member of the editorial board of Young physicist–journal for elementary and high school physics students published by Serbian Physical Society.
- 2004** Active member of committee for organizations of physics competitions in Serbia and Montenegro and author of theoretical problems.
- Jul–Aug 2004** Summer student, University of Ghent, Department of Applied Physics, Ghent, Belgium.
- Nov–Dec 2002** Exchange student, University of Sao Paulo, Institute of Physics, Sao Carlos, Brazil.
- 2001–2002** Mathematical Gymnasium, Belgrade, Serbia–preparing students for high school competitions in physics.
-